NATIONAL TECHNICAL UNIVERSITY OF ATHENS
School of Civil Engineering
Department of Structural Engineering
Institute of Steel Structure

ANALYSIS OF PALLET RACKING SYSTEMS WITH EQUIVALENT BEAM ELEMENTS

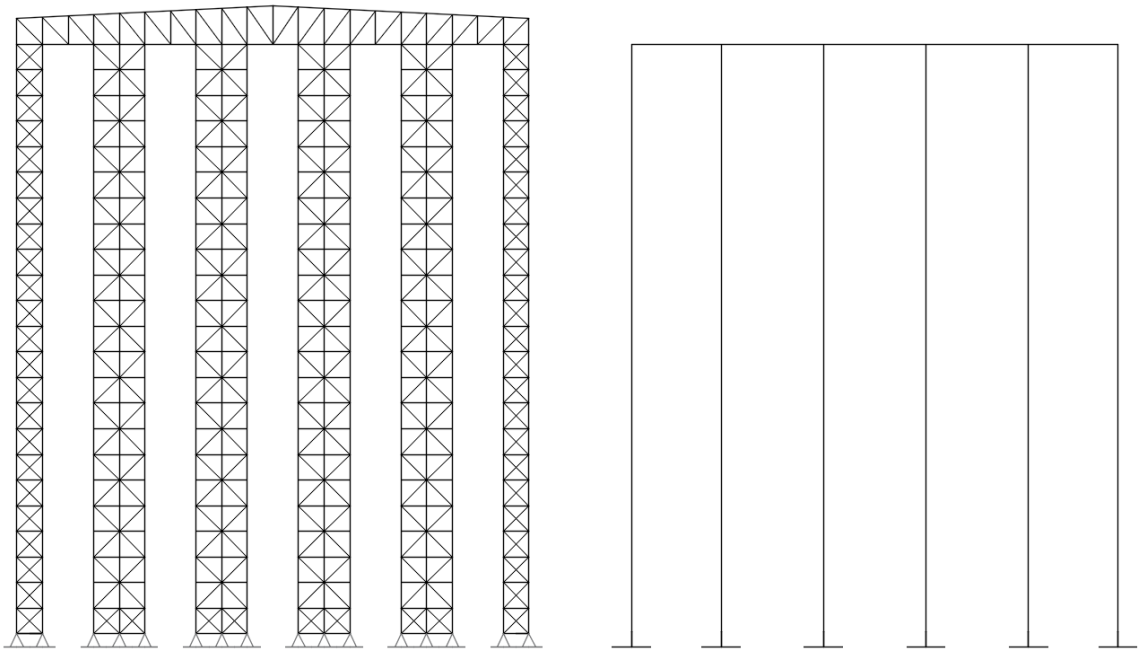

MASTER THESIS

Dimitrios A. Tsarpalis

Supervisor: prof. Ioannis Vayas

Athens, June 2018

ISS MT 2018/10

ΕΘΝΙΚΟ ΜΕΤΣΟΒΙΟ ΠΟΛΥΤΕΧΝΕΙΟ
Σχολή Πολιτικών Μηχανικών
Τομέας Δομοστατικής
Εργαστήριο Μεταλλικών Κατασκευών

ΑΝΑΛΥΣΗ ΣΥΣΤΗΜΑΤΩΝ ΑΠΟΘΗΚΕΥΣΗΣ ΠΑΛΕΤΩΝ ΜΕ ΙΣΟΔΥΝΑΜΑ ΓΡΑΜΜΙΚΑ ΣΤΟΙΧΕΙΑ

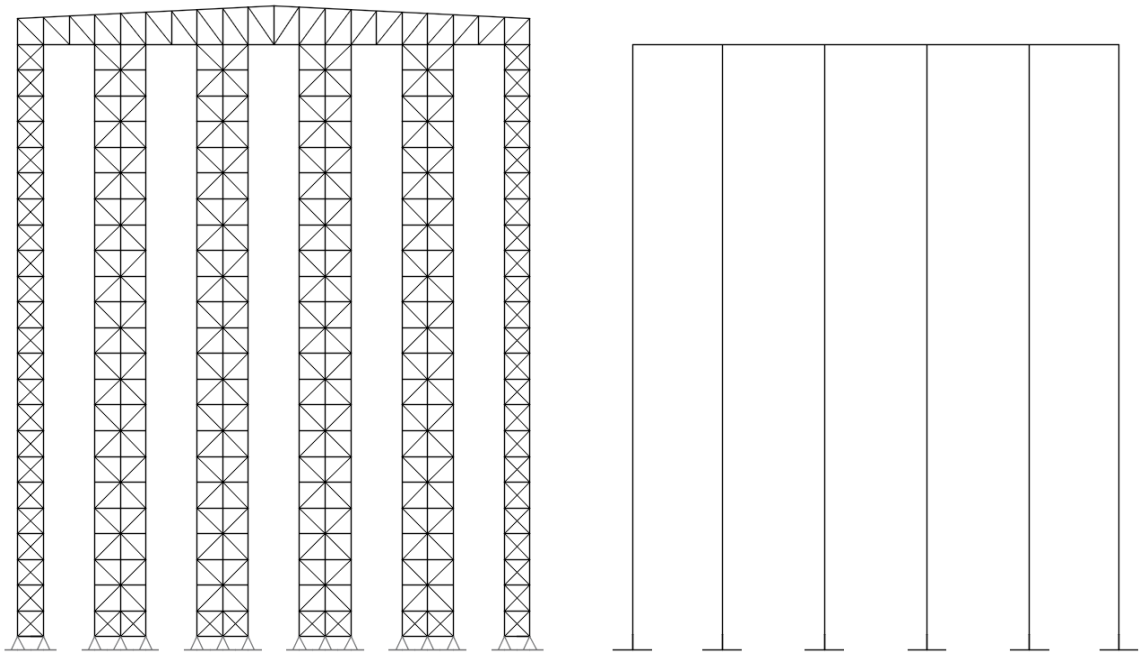

ΜΕΤΑΠΤΥΧΙΑΚΗ ΕΡΓΑΣΙΑ

Δημήτριος Α. Τσαρπαλής

Επιβλέπων: καθ. Ιωάννης Βάγιας

Αθήνα, Ιούνιος 2018

ΕΜΚ ΜΕ 2018/10

ANALYSIS OF PALLET RACKING SYSTEMS WITH EQUIVALENT BEAM ELEMENTS

MASTER THESIS

Dimitrios A. Tsarpalis

Supervisor: Ioannis Vayas

Τσαρπαλής Δ. Α. (2018).
Ανάλυση Συστημάτων Αποθήκευσης Παλετών με Ισοδύναμα Γραμμικά Στοιχεία
Μεταπτυχιακή Εργασία ΕΜΚ ΜΕ 2018/10
Εργαστήριο Μεταλλικών Κατασκευών, Εθνικό Μετσόβιο Πολυτεχνείο, Αθήνα.

Tsarpalis D. A. (2018).
Analysis of Pallet Racking Systems with Equivalent Beam Elements
Master Thesis ISS MT 2018/10
Institute of Steel Structures, National Technical University of Athens, Greece

Στα αδέρφια μου Παναγιώτη και Ηλία

Contents

NATIONAL TECHNICAL UNIVERSITY OF ATHENS
FACULTY OF CIVIL ENGINEERING
INSTITUTE OF STEEL STRUCTURES

MASTER THESIS
EMK ME 2018/10

Analysis of pallet racking systems with equivalent beam elements

Tsarpalis D. A. (supervised by Vayas I.)

Abstract

Automated Rack Supported Warehouses (ARSW) are the state of the art in storage technology, as they provide substantial savings in terms of cost, space and energy with respect to traditional warehouses. Despite their lightness, ARSWs carry very high live loads, by far higher than the dead load, opposite to what happens in usual civil engineering structures. Thus, standard design approaches are not applicable to this type of structures, especially when one considers seismic and wind loading.

The aforementioned lack of knowledge and design guidance for the ARSW makes clear the necessity for evaluation of reliable behavior factors (q) as well as the seismic fragility assessment of the designed warehouses. As a result, several test cases must be subjected to different loading scenarios and combinations, which may consist of steady (dead, pallet loads) or/and transient (seismic, wind loads) terms.

By examining the configuration of a typical ARSW it is obvious that the FEM modelling for these structures is a tedious task; they consist of hundreds or thousands steel members and nodes connected to each other through simple and semi-rigid joints. Modern computers accompanied with efficient computational algorithms can handle linear systems with great ease and thus, linear analysis can be performed by including all structural components in the analysis model. The problem arises when one examines nonlinear phenomena i.e. material and geometric nonlinearity. Simulations that take into account all ARSW's members and their nonlinear response may lead to prohibitive analysis costs in terms of time and CPU or even convergence and stability problems.

Considering the above, the complex ARSW system must be degraded into a simpler model that will balance between cost and accuracy. The objective of this thesis is to develop simplified models for the representation of complete warehouses in order to check their nonlinear response to seismic motion.

Particularly, the method followed in present thesis includes the substitution of upright frames for simple beam elements. In contrast to typical columns, upright frames are characterized by shear deformation and thus, Euler Bernoulli Beam Theory is not applicable. As a result, Timoshenko Beam Elements must be used, with linear properties (A, I, A_{eff})

suitably selected, depending on the type of the built-up column (D, Z, K and X configuration).

Apart from linear analysis, the equivalent model should also give adequately accurate results in the inelastic region. In present thesis, Opensees' Two Node Link Elements were chosen for the substitution of the upright frames expected to involve in structure's plastic mechanism. These elements are consisted of axial, shear and bending springs (3 for 2D and 6 for 3D) with the ability to assign any nonlinear material and thus, buckling, shear and bending failures can be taken into account.

The above procedure was applied to an ARSW 2D frame both for nonlinear Static and for Dynamic analyses and the results were quite promising. Author's next objective is to investigate applicability of this method in three dimensions, considering combinations of failure mechanisms.

ΕΘΝΙΚΟ ΜΕΤΣΟΒΙΟ ΠΟΛΥΤΕΧΝΕΙΟ
ΣΧΟΛΗ ΠΟΛΙΤΙΚΩΝ ΜΗΧΑΝΙΚΩΝ
ΕΡΓΑΣΤΗΡΙΟ ΜΕΤΑΛΛΙΚΩΝ ΚΑΤΑΣΚΕΥΩΝ

ΜΕΤΑΠΤΥΧΙΑΚΗ ΕΡΓΑΣΙΑ
ΕΜΚ ΜΕ 2018/10

Ανάλυση συστημάτων αποθήκευσης παλετών με ισοδύναμα γραμμικά στοιχεία

Τσαρπαλής Δ. Α. (Επιβλέπων: Βάγιας Ι.)

Περίληψη

Τα Αυτοματοποιημένα Συστήματα Αποθήκευση Παλετών (ΑΣΑΠ) αποτελούν την αιχμή του δόρατος στην τεχνολογία αποθήκευσης, αφού προσφέρουν πολλαπλά οφέλη σε όρους κόστους, χώρου και ενέργειας σε σχέση με τα παραδοσιακά συστήματα. Παρά το γεγονός ότι αποτελούν ελαφρές μεταλλικές κατασκευές, τα ΑΣΑΠ φέρουν πολύ υψηλά ωφέλιμα φορτία, κατά πολύ μεγαλύτερα από τα ίδια βάρη, αντίθετα με ότι συμβαίνει στις συνήθεις κατασκευές Πολιτικού Μηχανικού. Συνεπώς, οι τυπικές μέθοδοι σχεδιασμού δεν μπορούν να εφαρμοστούν για τα ΑΣΑΠ, ιδίως όταν λαμβάνονται υπόψη οριζόντιες δράσεις, όπως σεισμικές ή ανέμου.

Η προαναφερθείσα έλλειψη γνώσης και οδηγών σχεδιασμού για τα ΑΣΑΠ, καθιστούν σαφή την ανάγκη για προσδιορισμό αξιόπιστων συντελεστών συμπεριφοράς (q), καθώς και την εκτίμηση της σεισμικής τους επικινδυνότητας. Ως εκ τούτου, είναι απαραίτητο να μελετηθούν πληθώρα παραδειγμάτων σχεδιασμού σε διάφορες περιπτώσεις και συνδυασμούς φορτίσεων, σταθερές στο χρόνο (βάρη μεταλλικού σκελετού, παλετών, μηχανολογικού εξοπλισμού κ.λπ.) ή μεταβλητές (σεισμός, ριπές ανέμου).

Παρατηρώντας τη μορφολογία ενός τυπικού ΑΣΑΠ, είναι προφανές ότι η προσομοίωση σε περιβάλλον Πεπερασμένων Στοιχείων είναι μια απαιτητική διαδικασία· αποτελούνται από εκατοντάδες ή χιλιάδες χαλύβδινα μέλη τα οποία συνδέονται με ημιάκαμπτους ή αρθρωτούς κόμβους. Οι σύγχρονοι υπολογιστές με την υψηλή ισχύ που διαθέτουν, σε συνδυασμό με τη χρήση αποδοτικών αλγορίθμων, μπορούν να χειριστούν γραμμικά συστήματα με μεγάλη ευκολία και συνεπώς, οι γραμμικές αναλύσεις μπορούν να εκτελεστούν λαμβάνοντας υπόψη όλα τα δομικά μέλη στο στατικό προσομοίωμα. Το πρόβλημα γεννάται όταν εξετάζονται μη γραμμικά φαινόμενα, θεωρώντας δηλαδή μη γραμμικότητα υλικού ή γεωμετρίας. Η λεπτομερής μη γραμμική προσομοίωση όλων τα μελών ενός ΑΣΑΠ οδηγεί σε υπερβολικά χρονοβόρες αναλύσεις που πολλές φορές χαρακτηρίζονται από προβλήματα αριθμητικής σύγκλισης και αστάθειας.

Λαμβάνοντας υπόψη τα παραπάνω, το πολύπλοκο μοντέλο του ΑΣΑΠ πρέπει να υποκατασταθεί από ένα απλούστερο, το οποίο θα ισορροπεί μεταξύ κόστους και ακρίβειας. Σκοπός της εργασίας είναι η ανάπτυξη μιας μεθοδολογίας για την εύρεση απλοποιημένων

προσομοιωμάτων ώστε να μπορεί να μελετηθεί εύκολα και αξιόπιστα η σεισμική συμπεριφορά των ΑΣΑΠ.

Συγκεκριμένα, η μέθοδος που ακολουθήθηκε στην παρούσα εργασία στοχεύει στην αντικατάσταση των σύνθετων υποστυλωμάτων των ραφιών με γραμμικά στοιχεία δοκού. Σε αντίθεση με τα τυπικά υποστυλώματα, τα σύνθετα παρουσιάζουν σημαντικές διατμητικές παραμορφώσεις και επομένως η Θεωρία Δοκού Euler-Bernoulli δεν ισχύει. Συνεπώς, πρέπει να χρησιμοποιηθούν στοιχεία δοκού Timoshenko, με κατάλληλα επιλεγμένες γραμμικές ιδιότητες (A, I, A_{eff}), ανάλογα με τον τύπο του σύνθετου υποστυλώματος (διαμόρφωση D, Z, K και X).

Εκτός από τη γραμμική ανάλυση, το ισοδύναμο μοντέλο οφείλει να δίνει επαρκώς ακριβή αποτελέσματα και στη μη γραμμική περιοχή. Αποφασίστηκε η αντικατάσταση των σύνθετων υποστυλωμάτων που αναμένεται να συμμετάσχουν στον πλαστικό μηχανισμό της κατασκευής με Two Node Link Elements του λογισμικού OpenSees . Τα στοιχεία αυτά περιλαμβάνουν αξονικά και στροφικά ελατήρια (3 για 2D και 6 για 3D) με την ικανότητα να δέχονται οποιοδήποτε μη γραμμικό υλικό και επομένως μπορεί να ληφθεί υπόψη ο λυγισμός των στύλων αλλά και οι καμπτικές και διατμητικές αστοχίες.

Η παραπάνω διαδικασία εφαρμόστηκε σε ένα 2D πλαίσιο ΑΣΑΠ τόσο για Μη Γραμμική Στατική όσο και για Μη Γραμμική Δυναμική Ανάλυση και τα αποτελέσματα ήταν αρκετά ενθαρρυντικά. Ο επόμενος στόχος του συγγραφέα είναι η διερεύνηση της δυνατότητας επέκτασής της μεθοδολογίας αυτής στις τρεις διαστάσεις, λαμβάνοντας υπόψη συνδυασμούς αστοχιών.

Ευχαριστίες

Ολοκληρώνοντας τη μεταπτυχιακή μου εργασία, θα ήθελα να ευχαριστήσω όσους με βοήθησαν και με στήριξαν όλο αυτό το διάστημα.

Αρχικά θα ήθελα να ευχαριστήσω τον επιβλέποντά μου και καθηγητή Ε.Μ.Π. κ. Ιωάννη Βάγια για την ανάθεση του συγκεκριμένου θέματος, τη συνεχή καθοδήγησή του, το ενδιαφέρον του, τη βοήθειά του σε θέματα γνωστικού αντικειμένου, αλλά και για την εμπιστοσύνη που δείχνει στο πρόσωπό μου. Εύχομαι η αποδοτική μας σχέση να συνεχιστεί και τα επόμενα χρόνια στα πλαίσια της διδακτορικής μου διατριβής, την οποία έχω μόλις ξεκινήσει.

Ιδιαίτερες ευχαριστίες θα ήθελα να απευθύνω στον κ. Δημήτριο Βαμβάτσικο, Επίκουρο καθηγητή Ε.Μ.Π., για τις συμβουλές του και την άψογη συνεργασία που έχουμε. Οι γνώσεις του σε θέματα αντισεισμικής μηχανικής και στατικής, η μεταδοτικότητά του και η υπομονή του ήταν καθοριστικοί παράγοντες για την πρόοδο της συγκεκριμένης εργασίας.

Σε προσωπικό επίπεδο, θα ήθελα να ευχαριστήσω την οικογένειά μου για την αγάπη, τη βοήθεια και την υπομονή τους σε ό,τι κι αν αποφασίσω. Θέλω επίσης να ευχαριστήσω την νονά μου Ελένη για την συνεχή συμπαράσταση και υποστήριξή της στην μέχρι τώρα πορεία μου.

1 Introduction

1.1 Description of a Pallet Racking System

Pallet rack is a material handling storage aid system designed to store materials on pallets (or “skids”). Although there are many varieties of pallet racking, all types allow for the storage of palletized materials in horizontal rows with multiple levels. Forklift trucks are usually an integral part of any pallet rack system as they are usually required to place the loaded pallets onto the racks for storage. A typical structural design of a Racking System is illustrated in Figure 1.1

Figure 1.1: Structural Design of Adjustable Pallet Racking

There are several types of warehouse racking systems, which also are known as pallet racks or materials handling systems. Wooden, metal, or plastic pallets, or skids, are combined with larger racking systems comprised of shelves at various levels. Decking bases are available in different widths to support objects placed on the racks in storage. In many cases, warehouse racking is several feet high and requires forklifts for the loading process. Various warehouse racking system configurations are possible including selective racks, drive-in or drive-through racks, push-back racks, and flow racks.

Selective Racks – The most commonly used pallet system, selective racks provide access from an aisle. These warehouse racking systems are ideal for narrow aisle racking, standard systems, and deep-reach systems. Selective racks require special narrow lift trucks and accommodate a single pallet in depth

Drive-In and Drive-Through Racks – For high-density storage, drive-in racks and drive-through racks are ideal. Constructed of steel in most cases, these warehouse racking systems have enough space for a forklift to move into its bay. It’s important to note that drive-in racks have one entrance and exit, but drive-through racks allow access on both sides of the bay. As a result, drive-in racks are suited to the last in, first out (LIFO) process com-

monly used for nonperishable products or those with a low turnover. On the other hand, a drive-through system requires a first in, first out (FIFO) process. Drive-in and drive-through racks may be floor-to-ceiling structures

Push Back Racking Systems – Typically used for bulk storage, push back racking systems store products that span 2-5 pallets. When a pallet is loaded onto the system, it pushes the next pallet back, and when a pallet is unloaded, it is pushed to the front of the system. Push-back racking systems utilize the LIFO system and often feature inclined rails and sliding carts and double lanes

Flow Racks – Also known as gravity racks, flow racks are commonly used for high-density storage. With this type of warehouse racking system, items are loaded at the higher end and removed at the lower end using a FIFO system. The rotation of products becomes automatic as the racks flow with loading and unloading. Flow racks make use of gravity rollers that move in conjunction with the rack load and feature brakes or speed controllers to regulate item movement. One advantage of flow racks is they do not require electricity for operation because gravity powers them.

1.2 Structural Components

The structural design of a warehouse (geometry, materials, cross-sections etc.) varies depending on the material handling system, the designer's preferences and the owner's requirements However, the following structural components are always considered (Figure 1.2).

1) Upright Frame

Also known as built-up column, this component is constructed in cross-aisle direction of the warehouse. It is typically composed of two subcomponents (Figure 1.2):

- Uprights. Usually made of cold formed open cross-sections, these elements carry the gravity loads, such as self-weight of the structure, pallet loads, mechanical equipment etc.
- Bracings. These components (usually made of "C" cross-sections) transfer shear forces by uniaxial compression-tension mechanism. Their assembly strategy defines different upright frame types (D, Z, K, X etc. [1]).

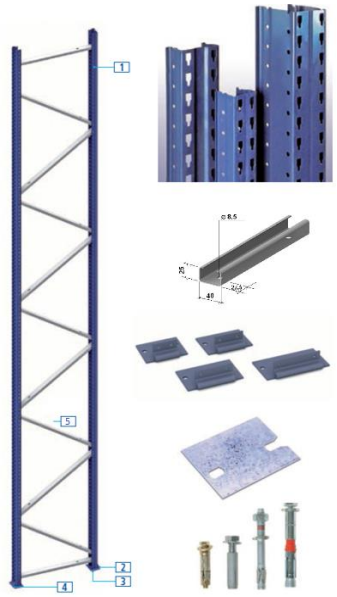

Figure 1.2: Elements of a upright frame: Upright (1), Base Plate (2), Level Plate (3), Anchors (4), Bracing (5)

2) Beam

Similarly to steel frames, beams carry the pallet loads and transfer them to the upright frames. Usually, they have connecting claws that ensure a decent connection to the frames without the use of bolts or screws. They are made of hollowed cross-section of high bending resistance and thus, their weakest point is typically the beam-to-upright connection.

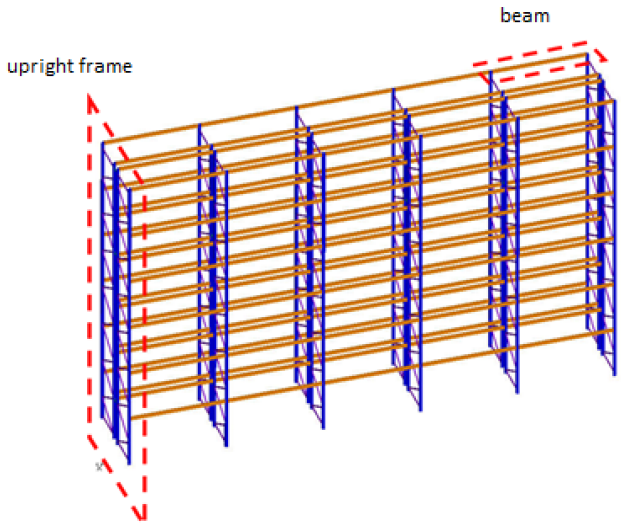

Figure 1.3: Configuration of a Portal Frame

In addition, in earthquake-prone areas, the racking systems are usually braced in down-aisle direction, to avoid soft story collapse mechanisms [2].

1.3 Automated Rack Supported Warehouses

A warehouse is a building where massive amount of goods can be stored before their "large distribution" to the consumers. Due to increasing mass production of goods and increasing consumption levels, demand for storage space increases. As the land becomes

everyday more valuable in terms of both economy and environment, highly optimized, reliable and safe warehouses are needed. Reduced running costs, automation and larger sizes are the future trends of the warehouse sector.

At present, Automated Rack Supported Warehouses (ARSW) or clad rack warehouses are usually built by manufacturers specialized in structural systems for logistics with the same or similar cold formed profiles used for warehouse storage pallet racks although in the case of ARSW the rack forms the load bearing structure of the whole building by itself. ARSWs can be much larger and taller with respect to usual pallet rack systems. They can be more than 40 m tall, 100 meters wide and 150 meters long.

Main advantages offered by Automated Rack Supporting Warehouses are:

- Significant cost savings in construction as no additional warehouse building is required.
- Short construction periods.
- Roof and cladding are directly fixed to the rack structure.
- Storage in height: Maximum use of available surface area for a high storage density.
- ARSW system is adjustable and eventually demountable.
- They can be fully automated which increases the efficiency of storage and logistics.
- Reduced responsibility for the owner of storage system as the system is assembled as a whole (building + storage).
- Energy efficiency, less carbon foot-print (less heating).
- No interference of rack with the building columns or the building vertical bracing system. Especially in high seismic zones this eliminates the need for seismic separation detailing between building and rack structure.
- Reduction of workers needed inside the warehouse.

1.4 Purpose of the Thesis

Collapse of ARSWs may have huge economic impacts not only for the owner but also, more in general, for the Community, in terms of loss of huge amounts of goods/merchandise. Furthermore, despite the limited number of workers required in automated warehouses, during collapse the life of the employees working inside and around the warehouse might be at risk. Hence, solution of the problems connected with safe and reliable design of clad rack buildings has a very large economic and safety impact.

The research made up to now is mainly limited to steel storage racks which are a much smaller scale of automated warehouses ([3], [4]). Automated storage systems, which will probably be the future of the warehouse sector, have not been investigated to such an extent so far. Moreover, in Europe (and in the world) there is no official reference document specific for the design of Automated high-rise warehouses. Designers are obliged to work

with a total lack of specific references and of commonly accepted design rules and procedures.

As a result, these structures are vulnerable in extreme load scenarios, such as high wind speeds and seismic actions. Examples of global and partial failures of ARSWs are shown in Figure 1.4 and Figure 1.5.

Figure 1.4: Partial collapse of a ARSW during construction phase

Figure 1.5: Collapse of a ARSW due to Emilia-Romagna earthquake, 2012

The aforementioned lack of knowledge and bibliography raises the demand for further research. Today, a variety of methods (Pushover, IDA etc.) exist to determine the nonlinear characteristics (overstrength, ductility, energy dissipation) of a structure, which require computationally expensive numerical analyses.

By examining the FEA model of an ARSW, it is obvious that a nonlinear simulation of the whole structure is nearly impossible. For example, the numerical model of the ARSW illustrated in Figure 1.6, consists of 137,000 nodes connected by 230,000 beam elements. Subtracting the fixed DOFs at the base of the uprights (nearly 11,000 DOF) the number of free DOFs to be solved is about 811,000.

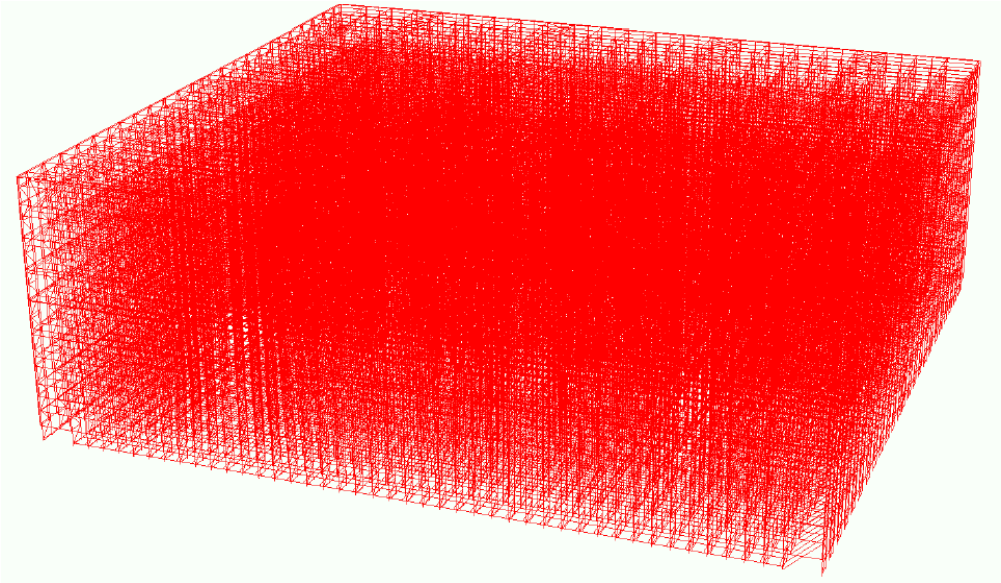

Figure 1.6: Numerical model of an ARSW

Objective of the present thesis is to develop simplified models for the representation of complete warehouses in order to check their non-linear response to seismic motion. The method that was followed includes the substitution of upright frames for simple beam elements that consider shear deformation. All analyses executed were 2D in cross-aisle direction, but the method is easily expandable to three dimensions, which will be the next research objective of the author.

1.5 Thesis Structure

Chapter 2 includes the derivation of linear and geometric stiffness matrices for Euler-Bernoulli and Timoshenko beam element. Upright frames are characterized by shear deformation and thus, equivalent element must consider this additional flexibility.

Chapter 3 discusses the linear properties of the equivalent beam element for upright frame configuration (D, Z, K and X column). In particular, cross-section area, moment of inertia and effective shear area are calculated for a variety of built-up columns and a general method for the estimation of shear area for arbitrary geometries is developed. Finally, a test case example on a D-column is conducted, assuming linear behavior.

Chapter 4 outlines the nonlinear phenomena that may develop in a built-up column. Specifically, the shear degradation mechanism is highlighted and a method for the substitution of an upright frame for Two Node Link Element is discussed. Afterwards, nonlinear static analyses are performed on a X-column.

Chapter 5 presents a numerical study of a 2D ARSW frame. Modal, Pushover and finally nonlinear Dynamic analyses were executed for the full and reduced-order model and the corresponding results were compared.

Although each of the chapters providing research results ends with the concluding comments, Chapter 6 draws main conclusions. It also provides recommendations for the future work.

2 Derivation of Timoshenko beam element's properties and matrices

2.1 Kinematics

2.1.1 Displacements

The use of finite element method in a solid continuum produces a discrete model consisted of a set of nodes, connected each other by the so-called finite elements [5]. Depending on the dimensions of the problem (1-D, 2-D, 3-D) and the assumptions made for the displacements (rotations, large displacements, plane strain etc.) one can produce stiffness and mass matrices for a variety of finite elements. In general, the continuum is discretized into a set of N nodes, the displacements of each is expressed by a vector $\overline{u_n}(t)=\left\{\overline{u_n^1},\overline{u_n^2},...,\overline{u_n^m}\right\}^T$, where n = 1,…,N the node index and m the degrees of freedom (DOF). The displacements of an arbitrary point whose coordinates are given by a vector $\vec{x}=\mathbf{x}=\{x_1,x_2,...\}^T$ can be obtained using the nodal displacements and the corresponding set of "shape functions" [6] N_{in} (i=1,..,m index of DOF, n=1,…,N index of node):

$$u_i(\mathbf{x},t)=\sum_{n=1}^{N}N_{in}(\mathbf{x})\cdot\bar{u}_n(t)=\left[N_i(\mathbf{x})\right]\bar{\mathbf{u}}(t) \qquad \text{Eq. (2.1)}$$

2.1.2 Strains

Depending on the characteristics of the problem, the deformed shape of the body may differ a lot from the initial configuration and thus, equilibrium must be established in the former (higher order theories). Although the significance can be sometimes crucial, in many practical problems of civil engineering the geometric effects are of minor importance and can be neglected. That is why the strains corresponding to the "theory of small displacements" are often called **engineering strains**:

$$\varepsilon_{ii}(\mathbf{x},t)=\frac{\partial u_i(\mathbf{x},t)}{\partial x_i}=u_{i,i}(\mathbf{x},t) \qquad \text{Eq. (2.2)}$$

$$\gamma_{ij}(\mathbf{x},t)=\frac{\partial u_i(\mathbf{x},t)}{\partial x_j}+\frac{\partial u_j(\mathbf{x},t)}{\partial x_i}=u_{\mathrm{j},i}(\mathbf{x},t)+u_{i,\mathrm{j}}(\mathbf{x},t) \qquad \text{Eq. (2.3)}$$

where,

ε_{ii} is axial strain

γ_{ij} is shear strain

The relation between the displacements and the engineering strains:

$$\varepsilon_{ii}\left(\mathbf{x},t\right)=\frac{\partial u_i\left(\mathbf{x},t\right)}{\partial x_i}=\frac{\partial\sum_{n=1}^{N}N_{in}\left(\mathbf{x}\right)\cdot\bar{u}_n\left(t\right)}{\partial x_i}=\sum_{n=1}^{N}N_{in,i}\left(\mathbf{x}\right)\cdot\bar{u}_n\left(t\right) \qquad \text{Eq. (2.4)}$$

$$\gamma_{ij}\left(\mathbf{x},t\right)=\frac{\partial u_i\left(\mathbf{x},t\right)}{\partial x_j}+\frac{\partial u_j\left(\mathbf{x},t\right)}{\partial x_i}=\sum_{n=1}^{N}\left(N_{in,\mathrm{j}}\left(\mathbf{x}\right)+N_{jn,i}\left(\mathbf{x}\right)\right)\cdot\bar{u}_n\left(t\right) \qquad \text{Eq. (2.5)}$$

Or in a matrix-vector form:

$$\varepsilon\left(\mathbf{x},t\right)=\left\{\varepsilon_{ii}\left(\mathbf{x},t\right),\gamma_{ij}\left(\mathbf{x},t\right)\right\}^T=\frac{\partial\left[N\left(\mathbf{x}\right)\right]}{\partial\mathbf{x}}\bar{\mathbf{u}}\left(t\right)=\left[B\left(\mathbf{x}\right)\right]\bar{\mathbf{u}}\left(t\right) \qquad \text{Eq. (2.6)}$$

In contrast to the engineering strains, Green-Lagrange strains are used when the effects of large displacements are examined (expressions in 3 dimensions):

$$\varepsilon_{ii}=\frac{\partial u_i}{\partial x_i}+\frac{1}{2}\left(\frac{\partial u_i}{\partial x_i}\right)^2+\frac{1}{2}\left(\frac{\partial u_j}{\partial x_i}\right)^2+\frac{1}{2}\left(\frac{\partial u_k}{\partial x_i}\right)^2 \qquad \text{Eq. (2.7)}$$

$$\gamma_{ij}=\frac{\partial u_i}{\partial x_j}+\frac{\partial u_j}{\partial x_i}+\frac{\partial u_i}{\partial x_j}\frac{\partial u_j}{\partial x_j}+\frac{\partial u_j}{\partial x_i}\frac{\partial u_i}{\partial x_i} \qquad \text{Eq. (2.8)}$$

For derivation of Eq. (2.7) and Eq. (2.8) see [7].

2.2 Strain Energy and Stiffness in Linear Elastic Continua

Strain energy is the energy stored by a system undergoing deformation. In finite element analysis, it is a function of the nodal displacements $\bar{\mathbf{u}}$:

$$\begin{aligned}U\left(\bar{\mathbf{u}}\right)&=\frac{1}{2}\int_{\Omega}\boldsymbol{\sigma}\left(\mathbf{x},t\right)^T\boldsymbol{\varepsilon}\left(\mathbf{x},t\right)d\Omega\overset{\boldsymbol{\sigma}=\left[S_e\right]\boldsymbol{\varepsilon}}{=}\frac{1}{2}\int_{\Omega}\boldsymbol{\varepsilon}\left(\mathbf{x},t\right)^T\left[S_e\right]\boldsymbol{\varepsilon}\left(\mathbf{x},t\right)d\Omega\\&=\frac{1}{2}\int_{\Omega}\bar{\mathbf{u}}\left(t\right)^T\left[B\left(\mathbf{x}\right)\right]^T\left[S_e\right]\left[B\left(\mathbf{x}\right)\right]\bar{\mathbf{u}}\left(t\right)d\Omega\\&=\frac{1}{2}\bar{\mathbf{u}}\left(t\right)^T\left(\int_{\Omega}\left[B\left(\mathbf{x}\right)\right]^T\left[S_e\right]\left[B\left(\mathbf{x}\right)\right]d\Omega\right)\bar{\mathbf{u}}\left(t\right)\end{aligned} \qquad \text{Eq. (2.9)}$$

where,

$\boldsymbol{\sigma}=\left[S_e\right]\boldsymbol{\varepsilon}$ is the stress-strain relation

Element's **elastic stiffness matrix** is defined as the second term in the RHS of Eq. (2.9):

$$\left[\overline{K}_e\right] \equiv \int_{\Omega} \left[B(\mathbf{x})\right]^T \left[S_e\right] \left[B(\mathbf{x})\right] d\Omega \qquad \text{Eq. (2.10)}$$

In order to derive the stiffness matrix that takes into consideration geometric effects, the Green-Lagrange strains have to be substituted in Eq. (2.9).

2.3 Stiffness Matrices of Euler-Bernoulli Beam Element

2.3.1 Shape Functions

The Euler-Bernoulli beam element is a structural finite element and so rotations must be used as degrees of freedom. In the case of two dimensions, this involves 2 displacements and 1 rotation at each node of the element (Figure 2.1).

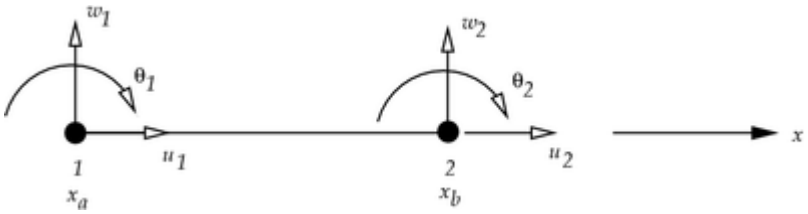

Figure 2.1: Degrees of freedom of Bernoulli beam element

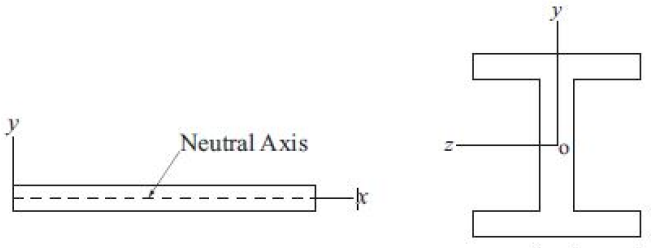

Figure 2.2: Neutral Axis of beam element

The shape functions establish a relation between the node displacements $\bar{u}_n(t)$ and the translation of points along beam's neutral axis $u_x(x,t)$ and $u_y(x,t)$ (Figure 2.2):

$$u_x(x,t) = \sum_{n=1}^{6} N_{xn}(x)\bar{u}_n(t) \qquad \text{Eq. (2.11)}$$

$$u_y(x,t) = \sum_{n=1}^{6} N_{yn}(x)\bar{u}_n(t) \qquad \text{Eq. (2.12)}$$

where,

x is the longitudinal axis and z is the axis along which rotation occurs

Translation $u_x(x,t)$ describes the extension of the neutral axis, so depends only on DOF u_1 and u_2. This implies that shape functions $N_{x,v_1}, N_{x,\theta_1}, N_{x,v_2}, N_{x,\theta_2}$ are zero. By the assumption that the axial force inside the element is constant, N_{x,u_1}, N_{x,u_2} can be calculated by:

$$N_{x,u_1} = 1 - \frac{x}{L} \qquad \text{Eq. (2.13)}$$

$$N_{x,u_2} = \frac{x}{L} \qquad \text{Eq. (2.14)}$$

Accordingly, by the assumption that internal bending moment is linear, the shape functions for translation $u_y(x,t)$ are cubic polynomials [8]:

$$N_{y,v_1} = 1 - 3\left(\frac{x}{L}\right)^2 + 2\left(\frac{x}{L}\right)^3 \qquad \text{Eq. (2.15)}$$

$$N_{y,\theta_1} = \left(\frac{x}{L} - 2\left(\frac{x}{L}\right)^2 + \left(\frac{x}{L}\right)^3\right)L \qquad \text{Eq. (2.16)}$$

$$N_{y,v_2} = 3\left(\frac{x}{L}\right)^2 - 2\left(\frac{x}{L}\right)^3 \qquad \text{Eq. (2.17)}$$

$$N_{y,\theta_2} = \left(-\left(\frac{x}{L}\right)^2 + \left(\frac{x}{L}\right)^3\right)L \qquad \text{Eq. (2.18)}$$

$$N_{y,u_1} = N_{y,u_2} = 0 \qquad \text{Eq. (2.19)}$$

In a matrix-vector form, Eq. (2.11) and Eq. (2.12) can be expressed more compactly as:

$$\begin{bmatrix} u_x(x,t) \\ u_y(x,t) \end{bmatrix} = \left[N(x)\right]\bar{u}(t) \qquad \text{Eq. (2.20)}$$

where,

$\left[N(x)\right]$ is the shape function matrix, defined by:

$$\left[N(x)\right] =$$

$$\left[\begin{array}{c|c|c|c|c|c} 1-\frac{x}{L} & 0 & 0 & 0 & \frac{x}{L} & 0 \\ \hline 0 & 1-3\left(\frac{x}{L}\right)^2+2\left(\frac{x}{L}\right)^3 & \left(\frac{x}{L}-2\left(\frac{x}{L}\right)^2+\left(\frac{x}{L}\right)^3\right)L & 0 & 3\left(\frac{x}{L}\right)^2-2\left(\frac{x}{L}\right)^3 & \left(-\left(\frac{x}{L}\right)^2+\left(\frac{x}{L}\right)^3\right)L \end{array}\right] \qquad \text{Eq. (2.21)}$$

Note that Eq. (2.21) gives the correct shape functions (same results as analytic solution) when axial force is constant and moment is linearly distributed along the element. This assumption is not so limitative for civil engineering problems, as it is common to concentrate the forces on the nodes instead of distributing them along the element (e.g. lumped masses).

2.3.2 Strain Energy and Elastic Stiffness Matrix

For the derivation of the stress-strain relation for the Euler-Bernoulli beam element we assume that each cross-section of the beam is at 90 degrees to the neutral axis. This is described mathematically by the following relation:

$$\boxed{\theta = \frac{\partial u_y}{\partial x}} \qquad \text{Eq. (2.22)}$$

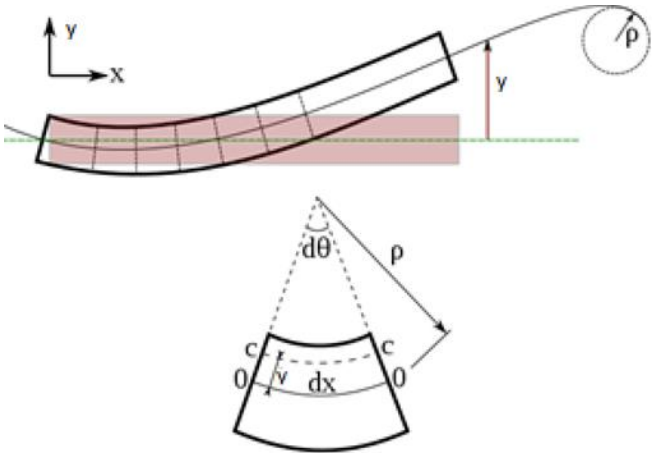

Figure 2.3: In the Euler-Bernoulli theory the cross section is perpendicular to the neutral axis

If deformations are small, then the engineering strains (see Eq. (2.2) and Eq. (2.3)) can be used to calculate the extensional strain ε_{xx}:

$$\varepsilon_{xx} = \frac{\partial u_x}{\partial x} - \frac{d\theta}{\partial x} y = \frac{\partial u_x}{\partial x} - \frac{\partial^2 u_y}{\partial x^2} y = \sum_{n=1}^{6} N'_{xn}(x)\bar{u}_n - \sum_{n=1}^{6} N''_{xn}(x) y \bar{u}_n = \\ = \sum_{n=1}^{6} B_n(x,y)\bar{u}_n = \left[\mathbf{B}(x,y)\right]\bar{\mathbf{u}} \qquad \text{Eq. (2.23)}$$

where,

$$\left[\mathbf{B}(x,y)\right]=\left[-\frac{1}{L},\frac{6y}{L^2}-\frac{12xy}{L^3},\frac{4y}{L}-\frac{6xy}{L^3},\frac{1}{L},-\frac{6y}{L^2}+\frac{12xy}{L^3},\frac{2y}{L}-\frac{6xy}{L^2}\right] \quad \text{Eq. (2.24)}$$

The strain energy of axial strains is calculated based on Eq. (2.9):

$$U\left(\bar{\mathbf{u}}\right)=\frac{1}{2}\int_{\Omega}\varepsilon_{xx}E\varepsilon_{xx}d\Omega \quad \text{Eq. (2.25)}$$

The **elastic stiffness matrix** of Euler-Bernoulli beam is defined as in Eq. (2.10):

$$\left[\overline{K}_e\right]\equiv\int_{x=0}^{L}\int_{\Omega}\left[\mathbf{B}(x,y)\right]^T E\left[\mathbf{B}(x,y)\right]dA\,dx \quad \text{Eq. (2.26)}$$

2.3.3 Euler-Bernoulli Stiffness Matrix with Geometric Strain Effects

Using Green-Lagrange strains (see Eq. (2.7) and Eq. (2.8)) instead of engineering strains, we can derive the following expression for the extensional strain:

$$\varepsilon_{xx}=\frac{\partial u_x}{\partial x}-\frac{\partial^2 u_y}{\partial x^2}y+\frac{1}{2}\left(\frac{\partial u_y}{\partial x}\right)^2 \quad \text{Eq. (2.27)}$$

The potential energy with geometric strain effects is:

$$\begin{aligned}U_e\left(\bar{\mathbf{u}}\right)&=\frac{1}{2}\int_{x=0}^{L}\int_{A}\varepsilon_{xx}E\varepsilon_{xx}dA\,dx\\&=\frac{1}{2}\int_{x=0}^{L}\int_{A}E\left(\frac{\partial u_x}{\partial x}-\frac{\partial^2 u_y}{\partial x^2}y+\frac{1}{2}\left(\frac{\partial u_y}{\partial x}\right)^2\right)^2dx\\&=\frac{1}{2}\int_{x=0}^{L}E\int_{A}\left(u_{x,x}^2-2u_{x,x}u_{y,xx}y+u_{x,x}u_{y,x}^2+u_{y,xx}^2y^2-u_{y,xx}u_{y,x}^2y+\overbrace{\frac{1}{4}u_{y,x}^4}^{H.O.T.}\right)dAdx\end{aligned} \quad \text{Eq. (2.28)}$$

Noting that $\int_A ydA=0$ (centre of mass) and $\int_A y^2dA\equiv I$, we can derive:

$$U\left(\bar{\mathbf{u}}\right)=\overbrace{\frac{1}{2}\int_{x=0}^{L}\left(EAu_{x,x}^2+EIu_{y,xx}^2\right)dx}^{U_e\ (Eq\ 2.27)}+\frac{1}{2}\int_{x=0}^{L}EA\left(u_{x,x}u_{y,x}^2\right)dx \quad \text{Eq. (2.29)}$$

Lastly, by substituting $u_{x,x} = \sum_{n=1}^{6} N'_{xn}(x)\bar{u}_n = \frac{N}{EA}$ (N is the axial force) we can get the following expression for the **full stiffness matrix of Euler-Bernoulli** beam element that takes into account geometric effects:

$$\overline{\mathbf{K}}_{tot} = \overline{\mathbf{K}}_e + \frac{N}{L}\overline{\mathbf{K}}_g \qquad \text{Eq. (2.30)}$$

where,

$\overline{\mathbf{K}}_e$ is the elastic stiffness matrix

$\overline{\mathbf{K}}_g$ is the geometric matrix

$\overline{\mathbf{K}}_{tot}$ is the total stiffness matrix [9]

2.3.4 Euler-Bernoulli Stiffness Matrices for prismatic homogeneous isotropic beams

For prismatic homogeneous isotropic beams in three dimensions (6 degrees of freedom at each node), the element stiffness matrices are:

$$\overline{\mathbf{K}}_e = \begin{bmatrix} \frac{EA}{L} & 0 & 0 & -\frac{EA}{L} & 0 & 0 \\ & \frac{12EI}{L^3} & \frac{6EI}{L^2} & 0 & -\frac{12EI}{L^3} & \frac{6EI}{L^2} \\ & & \frac{4EI}{L} & 0 & -\frac{6EI}{L^2} & \frac{2EI}{L} \\ & & & \frac{EA}{L} & 0 & 0 \\ & SYM & & & \frac{12EI}{L^3} & -\frac{6EI}{L^2} \\ & & & & & \frac{4EI}{L} \end{bmatrix} \qquad \text{Eq. (2.31)}$$

$$\overline{\mathbf{K}}_g = \begin{bmatrix} 0 & 0 & 0 & 0 & 0 & 0 \\ & \frac{6}{5} & \frac{L}{10} & 0 & -\frac{6}{5} & \frac{L}{10} \\ & & \frac{2L^2}{15} & 0 & -\frac{L}{10} & -\frac{L^2}{30} \\ & & & 0 & 0 & 0 \\ & SYM & & & \frac{6}{5} & -\frac{L}{10} \\ & & & & & -\frac{2L^2}{15} \end{bmatrix} \qquad \text{Eq. (2.32)}$$

2.4 Stiffness matrices of Timoshenko Beam Element

2.4.1 Shape Functions

In contrast to the Euler-Bernoulli beam theory, Timoshenko beam theory includes shear deformation and thus it violates the assumption that cross-sections remain perpendicular to the neutral axis. Again, as in Bernoulli theory, we describe the problem by considering the translation of points along the neutral axis of the beam $u_x(x)$ and $u_y(x)$ (see §2.3.1). The transverse deformation of a beam with shear and bending strains may be separated into a portion related to shear deformation and a portion related to bending deformation (Figure 2.4):

$$u_y(x,t) = u_{(b)y}(x) + u_{(s)y}(x) \qquad \text{Eq. (2.33)}$$

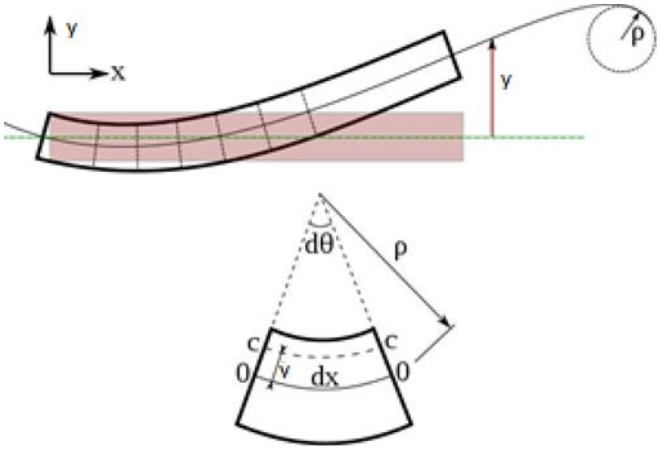

Figure 2.4: Deformation components of a Timoshenko beam element

Component $u_{(b)y}(x)$ is related to equilibrium of moments by the following expression:

$$EIu''_{(b)y}(x) = M(x) \qquad \text{Eq. (2.34)}$$

Accordingly, $u_{(s)y}(x)$ is related to equilibrium of shear forces by:

$$GA_{eff}u'_{(s)y}(x) = V(x) = V = const \qquad \text{Eq. (2.35)}$$

where,

A_{eff} is called **shear area**

It can be shown that the shape functions for the bending and shear components $N_{(b)yn}(x)$ and $N_{(s)yn}(x)$ are:

$$N_{(b)\mathrm{v}_1}(x)=\frac{1}{1+\Phi}\left[1-3\left(\frac{x}{L}\right)^2+2\left(\frac{x}{L}\right)^3\right] \quad \text{Eq. (2.36)}$$

$$N_{(s)\mathrm{v}_1}(x)=\frac{\Phi}{1+\Phi}\left[1-\frac{x}{L}\right] \quad \text{Eq. (2.37)}$$

$$N_{(b)\theta_1}(x)=\frac{L}{1+\Phi}\left(\frac{x}{L}-2\left(\frac{x}{L}\right)^2+\left(\frac{x}{L}\right)^3+\frac{1}{2}\left(2\frac{x}{L}-\left(\frac{x}{L}\right)^2\right)\Phi\right) \quad \text{Eq. (2.38)}$$

$$N_{(s)\theta_1}(x)=-\frac{L\Phi}{1+\Phi}\left[\frac{1}{2}\frac{x}{L}\right] \quad \text{Eq. (2.39)}$$

$$N_{(b)\mathrm{v}_2}(x)=\frac{1}{1+\Phi}\left[3\left(\frac{x}{L}\right)^2-2\left(\frac{x}{L}\right)^3\right] \quad \text{Eq. (2.40)}$$

$$N_{(s)\mathrm{v}_2}(x)=\frac{\Phi}{1+\Phi}\left[\frac{x}{L}\right] \quad \text{Eq. (2.41)}$$

$$N_{(b)\theta_2}(x)=\frac{L}{1+\Phi}\left[-\left(\frac{x}{L}\right)^2+\left(\frac{x}{L}\right)^3+\frac{1}{2}\left(\frac{x}{L}\right)^2\Phi\right] \quad \text{Eq. (2.42)}$$

$$N_{(s)\theta_2}(x)=-\frac{L}{1+\Phi}\left[\frac{1}{2}\frac{x}{L}\Phi\right] \quad \text{Eq. (2.43)}$$

The term Φ gives the relative importance of the shear deformation to the bending deformations:

$$\boxed{\Phi=\frac{12EI}{GA_{eff}L^2}} \quad \text{Eq. (2.44)}$$

2.4.2 Strain Energy and derivation of Stiffness Matrices

Using the engineering strains, the potential energy stored in the system due to bending and shear deformation is expressed by:

$$U_{b\&s}=\frac{1}{2}\int_0^L EI\left(\sum_{n=1}^{6}N''_{(b)yn}(x)\bar{u}_n\right)^2dx+\frac{1}{2}\int_0^L GA_{eff}\left(\sum_{n=1}^{6}N'_{(s)yn}(x)\bar{u}_n\right)^2dx \quad \text{Eq. (2.45)}$$

Substituting the shape functions described in Eq. (2.36) to Eq. (2.43) one can derive the **elastic stiffness matrix** for the Timoshenko beam element.

Finally, the components of the **full stiffness matrix** for a Timoshenko element may be derived as done for the Euler-Bernoulli element, using Green-Lagrange strains:

$$K_{ij}^{tot} = EA\int_0^L N'_{xi}(x)\,N'_{xj}(x)\,dx + EI\int_0^L N''_{(b)yi}(x)\,N''_{(b)yj}(x)\,dx + GA_{eff}\int_0^L N'_{(s)yi}(x)\,N'_{(s)yj}(x)\,dx + N\int_0^L N'_{yi}(x)\,N'_{yj}(x)\,dx \qquad \text{Eq. (2.46)}$$

2.4.3 Timoshenko Stiffness Matrices for prismatic homogeneous isotropic beams

For prismatic homogeneous isotropic beams in three dimensions (6 degrees of freedom at each node), the element stiffness matrices are:

$$\overline{\mathbf{K}}_e = \begin{bmatrix} \frac{EA}{L} & 0 & 0 & -\frac{EA}{L} & 0 & 0 \\ & \frac{12}{1+\Phi}\frac{EI}{L^3} & \frac{6}{1+\Phi}\frac{EI}{L^2} & 0 & -\frac{12}{1+\Phi}\frac{EI}{L^3} & \frac{6}{1+\Phi}\frac{EI}{L^2} \\ & & \frac{4+\Phi}{1+\Phi}\frac{EI}{L} & 0 & -\frac{6}{1+\Phi}\frac{EI}{L^2} & \frac{2-\Phi}{1+\Phi}\frac{EI}{L} \\ & & & \frac{EA}{L} & 0 & 0 \\ & SYM & & & \frac{12}{1+\Phi}\frac{EI}{L^3} & -\frac{6}{1+\Phi}\frac{EI}{L^2} \\ & & & & & \frac{4+\Phi}{1+\Phi}\frac{EI}{L} \end{bmatrix} \qquad \text{Eq. (2.47)}$$

$$\overline{\mathbf{K}}_g = \begin{bmatrix} 0 & 0 & 0 & 0 & 0 & 0 \\ & \frac{6/5+2\Phi+\Phi^2}{(1+\Phi)^2} & \frac{L/10}{(1+\Phi)^2} & 0 & \frac{-6/5-2\Phi-\Phi^2}{(1+\Phi)^2} & \frac{L/10}{(1+\Phi)^2} \\ & & \frac{2L^2/15+L^2\Phi/6+L^2\Phi^2/12}{(1+\Phi)^2} & 0 & \frac{-L/10}{(1+\Phi)^2} & \frac{-L^2/30-L^2\Phi/6-L^2\Phi^2/12}{(1+\Phi)^2} \\ & & & 0 & 0 & 0 \\ & SYM & & & \frac{6/5+2\Phi+\Phi^2}{(1+\Phi)^2} & \frac{-L/10}{(1+\Phi)^2} \\ & & & & & \frac{2L^2/15+L^2\Phi/6+L^2\Phi^2/12}{(1+\Phi)^2} \end{bmatrix} \qquad \text{Eq. (2.48)}$$

3 Equivalent Beam Element of a Single Upright Frame

As mentioned before, the full simulation of an Automated Rack Supported Warehouse consists of hundreds of thousands of elements and nodes yielding to an extremely computationally cumbersome model, which is not only hard to be designed in a CAD program, but also nearly impossible to be solved nonlinearly. These problems motivate the search for an equivalent model which will be computationally efficient but also respect the behaviour of the real structure. The solution suggested in the present thesis is to substitute the built-up columns and the roof for simple beam elements whose degrees of freedom will be way lesser. This is conceptually given in Figure 3.1.

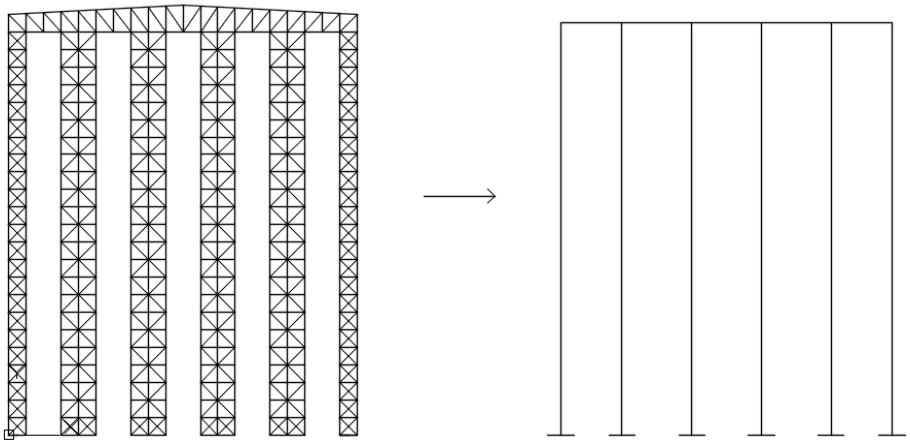

Figure 3.1: Suggested reduced-order model

3.1 Properties of equivalent beam element

The stiffness matrix of a **prismatic homogeneous two-dimensional beam element with doubly symmetric cross-section** depends on the following properties:

1. Material Properties, i.e. Young's Modulus E and Shear Modulus G.
2. Length, L.
3. Cross-section area, A.
4. Moment of inertia I.
5. Shear Area A_{eff}.

It is worth mentioning that shear deformation is usually neglected (and so the property A_{eff}) because in beams with typical lengths and cross sections this phenomenon is insignificant. However, in the case of upright frames, the "cross section" does not remain perpendicular to the neutral axis [10] and so shear must be considered (Figure 3.2). If one neglects the effects of shear deformation, the equivalent element may be 10 to 30% more stiff, depending on the characteristics of the structure and the distribution of loads.

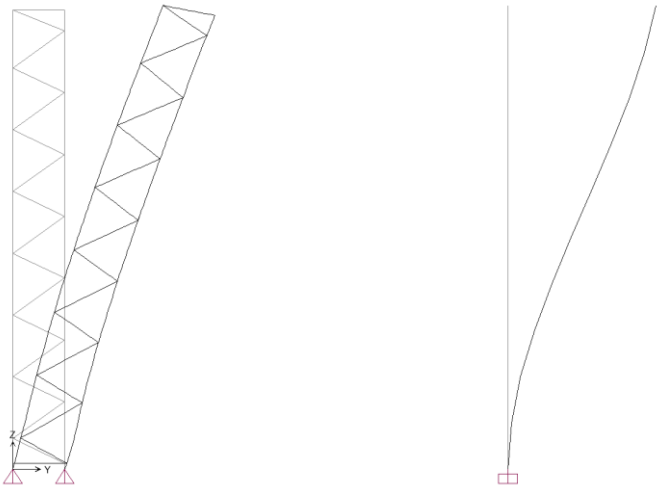

Figure 3.2: In built-up columns (left) “cross sections” do not remain perpendicular to the neutral axis. This effect must be considered when assigning equivalent element’s properties (right)

3.1.1 Material Properties and Length

There is no reason to change these properties as the equivalent element is made of the same materials and has the same length:

$$E_{eq} = E \qquad \text{Eq. (3.1)}$$

$$G_{eq} = G \qquad \text{Eq. (3.2)}$$

$$L_{eq} = L \qquad \text{Eq. (3.3)}$$

3.1.2 Cross-section Area

Cross-section area of the equivalent beam element is equal to the sum of uprights’ cross-section areas:

$$A_{eq} = \sum_{i=1}^{N} A_i \qquad \text{Eq. (3.4)}$$

where,

N is the total number of uprights

A_i is the cross section area of *i*-upright.

For example, the equivalent area for the upright frame in Figure 3.3 will be $A_{eq} = 3A_c$.

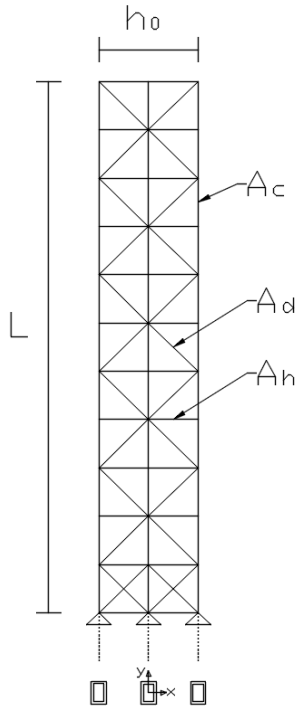

Figure 3.3: Example of a X- column with 3 uprights

3.1.3 Moment of Inertia

Let h_0 be the total width of the upright frame displayed in Figure 3.3. It easy to realize that the centre of gravity of the equivalent cross-section will be at $\frac{h_0}{2}$, as built-up columns are always symmetric (there is no point not to be). The equivalent moment of inertia is given by the following expression:

$$I_{eq} = A_c\left(-\frac{h_0}{2}\right)^2 + A_c \cdot 0 + A_c\left(\frac{h_0}{2}\right)^2 = A_c\frac{h_0^2}{2}$$

In general, the equivalent moment of inertia of a built-up column consisted of N uprights is given by:

$$\boxed{I_{eq} = \sum_{i=1}^{N} A_i \cdot h_i^2} \qquad \text{Eq. (3.5)}$$

where,

A_i is the cross section area of *i*-upright

h_i is the distance from the centre of gravity of *i*-upright

3.1.4 Shear Area

Shear area varies depending on the geometry and the type of the upright frame. Typical upright frames are: a) X-column b) D-column c) Z-column d) K-column (see Figure 3.4). We will proceed to the calculation of shear area for each of these types. Finally, we will

describe a method to calculate shear areas for arbitrary built-up columns (non-closed form).

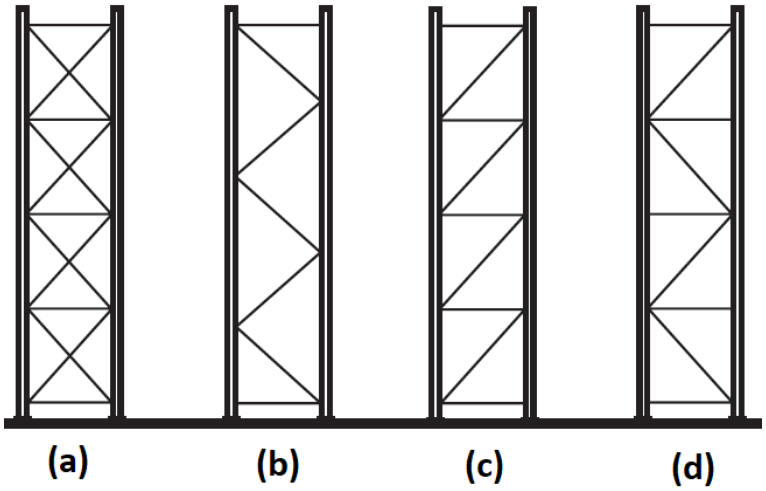

Figure 3.4: Typical upright frames: (a) X-column (b) D-column (c) Z-column (d) K-column

3.1.4.1 X-column

Consider the X-column with two uprights shown in Figure 3.5. The shear force is transferred through diagonal members only, while for conservation of symmetry, the horizontal bracings remain unstressed.

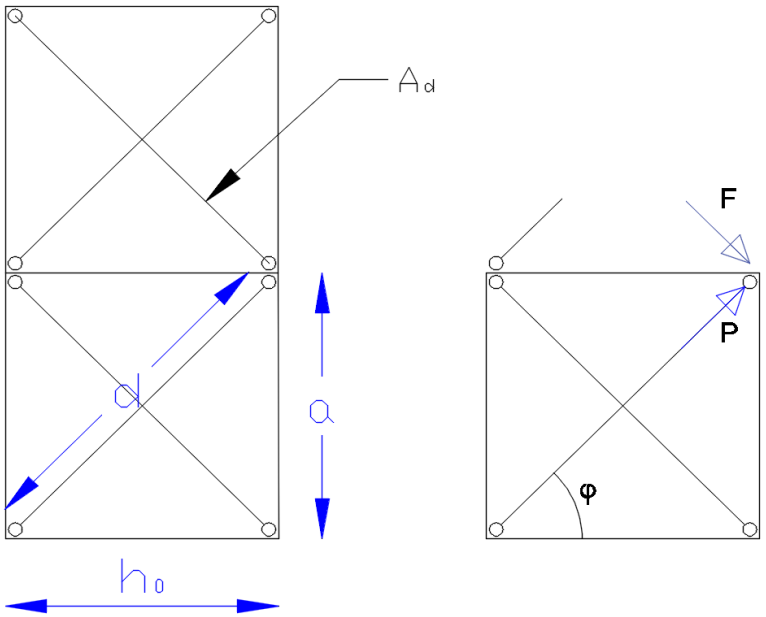

Figure 3.5: X-column configuration and shear transfer through diagonal bracings

Shear stress τ relates to shear deformation γ by:

$$\tau = \gamma G \qquad \text{Eq. (3.6)}$$

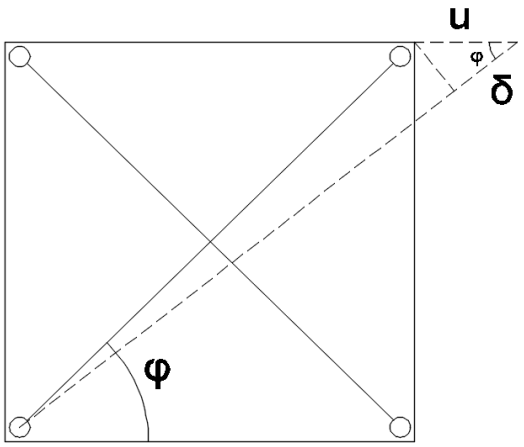

Figure 3.6: X-column's shear deformation

According to Figure 3.6 shear displacement u and extension of the diagonal bracing δ are geometrically related by the following expression:

$$\delta = u\cos\phi \qquad \text{Eq. (3.7)}$$

Now considering that each diagonal element transfers half the total shear ($Q/2$) and shear stress and shear force are related by $\tau = Q/A_{eff}$ [11]:

$$\tau = \frac{Q}{A_{eff}} = \frac{2P\cos\phi}{A_{eff}} = \frac{2\left(\frac{EA_d}{d}\delta\right)\cos\phi}{A_{eff}} \qquad \text{Eq. (3.8)}$$

Now combining Eq. (3.6), Eq. (3.7) and Eq. (3.8) we can derive an expression for the shear area:

$$\boxed{A_{eff} = 2\cdot\frac{EA_d}{G}\frac{h_0^2 a}{d^3}} \qquad \text{Eq. (3.9)}$$

3.1.4.2 D-column

Consider the D-column with two uprights shown in Figure 3.7. As in the case of X-column, shear forces are transferred via diagonal members and thus, the shear area will be given by:

$$\boxed{A_{eff} = \frac{EA_d}{G}\frac{h_0^2 a}{d^3}} \qquad \text{Eq. (3.10)}$$

, since the mechanism of shear deformation is the same as in X-column but with the difference that D-column has one diagonal bracing instead of two.

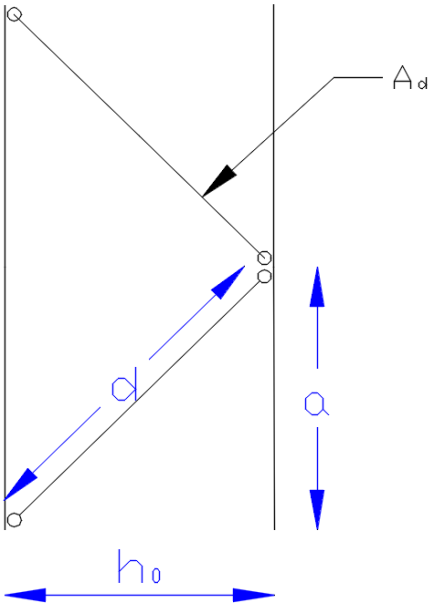

Figure 3.7: D-column configuration

3.1.4.3 Z-column

Consider the Z-column with two uprights shown in Figure 3.8. In contrast to the two previous mentioned types, in the case of Z-column two mechanisms produce shear deformation 1) axial deformation of the horizontal bracing and 2) axial deformation of the diagonal bracing.

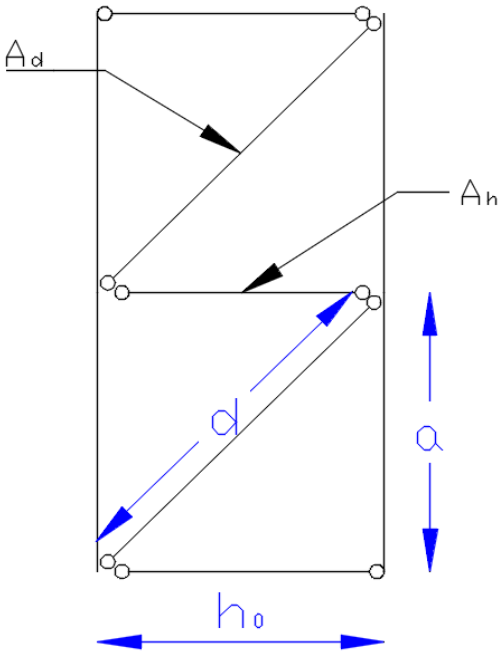

Figure 3.8: Z-column configuration

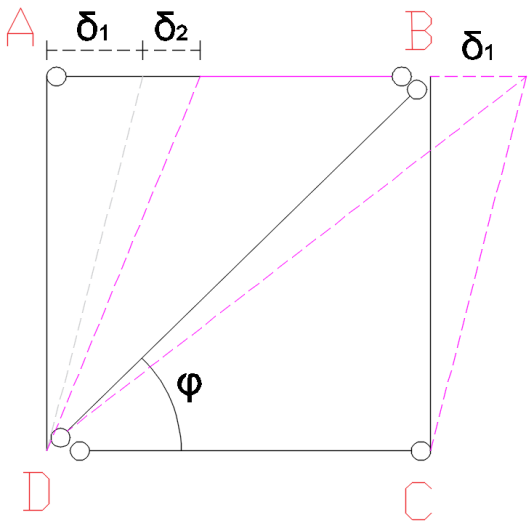

Figure 3.9: Z-column's shear deformation

Figure 3.9 shows the two components of shear deformation. Displacement δ_1 is related to the axial elongation of (DB) and displacement δ_2 to the elongation of (AB). Mathematically this is expressed by:

$$\delta_1 = \frac{Q}{\cos^2\phi}\frac{d}{EA_d} = \frac{Qa}{\cos^2\phi\cdot\sin\phi\cdot EA_d} \qquad \text{Eq. (3.11)}$$

$$\delta_2 = \frac{Qh_0}{EA_h} = \frac{Qa}{EA_h\tan\phi} \qquad \text{Eq. (3.12)}$$

Now following the same procedure as in 3.1.4.1 we can derive a formula for the shear area of Z-column:

$$\gamma = \frac{\delta_1+\delta_2}{a} \overset{Eq.\ 3.11\&3.12}{=} \frac{Q}{\cos^2\phi\cdot\sin\phi\cdot EA_d} + \frac{Q}{EA_h\tan\phi} \Rightarrow$$

$$\frac{Q}{\cos^2\phi\cdot\sin\phi\cdot EA_d} + \frac{Q}{EA_h\tan\phi} = \frac{Q}{A_{eff}} \Rightarrow$$

$$\boxed{A_{eff} = \frac{\frac{E}{G}A_d\frac{h_0^2}{d^2}\frac{a}{d}}{1+\frac{h_0^3}{d^3}\frac{A_d}{A_h}}} \qquad \text{Eq. (3.13)}$$

3.1.4.4 K-column

Consider the K-column with two uprights shown in Figure 3.10. As in D-column, shear deformation depends only on the diagonal bracings while the horizontal ones remain unstressed. Thus, the following expression hold for the shear area of the K-system:

$$A_{eff} = \frac{EA_d}{G}\frac{h_0^2 a}{d^3}$$ Eq. (3.14)

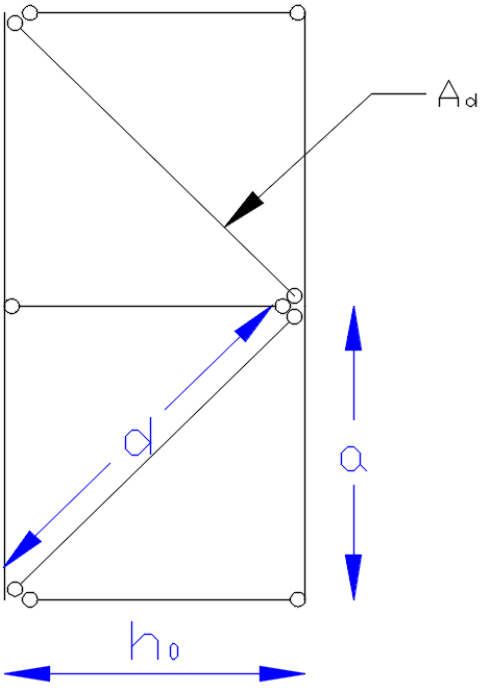

Figure 3.10: K-column configuration

3.1.4.5 General Method for the Calculation of Shear Area in Arbitrary Built-Up Columns

Let us consider an upright frame whose shear area in not given in closed form (e.g. Figure 3.11) or the diagonal and horizontal bracings vary with height. Then, we can approximate element's shear area (in a non-closed form) by executing the following procedure:

1. Isolate the column under consideration and pin the nodes at one end.
2. Apply a point load at the free end. If P is the applied load, then the corresponding displacement of the free end δ_{tot} is given by:

$$P = \frac{12}{4+\Phi}\frac{EI_{eq}}{L^3}\delta_{tot}$$ Eq. (3.15)

3. Solve Eq. (3.15) for Φ:

$$\Phi = \frac{12EI_{eq}}{L^3}\delta_{tot} - 4$$ Eq. (3.16)

Another way to calculate Φ is to set the cross-section area of the bracings to a very large value, so no shear deformation will be developed:

$$P = 3\frac{EI_{eq}}{L^3}\delta_b \qquad \text{Eq. (3.17)}$$

Then combining Eq. (3.15) and Eq. (3.17) we can derive the following:

$$3\frac{EI_{eq}}{L^3}\delta_b = \frac{12}{4+\Phi}\frac{EI_{eq}}{L^3}\delta_{tot} \Rightarrow \delta_b = \frac{4}{4+\Phi}\delta_{tot}$$

$$\boxed{\Phi = 4\left(\frac{\delta_{tot}}{\delta_b} - 1\right)} \qquad \text{Eq. (3.18)}$$

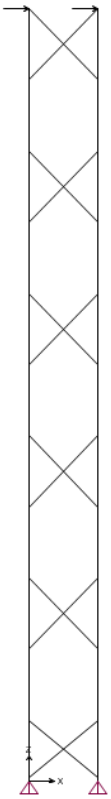

Figure 3.11: Upright frame with arbitrary configuration

3.1.4.6 Tables of Properties for typical upright frames

Table 3.1: Properties of X-columns

	X-COLUMN SINGLE	**X-COLUMN DOUBLE A**	**X-COLUMN DOUBLE B**
	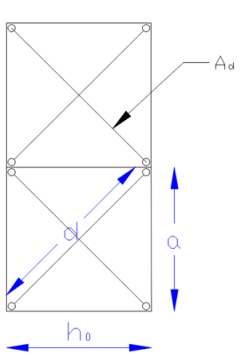	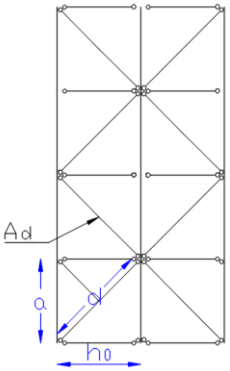	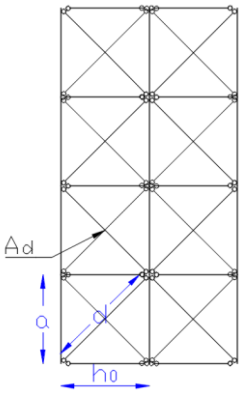
Nº uprights	2	3	3
A_{eq}	$2A_c$	$3A_c$	$3A_c$
I_{eq}	$A_c \frac{h_0^2}{2}$	$2A_c h_0^2$	$2A_c h_0^2$
A_{eff}	$2 \cdot \frac{EA_d}{G} \frac{h_0^2 a}{d^3}$	$2 \cdot \frac{EA_d}{G} \frac{h_0^2 a}{d^3}$	$4 \cdot \frac{EA_d}{G} \frac{h_0^2 a}{d^3}$

Table 3.2: Properties of D-columns

	D-COLUMN SINGLE	**D-COLUMN DOUBLE A**	**D-COLUMN DOUBLE B**
	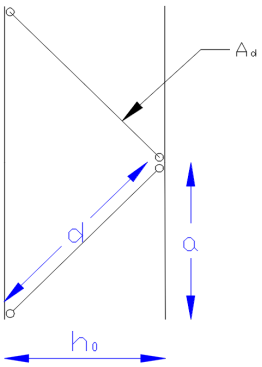	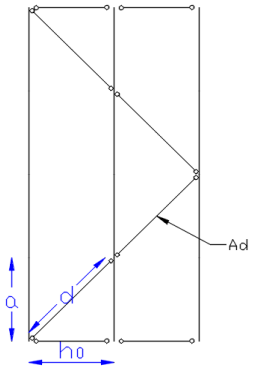	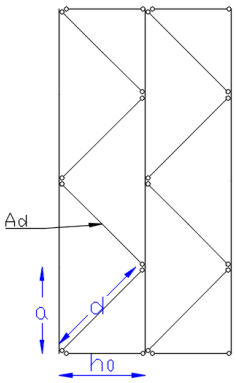
Nº uprights	2	3	3
A_{eq}	$2A_c$	$3A_c$	$3A_c$
I_{eq}	$A_c \frac{h_0^2}{2}$	$2A_c h_0^2$	$2A_c h_0^2$
A_{eff}	$\frac{EA_d}{G} \frac{h_0^2 a}{d^3}$	$\frac{EA_d}{G} \frac{h_0^2 a}{d^3}$	$2 \cdot \frac{EA_d}{G} \frac{h_0^2 a}{d^3}$

Table 3.3: Properties of Z-columns

	Z-COLUMN SINGLE	**Z-COLUMN DOUBLE A**	**Z-COLUMN DOUBLE B**
	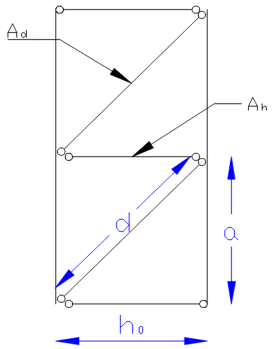	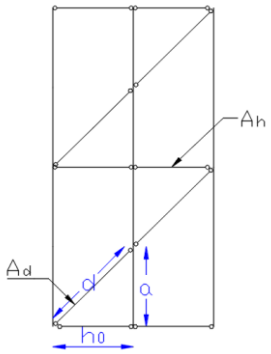	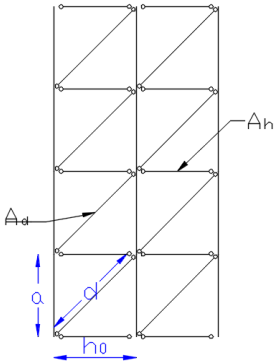
Nº uprights	2	3	3
A_{eq}	$2A_c$	$3A_c$	$3A_c$
I_{eq}	$A_c \frac{h_0^2}{2}$	$2A_c h_0^2$	$2A_c h_0^2$
A_{eff}	$\frac{\frac{EA_d}{G}\frac{h_0^2}{d^2}\frac{a}{d}}{1+\frac{h_0^3}{d^3}\frac{A_d}{A_h}}$	$\frac{\frac{EA_d}{G}\frac{h_0^2}{d^2}\frac{a}{d}}{1+\frac{h_0^3}{d^3}\frac{A_d}{A_h}}$	$2\cdot\frac{\frac{EA_d}{G}\frac{h_0^2}{d^2}\frac{a}{d}}{1+\frac{h_0^3}{d^3}\frac{A_d}{A_h}}$

Table 3.4: Properties of K-columns

	Z-COLUMN SINGLE	**Z-COLUMN DOUBLE A**	**Z-COLUMN DOUBLE B**
	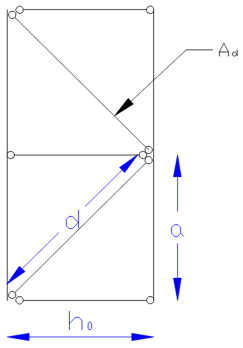	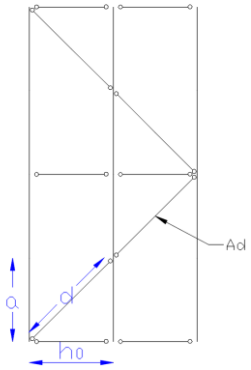	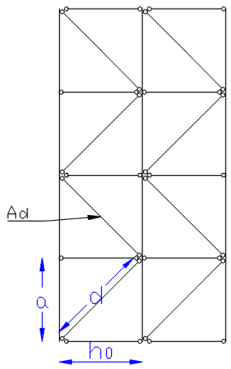
Nº uprights	2	3	3
A_{eq}	$2A_c$	$3A_c$	$3A_c$
I_{eq}	$A_c \frac{h_0^2}{2}$	$2A_c h_0^2$	$2A_c h_0^2$
A_{eff}	$\frac{EA_d}{G}\frac{h_0^2 a}{d^3}$	$\frac{EA_d}{G}\frac{h_0^2 a}{d^3}$	$2\cdot\frac{EA_d}{G}\frac{h_0^2 a}{d^3}$

3.2 D-column test case: Modal and Linear Buckling Analysis

The method described in previous sections will be tested on a D type column which geometry is shown in Figure 3.12. In addition, structural properties of the test example are summed in Table 3.5.

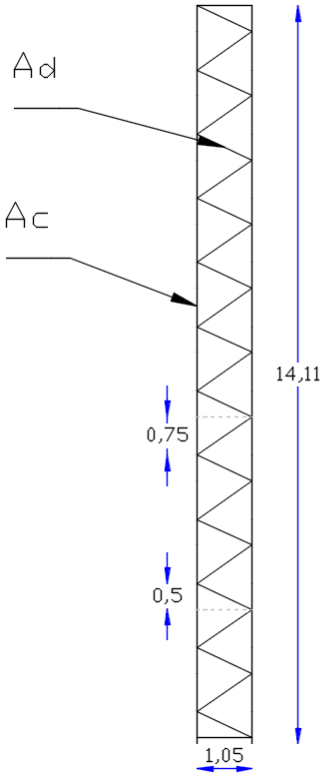

Figure 3.12: Geometric properties of D-column test case

Table 3.5: Structural properties of D-column test case

	Material	Cross-Section Area (m^2)	Moment of Inertia (m^4)	Shear Area (m^2)
Upright	S275	9.875e-4	1.01e-6	4.301e-4
Bracing	S275	0.9875e-4	0.101e-6	0.4301e-4

Note that the D bracing consists of two unequally parts, one 0.5 meters and the other 0.75 meters, a case that is not explicitly provided in Table 3.2 for the calculation of shear area. Thus, one must follow the general method that was developed in §3.1.4.5 or, more efficiently, to calculate the shear areas for 0.5m and 0.75m and then use the average. Both methods were performed, and the results were compared.

Using Table 3.2we derive:

$$\boxed{A_{eq} = 2A_c = 1.975e^{-3}\ m^2}$$

$$\boxed{I_{eq} = A_c \frac{h_0^2}{2} = 5.444e^{-3}\ m^4}$$

$$A_{eff}\left(0.5\right) = \frac{EA_d}{G}\frac{h_0^2 a}{d^3} = 9.00e^{-5}\ m^2$$

$$A_{eff}\left(0.75\right) = \frac{EA_d}{G}\frac{h_0^2 a}{d^3} = 9.88e^{-5}\ m^2$$

$$\boxed{\overline{A}_{eff} = \frac{A_{eff}\left(0.5\right) + A_{eff}\left(0.75\right)}{2} = 9.44e^{-5}\ m^2}$$

$$\boxed{\overline{\Phi} = \frac{12EI}{G\overline{A}_{eff}L^2} = 0.90369}$$

Now Φ will be calculated with the general method. As discussed in §3.1.4.5, firstly, bracings' cross-section areas are modified (left model in Figure 3.13), then point loads are applied (10 kN) to the free ends and finally the corresponding deflections are calculated:

$$\boxed{\Phi_{gen} = 4\left(\frac{\delta_{tot}}{\delta_b} - 1\right) = 4\left(\frac{0.1008}{0.0819} - 1\right) = 0.923077}$$

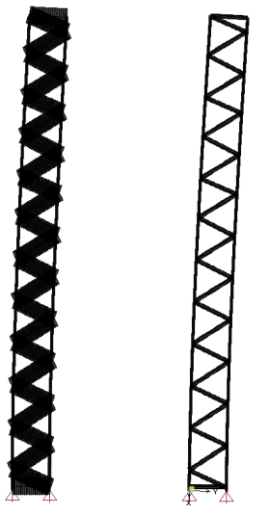

Figure 3.13: Finite element model of full structure without shear deformation (left) and with shear deformation (right)

The difference is about 2%, so one can proceed with the average shear than performing the general method.

3.2.1 Linear Elastic Analysis

Next, linear elastic analysis is performed for horizontal point loads (10 kN) applied to upright frame's free end (Figure 3.14), which yields to the following deflections:

$$\left.\begin{aligned} d_{full} &= 0.1008\ m \\ d_{eq} &= 0.1004\ m \end{aligned}\right\} \rightarrow \frac{d_{full} - d_{eq}}{d_{full}} = 0.4\%$$

Similar tests have been performed for several types of upright frames and load distributions and the results were always almost identical.

It is also worth mentioning that if equivalent element's shear area is set to a large value (no shear deformation), then the deflection is decreased by 20%. This yields to the result that *shear deformation should always be under consideration when accurate displacements are desired.*

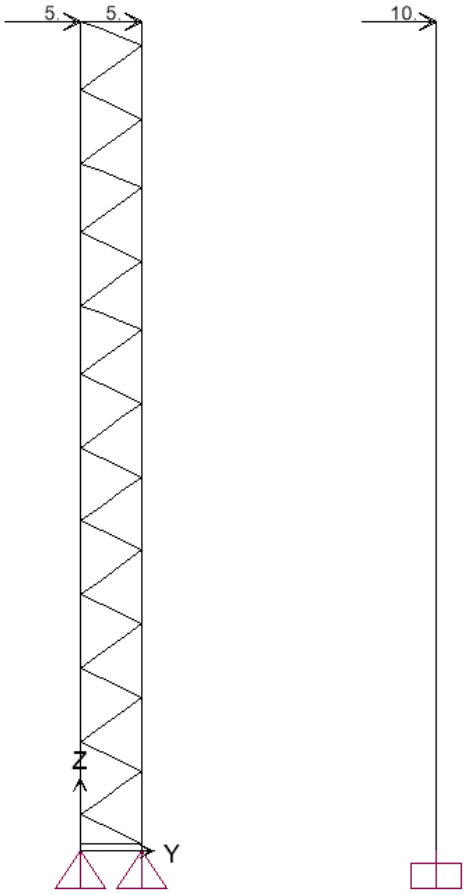

Figure 3.14: Finite element model of full structure (left) and equivalent column (right)

3.2.2 Modal Analysis

Another comparison between the two models can be made for the modes of free vibration. A 400 kg lumped mass at the top node (z=14.11m) results in the following first eigenvalues (see Figure 3.15):

$$\left.\begin{array}{l} T_{full} = 1.286 \text{ sec} \\ T_{eq} = 1.28 \text{ sec} \end{array}\right\} \rightarrow \frac{T_{full} - T_{eq}}{T_{full}} = 0.47\%$$

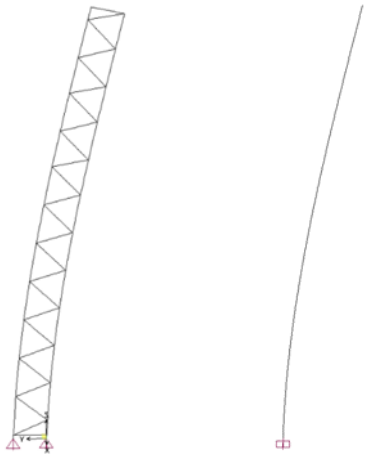

Figure 3.15: First mode of vibration for the full structure (left), T_1=1.286 sec and the equivalent column (right), T_1=1.28 sec

3.2.3 Linear Buckling Analysis

Finally, Linear Buckling Analysis (LBA) was performed, for same dead load as in §3.2.2.

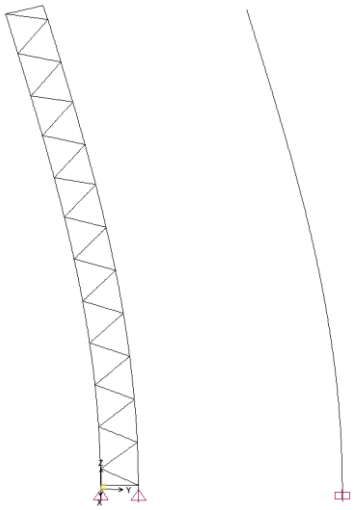

Figure 3.16: First buckling mode for the full structure (left), λ=29.32 and the equivalent column (right), λ=29.39

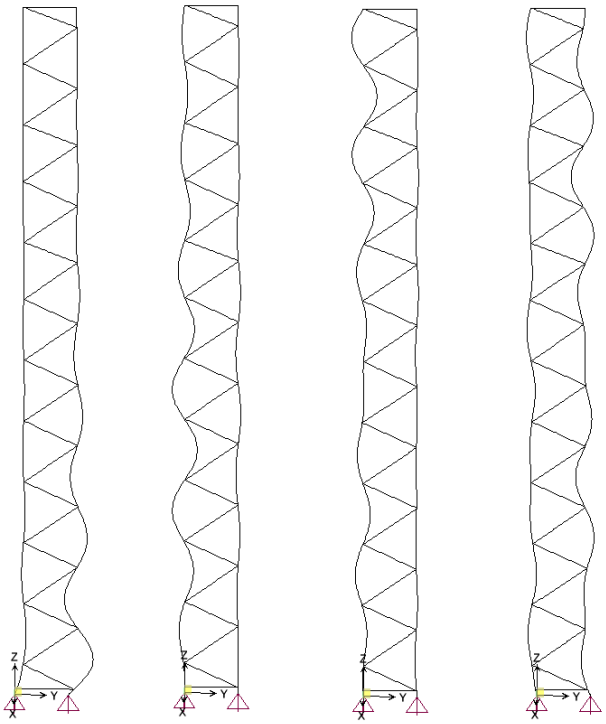

Figure 3.17: Local buckling of the uprights is not considered in equivalent element

As indicated by Figure 3.16, the first buckling mode (global buckling) is almost identical for the two systems. *However, it should be mentioned that the equivalent element cannot consider local buckling of the uprights (Figure 3.17) or buckling of the bracings.*

4 Nonlinear Behaviour of a Single Upright Frame

4.1 Failure modes

The test case analysed in previous section demonstrates the capabilities of the equivalent element to predict extremely well the response of a built-up column in linear analysis. One step further is to include nonlinear properties in order to achieve adequate accuracy for Pushover and Dynamic Analysis. The nonlinear behaviour of an upright frame can be distinguished in three main categories:

1. Axial Failure. This type of failure refers to flexural (Figure 3.16 and Figure 3.17) local, distortional and lateral torsional buckling of the uprights [12] (see Figure 4.1). It is common in rack-system technology to perform laboratory tests to evaluate uprights' compression resistance and thus, $N_{rd,upright}$ is usually a known value.

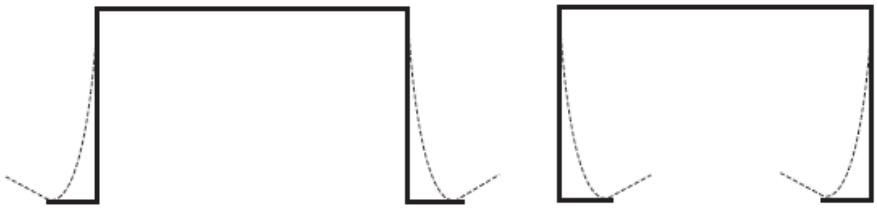

Figure 4.1: Distortional mode of an open cross-section with simple lips

2. Bending Failure. Loads are not primarily carried by bending mechanisms, as bracings are considered to be pinned and uprights are usually simply supported to the foundation. However, bending moments may develop in the uprights when an adequate number of bracings have failed. This phenomenon will be discussed in more detail later.
3. Shear Failure. As mentioned in previous sections, shear forces are transferred via bracings, which may fail due to buckling or tensile yielding.

4.1.1 Method to implement nonlinearity

The equivalent element should be able to provide the potential for all types of failures mentioned above. The most common ways to consider plasticity and nonlinearity in beam elements are:

a) Rotational hinges

Equivalent element's bending moment M_{eq} is linked to a set of axial forces N_b on the uprights, of opposite direction (see Figure 4.2):

$$M_{eq} = N_b \cdot h_0$$

On the other hand, equivalent axial force N_{eq} is related to a set of axial forces $\frac{N_{eq}}{2}$ on the uprights, of the same direction (Figure 4.2).

Summing all together, if $N_{rd,upright}$ is upright's compression resistance and N, M the axial force and the bending moment acting on the equivalent element respectively, then the condition for axial failure is:

$$N_{rd,upright} = \frac{N_{eq}}{2} + \frac{M_{eq}}{h_0} \qquad \text{Eq. (4.1)}$$

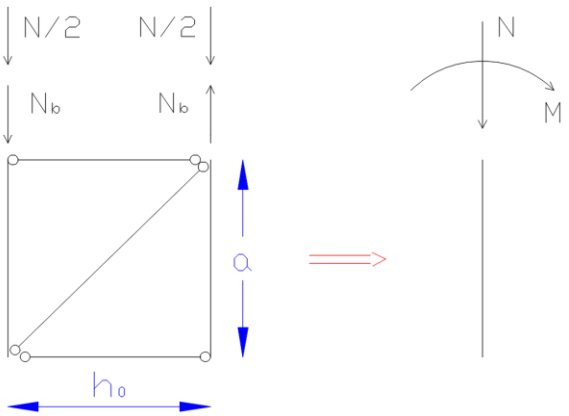

Figure 4.2: Relation between axial forces and bending moments of the two models

Eq. (4.1) indicates a linear interaction between moment and axial force of the equivalent element, which is conceptually illustrated in Figure 4.3.

Overall, nonlinear rotational hinges with axial force interaction can be used to take into consideration the compression failure of the uprights. *However, this type of nonlinear elements cannot predict shear failure of the system, which is related to bracings' buckling or tensile yielding.*

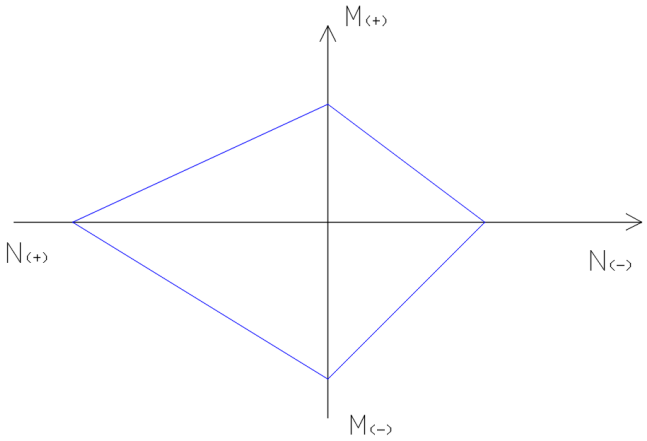

Figure 4.3: Interaction between the bending moment and axial force of the equivalent element

b) Shear Springs

An important factor that dominates the nonlinear behaviour of an upright frame in seismic loading is bracings' failure, as indicated in [13]. These structural components are responsible for the transfer of seismic shear forces to structure's foundation. If V_{eq} is equivalent

element's shear force and $N_{rd,bracing}$ the axial resistance of the bracing shown in Figure 4.4, then failure occurs when:

$$N_{rd,upright} = \frac{V_{eq}}{\cos\varphi} \qquad \text{Eq. (4.2)}$$

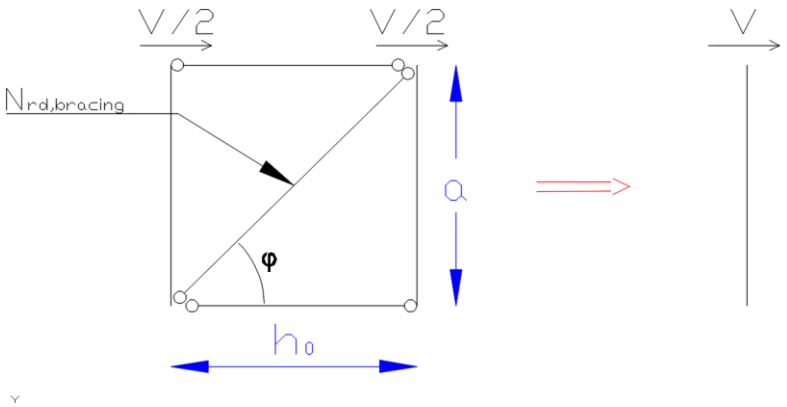

Figure 4.4: Relation between equivalent element's shear force and bracing's axial force (Z-Column)

Similarly, one can relate the bracings' axial resistances to the shear resistance of the equivalent element for any type of built-up column. *Of course, in contrast to the rotational hinges, this type of elements cannot provide the potential for uprights' axial failure.*

4.1.2 Concept of Two Node Link Element

Rotational hinges together with shear springs must be combined to simulate the nonlinear response of an upright frame. Thus, at each node of the equivalent element a set of nonlinear bending and shear springs must be assigned (Figure 4.5).

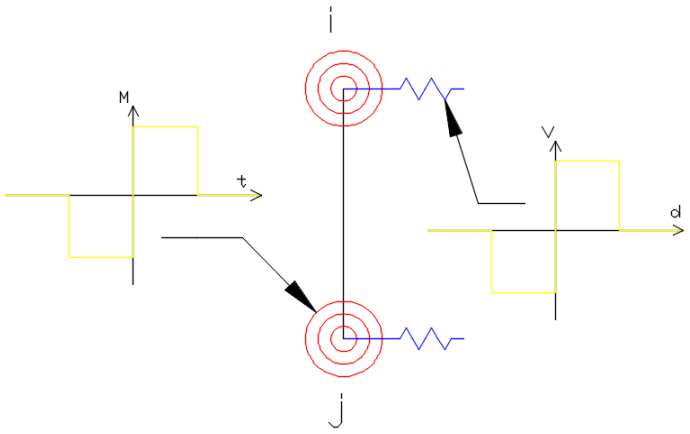

Figure 4.5: Set of nonlinear springs at each node of the equivalent element

This method to implement nonlinearity is characterized by the incapability to provide the post-capping response of the element; before failure the system is linear and after failure the system cannot carry any load. This is conceptually illustrated in Figure 4.6. Of course, one can assign multilinear curves for M-θ and V-δ, but there is no straightforward way to calculate the unknown values (i.e. θ_y, θ_{ult}, δ_y, δ_{ult} etc.).

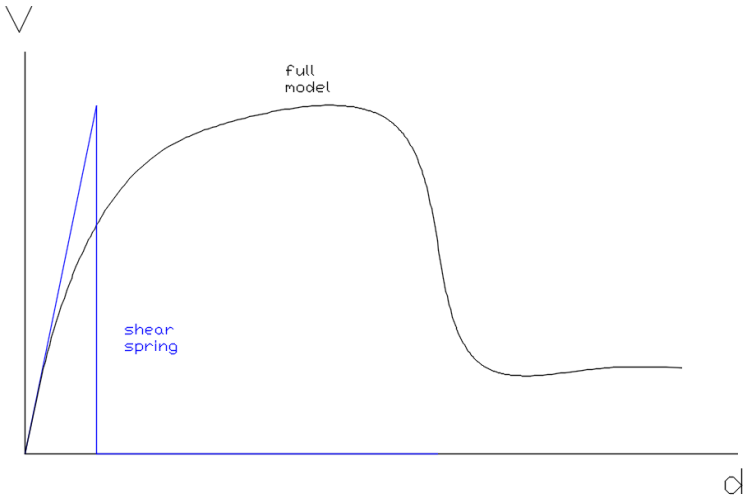

Figure 4.6: Incapability of the spring elements to predict an accurate nonlinear curve

The aforementioned difficulty can be bypassed by using nonlinear elements instead of non-linear nodes (hinges). This way, nonlinearity is an inner property of the equivalent element and can be explicitly linked to the stiffness degradation of the real structure. The only disadvantage is the computational cost of adding inner degrees of freedom in each element. However, these DOFs contribute only locally (on local stiffness matrix of the corresponding element) and so problem's global stiffness matrix does not increase in size.

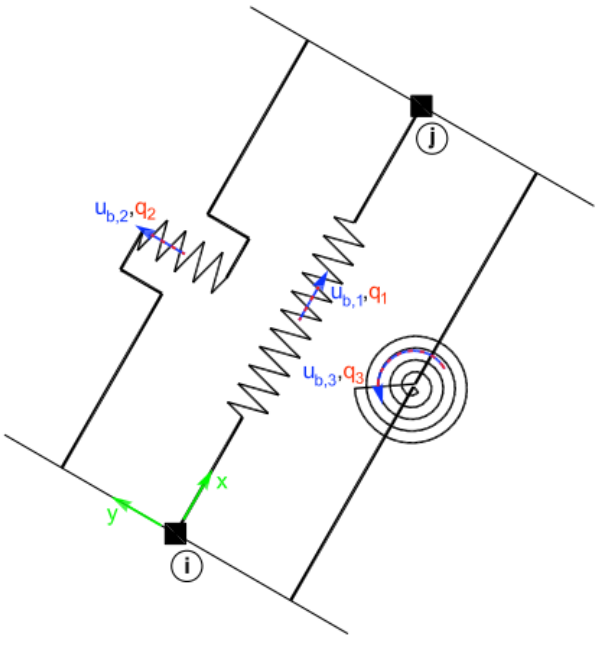

Figure 4.7: Concept of Two Node Link Element

Open-source software OpenSees [14] provides the **Two Node Link Elements** (aka Link Elements) (see Figure 4.7) with the capability to assign axial, rotational and shear springs. In the following section we will focus on the calculation of springs' linear properties and then we will introduce a method to consider nonlinearity.

4.1.3 Linear4 Properties of Two Node Link Element for the Bernoulli and Timoshenko Beam

First and foremost, the Link Element must be capable to restore the exact stiffness matrix for the case of homogeneous, linear and elastic Euler-Bernoulli Beam (see Eq. (2.30)). Let K_{axial}, K_{shear} and C be the linear stiffness of axial, shear and rotational spring respectively. We will determine relations between beam's properties (L, E, A, I) and springs' stiffnesses:

- $k_{11} = \frac{EA}{L}$

This component is associated with beam's axial deformation. An acting axial force N causes a displacement d_a:

$$N = \frac{EA}{L} \cdot d_a$$

The total energy stored in Link Element's axial spring due to N is:

$$U = \frac{1}{2} K_{axial} d_a^2 - N d_a$$

Equilibrium is restored in the system when the total energy is minimized [15]:

$$\frac{\partial U}{\partial d_a} = 0 \Rightarrow K_{axial} d_a - N = 0$$

Finally, Link Element's axial stiffness is equal to:

$$\boxed{K_{axial} = \frac{EA}{L}} \qquad \text{Eq. (4.3)}$$

- $k_{22} = \frac{12EI}{L^3}$

A shear force F acting on node j (see Figure 4.8) yields to a displacement d_s:

$$F = \frac{12EI}{L^3} d_s$$

The total energy stored by the shear spring due to F is:

$$U = \frac{1}{2} K_{shear} d_s^2 - F d_s$$

Again, equilibrium is established when:

$$\frac{\partial U}{\partial d_s} = 0 \Rightarrow K_{shear} d_s - F = 0$$

Link Element's shear stiffness is equal to:

$$\boxed{K_{shear} = \frac{12EI}{L^3}}$$ Eq. (4.4)

- $k_{33} = \frac{4EI}{L}$

A bending moment M applied to beam's end, causes a rotation θ:

$$M = \frac{4EI}{L} \theta$$

The rotation θ at node j produces both a rotation t to the rotational spring and a displacement d to the shear spring. Observing the geometry of the Link Element we derive:

$$\boxed{t = \theta}$$ Eq. (4.5)

$$\boxed{d = \theta \cdot L / 2}$$ Eq. (4.6)

It is highlighted that Eq. (4.6) holds only when small displacements are considered.

Summing up, the total energy stored in shear and rotational spring is given by:

$$U = \frac{1}{2} K_{shear} \cdot d^2 + \frac{1}{2} C \cdot t^2 - M \cdot t \overset{Eq.(4.5)\&(4.6)}{=} \frac{1}{2} K_{shear} \cdot \frac{L^2}{4} \theta^2 + \frac{1}{2} C \cdot \theta^2 - M \cdot \theta$$

Finally, the condition for system's equilibrium:

$$\frac{dU}{d\theta}=0\Rightarrow K_{shear}\cdot\frac{L^2}{4}\theta+C\cdot\theta-M=0\Rightarrow C=\frac{M-K_{shear}\dfrac{L^2}{4}\theta}{\theta}$$

$$\Rightarrow C=\frac{\dfrac{4EI}{L}\cancel{\theta}-K_{shear}\dfrac{L^2}{4}\cancel{\theta}}{\cancel{\theta}}\overset{(4)}{\Rightarrow}$$

$$\boxed{C=\frac{EI}{L}}$$ Eq. (4.7)

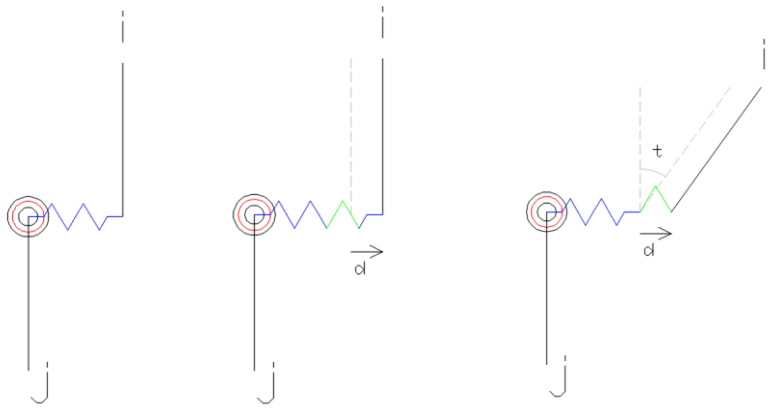

(a) (b) (c)

Figure 4.8: Possible deformed configurations (no axial deformation) of the Link Element: (a) initial configuration (b) shear deformation (c) rotational deformation

Similar procedure can be followed for the case of Timoshenko stiffness matrix. Table 4.1 sums up Link Element's spring properties for both cases.

Table 4.1: Springs' Linear Properties for Two Node Link Element

Type of beam	**EULER-BERNOULLI**	**TIMOSHENKO** $\left(\Phi=\dfrac{12EI}{L^2GA_{eff}}\right)$
Axial Spring	$\dfrac{EA}{L}$	$\dfrac{EA}{L}$
Shear Spring	$\dfrac{12EI}{L^3}$	$\dfrac{1}{1+\Phi}\cdot\dfrac{12EI}{L^3}$
Bending Spring	$\dfrac{EI}{L}$	$\dfrac{EI}{L}$
P-delta input value (OpenSees users)	-0.1	$\dfrac{-0.1}{(1+\Phi)^2}$

Note for OpenSees users

Two Node Link Element has an option to add P-delta effects by defining moment contribution ratios for each node. By examining the source code of OpenSees, it was concluded that the additional moment due to P-delta effects is calculated by:

$$M_{p-delta} = \frac{N}{L} \cdot (1 - M_1 - M_2) \cdot (d_2 - d_1) \qquad \text{Eq. (4.8)}$$

The analytic expression of P-delta moment is (see Eq. (2.32)):

$$M_{p-delta} = \frac{6}{5} \frac{N}{L} \cdot (d_2 - d_1) \qquad \text{Eq. (4.9)}$$

Thus, we can determine the moment contribution ratios combining Eq. (4.8) and Eq. (4.9) and assuming that $M_1 = M_2 = M$:

$$\frac{N}{L} \cdot (1 - M_1 - M_2) \cdot (d_2 - d_1) = \frac{6}{5} \frac{N}{L} \cdot (d_2 - d_1) \Rightarrow$$

$$\boxed{M_1 = M_2 = M = -0.1}$$

Similarly, for the case of Timoshenko beam:

$$\frac{N}{L} \cdot (1 - M_1 - M_2) \cdot (d_2 - d_1) = \frac{6/5 + 2\Phi + \Phi^2}{(1+\Phi)^2} \frac{N}{L} \cdot (d_2 - d_1) \Rightarrow$$

$$\boxed{M_1 = M_2 = M = \frac{-0.1}{(1+\Phi)^2}}$$

4.2 X-column test case: Pushover Analysis (Point and Triangular Distribution)

The method that was developed in previous section will be tested on a single X-column and the results will be compared with the detailed structure. Specifically, they will be three models of decreasing accuracy:

1. Fiber Model. All structural members (uprights, diagonal and horizontal bracings) will be simulated as fiber elements with 3 integration points. Especially for the diagonal bracings in compression, an imperfection L/200 is assumed, where L is the length of the element.
2. Truss Model. In this case, uprights are assumed to behave linearly, while the bracings are simulated by nonlinear truss elements (whose material law will be discussed later).

3. Link Model. As described in §4.1.2, the whole upright frame will be substituted for a Two Node Link Element that includes shear degradation (failure of the bracings).

4.2.1 Geometry and structural properties

The examined test case is a two-dimensional X-column which consists of 20 X-boxes and is pin-connected to the ground (see Figure 4.9). Table 4.2 contains information about the geometry of each X-box, while the cross-sectional properties are given in Table 4.3

Table 4.2: Geometry of X-column test case

Box No.	vertical distance **a** (m)	horizontal distance $\mathbf{h_0}$ (m)	diagonal length **d** (m)
1	0.06	1.20	-
2	1.00	1.20	1.56
3	1.25	1.20	1.73
4	1.25	1.20	1.73
5	1.25	1.20	1.73
6	1.25	1.20	1.73
7	1.25	1.20	1.73
8	1.5	1.20	1.73
9	1.2	1.20	1.73
10	1.25	1.20	1.73
11	1.25	1.20	1.73
12	1.25	1.20	1.73
13	1.25	1.20	1.73
14	1.25	1.20	1.73
15	1.25	1.20	1.73
16	1.25	1.20	1.73
17	1.25	1.20	1.73
18	1.25	1.20	1.73
19	1.07	1.20	1.61
20	1.07	1.20	1.61

Table 4.3: Cross-sections of X-column test case

Box No.	Upright	Diagonal Bracings	Horizontal Bracing
1	RHS 120x80x10 (S355)	-	DC 80x50x3 (S355)
2	RHS 120x80x10 (S355)	L 40x40x5 (S355)	DC 80x50x3 (S355)
3	RHS 120x80x10 (S355)	L 40x40x5 (S355)	DC 80x50x3 (S355)
4	RHS 120x80x10 (S355)	L 40x40x4 (S275)	DC 80x50x3 (S355)
5	RHS 120x80x10 (S355)	L 40x40x4 (S275)	DC 80x50x3 (S355)
6	RHS 120x80x6 (S355)	L 40x40x4 (S275)	DC 80x50x3 (S355)
7	RHS 120x80x6 (S355)	L 40x40x4 (S275)	DC 80x50x3 (S355)
8	RHS 120x80x6 (S355)	L 40x40x4 (S275)	DC 80x50x3 (S355)
9	RHS 120x80x6 (S355)	L 35x35x4 (S275)	DC 80x50x3 (S355)
10	RHS 120x80x4 (S355)	L 35x35x4 (S235)	DC 80x50x3 (S355)
11	RHS 120x80x4 (S355)	L 35x35x4 (S235)	DC 80x50x3 (S355)
12	RHS 120x80x4 (S355)	L 35x35x4 (S235)	DC 80x50x3 (S355)
13	RHS 120x80x4 (S355)	L 30x30x4 (S235)	DC 80x50x3 (S355)
14	RHS 120x80x4 (S355)	L 30x30x4 (S235)	DC 80x50x3 (S355)
15	RHS 120x80x4 (S355)	L 30x30x4 (S235)	DC 80x50x3 (S355)
16	RHS 120x80x4 (S355)	L 30x30x4 (S235)	DC 80x50x3 (S355)
17	RHS 120x80x4 (S355)	L 30x30x4 (S235)	DC 80x50x3 (S355)
18	RHS 120x80x4 (S355)	L 30x30x4 (S235)	DC 80x50x3 (S355)
19	RHS 120x80x4 (S355)	L 30x30x4 (S235)	DC 80x50x3 (S355)
20	RHS 120x80x4 (S355)	L 30x30x4 (S235)	-

(**RHS**: Rectangular Hollowed Section **L**: Angle Section, **DC**: Double Channel)

In addition to Table 4.2 and Table 4.3, the following structural properties are highlighted:

a) Steel is assumed with no strain-hardening.

b) All uprights have symmetric rectangular cross-sections, oriented with their strong axis inside built-up column's plane.

c) All bracings are pinned to the uprights and they do not intersect with each other.

d) Diagonal bracings in compression have an initial imperfection L/200 to consider buckling phenomena.

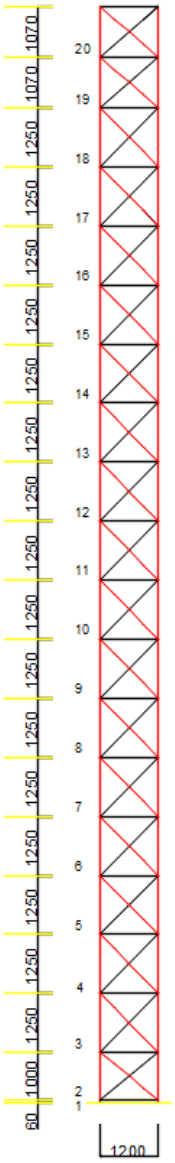

Figure 4.9: Configuration of X-column test case

4.2.2 Fiber Model

The Fiber element Model is the most straightforward to implement, as no additional calculations and preparation of data are needed. Moreover, force-based elements are known for their pre-capping accuracy and their ability to reduce the total DOFs of the problem as they do not require internal mesh. However, convergence problems are usually witnessed, especially when large displacements and deformations are observed (e.g. fracture phenomena).

In addition to the properties given in §4.2.1, Table 4.4 contains further information and assumptions about the Fiber Model.

Table 4.4: Fiber Model analysis assignments

	uprights	**diagonal bracings (tension)**	**diagonal bracings (compression)**	**horizontal bracings**
Geometric Transformation	P-delta	Corotational	Corotational	Linear
Element Type	Force-Based	Force-Based	Force-Based	Force-Based
Integration Points	3	3	3	3
Material	Steel02 (Osees)	Steel02 (Osees)	Steel02 (Osees)	Steel02 (Osees)
Imperfection	no	no	L/200	no
Group Elements	40	19	38	20
Group Nodes	42	38	57	40
Total Elements	117			
Total Nodes	171			

4.2.3 Truss Model

In this model, uprights and horizontal bracings are simulated by linear elastic elements, as it is not expected to behave nonlinearly. On the other hand, the diagonal elements are substituted for equivalent truss elements, whose material law is suitably chosen. Specifically, we implemented the method that was developed in [16], which consists of the following steps (see Figure 4.10):

1. Isolate each diagonal bracing from the rest structure. A pin support is assigned at one end and a roller at the other. The bracing is simulated by force-based fiber elements and an imperfection of L/200 is assumed.
2. Apply a compression point load F^- at the node with the roller, perform nonlinear analysis (displacement control) until non-convergence and monitor the axial displacement δ^-.
3. Apply a tensile point load F^+ at the node with the roller, perform nonlinear analysis (displacement control) until non-convergence and monitor the axial displacement δ^+.
4. Combine the results from step 2 and 3. This will yield to the full diagram $F-\delta$ for the bracing under examination.

5. Select 8 points (4 for compression and 4 for tension) that represent adequate accurately the full diagram $F-\delta$ that was derived in step 4.
6. Convert the 8-point diagram $F-\delta$ to a material law $\sigma-\varepsilon$. This can be easily done by assuming that the truss element has cross-section area equal to 1:

$$\sigma=\frac{F}{A}=F$$

$$\varepsilon=\frac{\delta}{L}$$

where,

L is bracing's length.

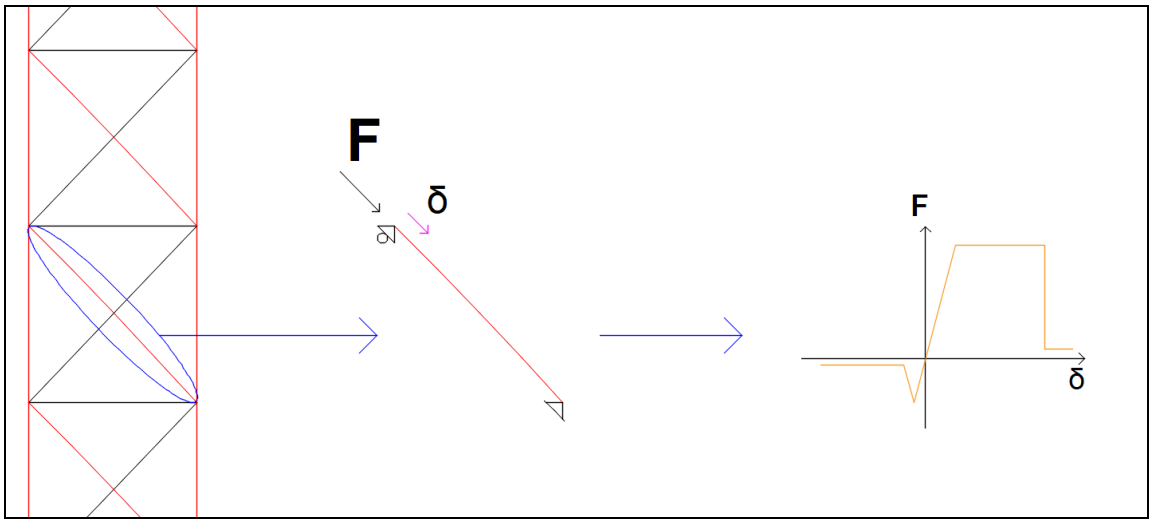

Figure 4.10: Isolation of a diagonal bracing for tension-compression test

Table 4.5: Axial (positive and negative) strength of the equivalent truss elements

Box No.	Element tag	Tensile strength N^+ (kN)	Buckling strength N^- (kN)
2	L40x40x5xS355_156	131.07	-17.91
3	L40x40x5xS355_173	131.07	-14.92
4	L40x40x5xS355_173	131.07	-14.92
5	L40x40x4xS275_173	82.388	-11.52
6	L40x40x4xS275_173	82.388	-11.52
7	L40x40x4xS275_173	82.388	-11.52
8	L40x40x4xS275_173	82.388	-11.52
9	L40x40x4xS275_173	82.388	-11.52

Table 4.5: Axial (positive and negative) strength of the equivalent truss elements (continuation)

Box No.	Element tag	Tensile strength N+ (kN)	Buckling strength N- (kN)
10	L40x40x4xS275_173	82.3888	-11.52
11	L35x35x4xS275_173	71.55	-7.87
12	L35x35x4xS235_173	61.18	-7.58
13	L35x35x4xS235_173	61.18	-7.58
14	L35x35x4xS235_173	61.18	-7.58
15	L30x30x4xS235_173	51.91	-4.87
16	L30x30x4xS235_173	51.91	-4.87
17	L30x30x4xS235_173	51.91	-4.87
18	L30x30x4xS235_173	51.91	-4.87
19	L30x30x4xS235_160	51.91	-5.55
20	L30x30x4xS235_160	51.91	-5.55

Table 4.6: Truss Model analysis assignments

	uprights	**diagonal bracings (tension)**	**diagonal bracings (compression)**	**horizontal bracings**
Geometric Transformation	P-delta	Linear	Linear	Linear
Element Type	Elastic E-B Beam	Truss	Truss	Truss
Material	-	Pinching4 (Osees)	Pinching4 (Osees)	Elastic
Preparation of data	NO	YES	YES	NO
Group Elements	40	19	19	20
Group Nodes	42	0	0	0
Total Elements	98			
Total Nodes	42			

OpenSees' material Pinching4 was selected for the diagonal bracings, which is based on an 8-point response envelope and supports cyclic degradation and pinching effects (it will be helpful when performing dynamic analyses). Truss elements' ultimate strengths (positive

and negative) are given in Table 4.5, while Table 4.6 sums up all the information about the Truss Model. Note that the nodes (and so the size of the stiffness matrix) have reduced to about 25% of the Fiber Model.

4.2.4 Link Model

In Link Model, the upright-bracing system is substituted for Two Node Link Elements whose linear properties are calculated according to Table 4.1. The shear and bending stiffnesses of the link elements are given in Table 4.7. Note also the first X-box (see Table 4.2) has negligible length and thus, 19 link elements are considered instead of 20.

Table 4.7: Linear Properties of Two Node Link Elements

Link No.	Equivalent Area A_{eq} (m^2)	Equivalent Inertia I_{eq} (m^4)	Shear Area A_{eff} (m^2)	Shear Stiffness k_{shear} (N/m)	Bending Stiffness C_{rot} (Nm/rad)
1	3.60E-03	2.59E-03	7.25E-04	5.47E+07	5.14E+08
2	3.60E-03	2.59E-03	6.75E-04	4.30E+07	4.35E+08
3	3.60E-03	2.59E-03	6.75E-04	4.30E+07	4.35E+08
4	3.60E-03	2.59E-03	5.47E-04	3.50E+07	4.35E+08
5	2.26E-03	1.62E-03	5.47E-04	3.48E+07	2.73E+08
6	2.26E-03	1.62E-03	5.47E-04	3.48E+07	2.73E+08
7	2.26E-03	1.62E-03	5.47E-04	3.48E+07	2.73E+08
8	2.26E-03	1.62E-03	5.47E-04	3.48E+07	2.73E+08
9	1.54E-03	1.11E-03	5.47E-04	3.45E+07	1.86E+08
10	1.54E-03	1.11E-03	4.75E-04	3.00E+07	1.86E+08
11	1.54E-03	1.11E-03	4.75E-04	3.00E+07	1.86E+08
12	1.54E-03	1.11E-03	4.75E-04	3.00E+07	1.86E+08
13	1.54E-03	1.11E-03	4.75E-04	3.00E+07	1.86E+08
14	1.54E-03	1.11E-03	4.03E-04	2.56E+07	1.86E+08
15	1.54E-03	1.11E-03	4.03E-04	2.56E+07	1.86E+08
16	1.54E-03	1.11E-03	4.03E-04	2.56E+07	1.86E+08
17	1.54E-03	1.11E-03	4.03E-04	2.56E+07	1.86E+08
18	1.54E-03	1.11E-03	4.32E-04	3.21E+07	2.17E+08
19	1.54E-03	1.11E-03	4.32E-04	3.21E+07	2.17E+08

Next, the nonlinear behaviour of the system will be approximated. First, by noting that the uprights have rectangular hollowed sections of considerable size, it is logical to assume that they will respond linearly (this assumption was tested by substituting the uprights in

the Fiber Model for linear elastic beams and concluded that the results were unaffected). Thus, we will focus on the shear failure mode (buckling and tensile failure of bracings).

In initial configuration (Figure 4.12.a), shear forces are transferred through the diagonal bracings, while the horizontal bracing is unstressed due to symmetry. We define $N_{(+)}, N_{(-)}$ diagonal bracing's strength in tension and compression respectively (see Table 4.5) and N_h the horizontal element's strength in compression and we assume that:

- $N_{(+)} > N_{(-)}$, as in compression buckling phenomena are witnessed.
- $N_h > N_{(-)}$, as $h_0 < d$.

The first member that exceeds its ultimate strength will be the diagonal bracing in compression, which corresponds to a **"yield shear strength"**:

$$V_y = 2N_{(-)}\frac{h_0}{d} \qquad \text{Eq. (4.10)}$$

Figure 4.12.b shows the structural model after buckling of the diagonal element. One can claim that the system has transformed from a X-column to a Z-column and thus the shear area has changed. This will be referred as **"shear degradation"**. Link element's reduced shear stiffness after the degradation will be:

$$k_{y,shear} = \frac{12EI}{\left(1+\Phi_y\right)L^3} \qquad \text{Eq. (4.11)}$$

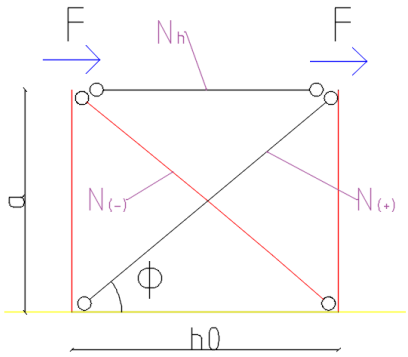

Figure 4.11: Shear distribution on a single X-box (initial configuration)

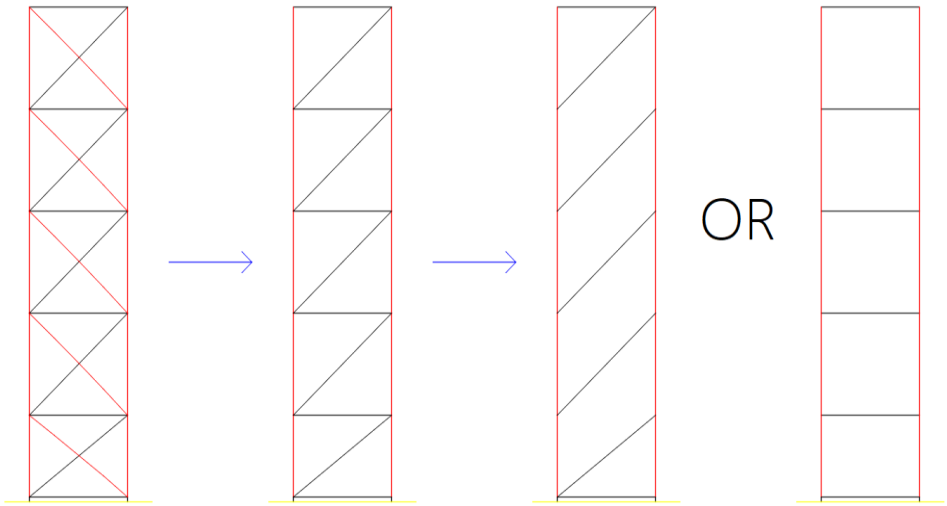

Figure 4.12: Shear failure mechanism of a X-column

The **yield shear displacement** is derived by combining Eq. (4.10) and Eq. (4.11):

$$\delta_y = \frac{V_y}{k_{shear}} \qquad \text{Eq. (4.12)}$$

Table 4.8: Shear degradation when buckling of the diagonal bracing occurs (Figure 4.12.b)

Link No.	Yield Shear Area $A_{eff,y}$ (m^2)	Yield Shear Stiffness $k_{y,shear}$ (N/m)	Yield Shear Force V_y (kN)	Yield Shear Displacement δ_y (m)
1	3.15E-04	2.39E+07	26.843	0.0004907
2	3.01E-04	1.94E+07	20.637	0.0004802
3	3.01E-04	1.94E+07	20.637	0.0004802
4	2.49E-04	1.60E+07	15.928	0.0004564
5	2.49E-04	1.60E+07	15.928	0.0004592
6	2.49E-04	1.60E+07	15.928	0.0004592
7	2.49E-04	1.60E+07	15.928	0.0004592
8	2.49E-04	1.60E+07	15.928	0.0004592
9	2.49E-04	1.59E+07	15.928	0.0004628
10	2.19E-04	1.40E+07	10.900	0.0003630
11	2.19E-04	1.40E+07	10.499	0.0003494
12	2.19E-04	1.40E+07	10.499	0.0003494
13	2.19E-04	1.40E+07	10.499	0.0003494
14	1.88E-04	1.21E+07	6.745	0.0002637
15	1.88E-04	1.21E+07	6.745	0.0002637

Table 4.8: Shear degradation when buckling of the diagonal bracing occurs (Figure 4.12.b) (continuation)

Link No.	Yield Shear Area Aeff,y (m2)	Yield Shear Stiffness ky,shear (N/m)	Yield Shear Force Vy (kN)	Yield Shear Dis-placement δy (m)
16	1.88E-04	1.21E+07	6.745	0.0002637
17	1.88E-04	1.21E+07	6.745	0.0002637
18	1.98E-04	1.49E+07	8.285	0.0002579
19	1.98E-04	1.49E+07	8.285	0.0002579

The degraded properties of each X-box are given in Table 4.8. As mentioned before, the upright frame has transformed from a X-type to a Z-type and thus, horizontal bracing is now compressed. The next structural member that will fail depends on their tensile and compressive strength:

- If $N_h < \cos\phi N_{(+)} = \frac{h_0}{d} N_{(+)}$, the horizontal bracing in compression will fail (Figure 4.12.c1).
- If $N_h > \cos\phi N_{(+)} = \frac{h_0}{d} N_{(+)}$, the diagonal bracing in tension will fail (Figure 4.12.c2).

In this example, horizontal bracings were considerably stiff, so it is not expected to behave nonlinearly. Thus, the **"ultimate shear strength"** of the system is given by:

$$V_{ult} = V_y + \left(N_{(+)} - N_{(-)}\right)\cos\phi = V_y + \left(N_{(+)} - N_{(-)}\right)\frac{h_0}{d} \Rightarrow$$

$$\boxed{V_{ult} = \left(N_{(+)} + N_{(-)}\right)\frac{h_0}{d}} \qquad \text{Eq. (4.13)}$$

In general, Eq. (4.13) is modified to include potential buckling of the horizontal bracing:

$$\boxed{V_{ult} = V_y + \min\left[\left(N_{(+)} - N_{(-)}\right)\cos\phi \;;\; N_h\right]} \qquad \text{Eq. (4.14)}$$

The **ultimate shear displacement** is given by:

$$\boxed{\delta_{ult} = \delta_y + \frac{V_{ult} - V_y}{k_{y,shear}}} \qquad \text{Eq. (4.15)}$$

Table 4.9 contains the degraded shear properties for each link element. Note that after ultimate shear strength V_{ult} is exceeded, we assume zero **ultimate shear stiffness** $k_{ult,shear}$. This is valid due to two reasons:

- We selected a steel material without strain-hardening and thus, the bracings in tension do not have overstrength.
- The shear stiffness of damaged configuration illustrated in Figure 4.12.c2 (or Figure 4.12.c1) is nearly equal to zero. This assumption is discussed thoroughly in Annex A.

Finally, assuming steel's fracture strain is equal to 10%, the corresponding **residual shear displacement** (see Figure 4.13) is equal to (for proof see Annex B):

$$\delta_{res} = 10\% \frac{d^2}{h_0} \qquad \text{Eq. (4.16)}$$

Table 4.9: Shear degradation when diagonal bracing fails in tension (see Figure 4.12.c2)

Link No.	Ult. Shear Area $A_{eff,ult}$ (m^2)	Ult. Shear Stiffness $k_{ult,shear}$ (N/m)	Ult. Shear Force V_{ult} (kN)	Ult. Shear Displacement δ_{ult} (m)
1	0.00	0.00	98.63	0.003569
2	0.00	0.00	105.32	0.004828
3	0.00	0.00	105.32	0.004828
4	0.00	0.00	67.75	0.003664
5	0.00	0.00	67.75	0.003676
6	0.00	0.00	67.75	0.003676
7	0.00	0.00	67.75	0.003676
8	0.00	0.00	67.75	0.003676
9	0.00	0.00	67.75	0.003691
10	0.00	0.00	57.29	0.003655
11	0.00	0.00	49.60	0.003123
12	0.00	0.00	49.60	0.003123
13	0.00	0.00	49.60	0.003123
14	0.00	0.00	40.96	0.003091
15	0.00	0.00	40.96	0.003091
16	0.00	0.00	40.96	0.003091
17	0.00	0.00	40.96	0.003091
18	0.00	0.00	38.24	0.002305
19	0.00	0.00	38.24	0.002305

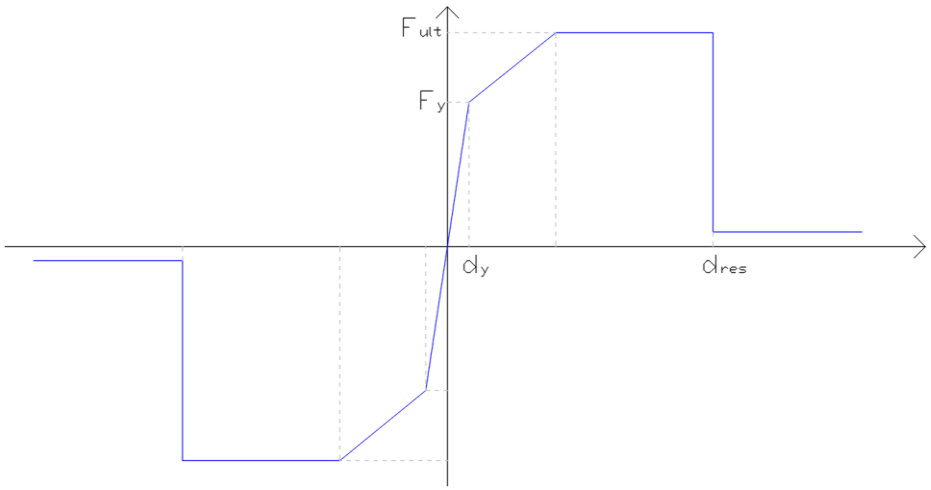

Figure 4.13: Force-Displacement diagram of nonlinear shear spring

Table 4.10: Link Model analysis assignments

	Equivalent link element
Geometric Transformation	P-delta
Element Type	Two Node Link Element
Material	Pinching4 (Osees)
Preparation of data	YES
Total Elements	19
Total Nodes	20

4.2.5 Point Load Analysis

A nonlinear static analysis (displacement-control) is performed for each of the three models (Fiber, Truss and Link). Horizontal nodal point forces are applied to level 23.2m, which corresponds to X-column's highest points and the corresponding Pushover Diagrams are shown in Figure 4.14. We conclude on the following:

- Fiber Model is characterized by early non-convergence. This is attributed to lack of strain-hardening of steel materials.
- Truss and Link Model predict about the same ultimate strength, which corresponds to a Base Shear equal to 38 kN.
- Link Model is quite stiffer than the Truss Model, which implies that a degradation mechanism is not taken into consideration. However, the results are adequately accurate.

- At top node displacement equal to 800mm both Truss and Link Model analyses did not converge. This happens due to fracture of the diagonal bracing in tension (δ_{res} for the Link Model).

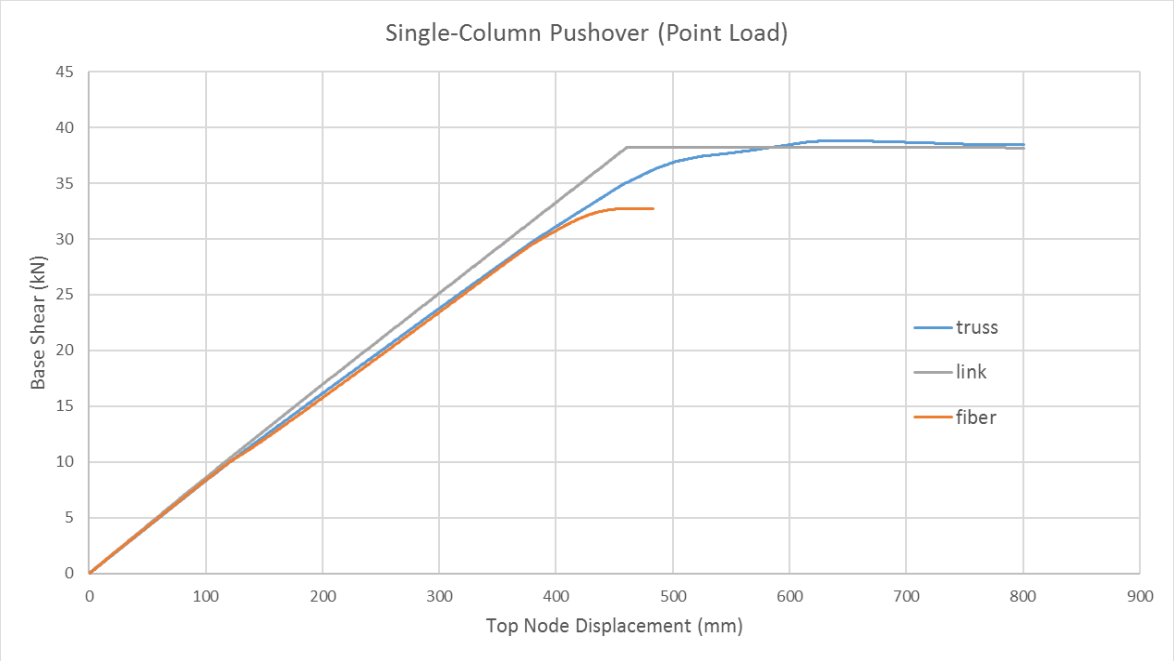

Figure 4.14: Pushover Diagram for Point Load applied at top nodes

4.2.6 Triangular Distribution Analysis

Finally, a nonlinear static analysis (displacement-control) with triangular distribution was performed, which roughly simulates the first eigenmode of a cantilever. The results are shown in Figure 4.15. Again, Fiber Model is characterized by numerical instabilities and the analysis stopped when a diagonal bracing failed due to tension yielding.

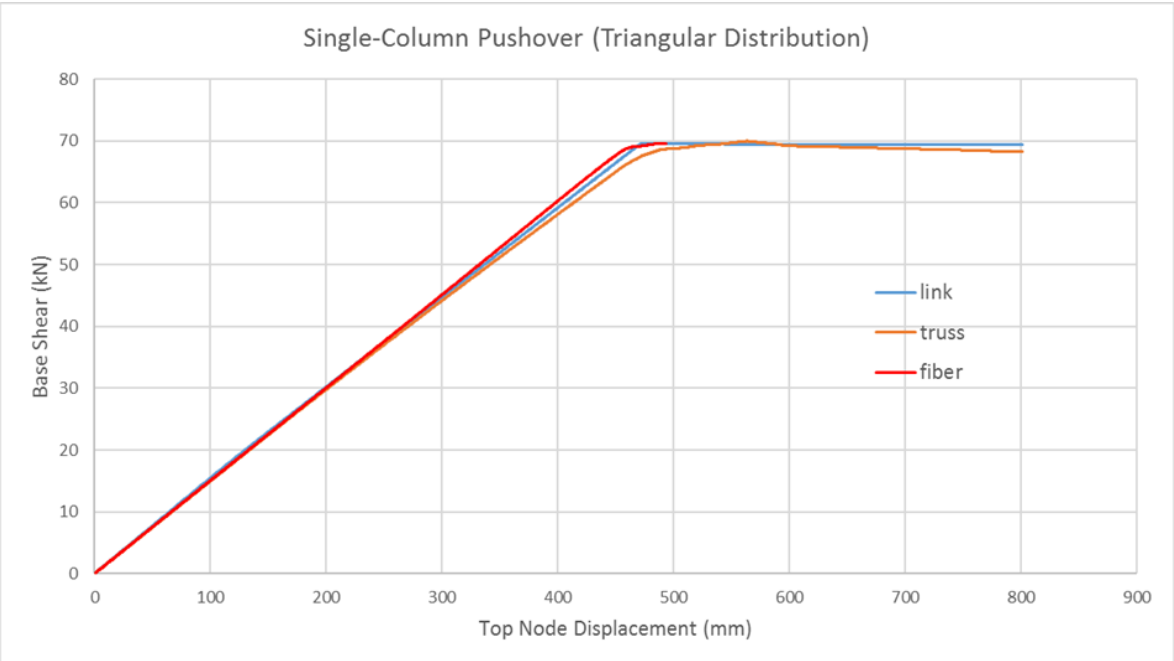

Figure 4.15: Pushover diagram for Triangular Distribution

5 Nonlinear Behaviour of a Single ARSW Frame

In this section, the nonlinear behaviour of a single ARSW frame is examined in static and dynamic analysis. This frame is a part of an existing ARSW, which is shown under construction in Figure 5.1. As before, we consider three Finite Element Models of decreased accuracy:

1. Fiber Model
2. Truss Model
3. Link Model

5.1 Configuration of Test Case and Structural Characteristics

The ARSW frame under consideration (geometry illustrated in Figure 5.2) consists of 2 external **single X-columns**, 4 internal **double X-columns** and 1 **truss beam** that connects all X-columns together. For their structural properties see Table 5.1, Table 5.2 and Table 5.3 respectively.

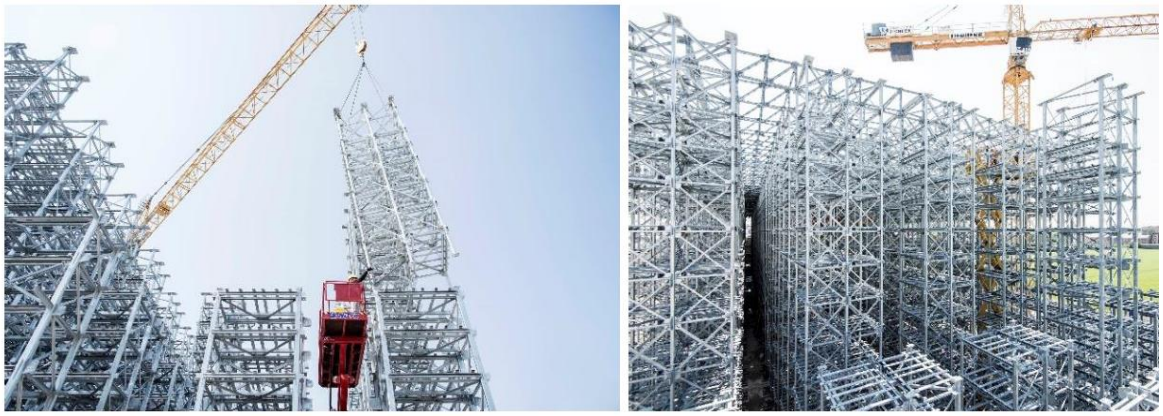

Figure 5.1: Example of an ARSW with X-columns under construction

Table 5.1: Cross-sections of single X-column

Box No.	Upright	Diagonal Bracings	Horizontal Bracing
1	RHS 120x80x10 (S355)	-	DC 80x50x3 (S355)
2	RHS 120x80x10 (S355)	L 40x40x5 (S355)	DC 80x50x3 (S355)
3	RHS 120x80x10 (S355)	L 40x40x5 (S355)	DC 80x50x3 (S355)
4	RHS 120x80x10 (S355)	L 40x40x4 (S275)	DC 80x50x3 (S355)
5	RHS 120x80x10 (S355)	L 40x40x4 (S275)	DC 80x50x3 (S355)
6	RHS 120x80x6 (S355)	L 40x40x4 (S275)	DC 80x50x3 (S355)
7	RHS 120x80x6 (S355)	L 40x40x4 (S275)	DC 80x50x3 (S355)
8	RHS 120x80x6 (S355)	L 40x40x4 (S275)	DC 80x50x3 (S355)

Table 5.1: Cross-sections of single X-column (continuation)

Box No.	Upright	Diagonal Bracings	Horizontal Bracing
9	RHS 120x80x6 (S355)	L 35x35x4 (S275)	DC 80x50x3 (S355)
10	RHS 120x80x4 (S355)	L 35x35x4 (S235)	DC 80x50x3 (S355)
11	RHS 120x80x4 (S355)	L 35x35x4 (S235)	DC 80x50x3 (S355)
12	RHS 120x80x4 (S355)	L 35x35x4 (S235)	DC 80x50x3 (S355)
13	RHS 120x80x4 (S355)	L 30x30x4 (S235)	DC 80x50x3 (S355)
14	RHS 120x80x4 (S355)	L 30x30x4 (S235)	DC 80x50x3 (S355)
15	RHS 120x80x4 (S355)	L 30x30x4 (S235)	DC 80x50x3 (S355)
16	RHS 120x80x4 (S355)	L 30x30x4 (S235)	DC 80x50x3 (S355)
17	RHS 120x80x4 (S355)	L 30x30x4 (S235)	DC 80x50x3 (S355)
18	RHS 120x80x4 (S355)	L 30x30x4 (S235)	DC 80x50x3 (S355)
19	RHS 120x80x4 (S355)	L 30x30x4 (S235)	DC 80x50x3 (S355)
20	RHS 120x80x4 (S355)	L 30x30x4 (S235)	-

(**RHS**: Rectangular Hollowed Section **L**: Angle Section, **DC**: Double Channel)

Table 5.2: Cross-sections of double X-column

Box No.	Upright	Diagonal Bracings	Horizontal Bracing
1	RHS 120x80x10 (S355)	-	DC 80x50x3 (S355)
2	RHS 120x80x10 (S355)	L 40x40x5 (S355)	DC 80x50x3 (S355)
3	RHS 120x80x10 (S355)	RHS 30x30x2.5 (S355)	DC 80x50x3 (S355)
4	RHS 120x80x10 (S355)	RHS 30x30x2.5 (S355)	DC 80x50x3 (S355)
5	RHS 120x80x10 (S355)	RHS 30x30x2.5 (S355)	DC 80x50x3 (S355)
6	RHS 120x80x6 (S355)	RHS 30x30x2.5 (S355)	DC 80x50x3 (S355)
7	RHS 120x80x6 (S355)	RHS 30x30x2.5 (S355)	DC 80x50x3 (S355)
8	RHS 120x80x6 (S355)	RHS 30x30x2.5 (S275)	DC 80x50x3 (S355)
9	RHS 120x80x6 (S355)	RHS 30x30x2.5 (S275)	DC 80x50x3 (S355)
10	RHS 120x80x4 (S355)	RHS 30x30x2.5 (S275)	DC 80x50x3 (S355)
11	RHS 120x80x4 (S355)	RHS 30x30x2.5 (S275)	DC 80x50x3 (S355)
12	RHS 120x80x4 (S355)	RHS 30x30x2.5 (S275)	DC 80x50x3 (S355)
13	RHS 120x80x4 (S355)	RHS 120x80x4 (S355)	DC 80x50x3 (S355)
14	RHS 120x80x4 (S355)	RHS 120x80x4 (S355)	DC 80x50x3 (S355)
15	RHS 120x80x4 (S355)	RHS 120x80x4 (S355)	DC 80x50x3 (S355)
16	RHS 120x80x4 (S355)	RHS 30x30x2 (S235)	DC 80x50x3 (S355)
17	RHS 120x80x4 (S355)	RHS 30x30x2 (S235)	DC 80x50x3 (S355)

Table 5.2: Cross-sections of double X-column (continuation)

Box No.	Upright	Diagonal Bracings	Horizontal Bracing
18	RHS 120x80x4 (S355)	RHS 30x30x2 (S235)	DC 80x50x3 (S355)
19	RHS 120x80x4 (S355)	RHS 30x30x2 (S235)	DC 80x50x3 (S355)
20	RHS 120x80x4 (S355)	RHS 30x30x2 (S235)	-

(**RHS**: Rectangular Hollowed Section **L**: Angle Section, **DC**: Double Channel)

Table 5.3: Cross-sections of truss beam (Figure 5.2, from left to right)

Box No.	Upright	Diagonal Bracings	Horizontal Bracing
1	DA 45x45x4 (S355)	DA 55x55x4 (S355)	DA 55x55x4 (S355)
2	DA 45x45x4 (S355)	DA 55x55x4 (S355)	DA 55x55x4 (S355)
3	DA 45x45x4 (S355)	DA 55x55x4 (S355)	DA 55x55x4 (S355)
4	DA 45x45x4 (S355)	DA 55x55x4 (S355)	DA 55x55x4 (S355)
5	DA 45x45x4 (S355)	DA 55x55x4 (S355)	DA 55x55x4 (S355)
6	DA 45x45x4 (S355)	DA 55x55x4 (S355)	DA 55x55x4 (S355)
7	DA 45x45x4 (S355)	DA 55x55x4 (S355)	DA 55x55x4 (S355)
8	DA 45x45x4 (S355)	DA 55x55x4 (S355)	DA 55x55x4 (S355)
9	DA 45x45x4 (S355)	DA 55x55x4 (S355)	DA 55x55x4 (S355)
10	DA 45x45x4 (S355)	DA 55x55x4 (S355)	DA 55x55x4 (S355)
11	DA 45x45x4 (S355)	DA 55x55x4 (S355)	DA 55x55x4 (S355)
12	DA 45x45x4 (S355)	DA 55x55x4 (S355)	DA 55x55x4 (S355)
13	DA 45x45x4 (S355)	DA 55x55x4 (S355)	DA 55x55x4 (S355)
14	DA 45x45x4 (S355)	DA 55x55x4 (S355)	DA 55x55x4 (S355)
15	DA 45x45x4 (S355)	DA 55x55x4 (S355)	DA 55x55x4 (S355)
16	DA 45x45x4 (S355)	DA 55x55x4 (S355)	DA 55x55x4 (S355)
17	DA 45x45x4 (S355)	DA 55x55x4 (S355)	DA 55x55x4 (S355)
18	DA 45x45x4 (S355)	DA 55x55x4 (S355)	DA 55x55x4 (S355)
19	DA 45x45x4 (S355)	DA 55x55x4 (S355)	DA 55x55x4 (S355)
20	DA 45x45x4 (S355)	DA 55x55x4 (S355)	DA 55x55x4 (S355)

(**DA:** Double Angle Section)

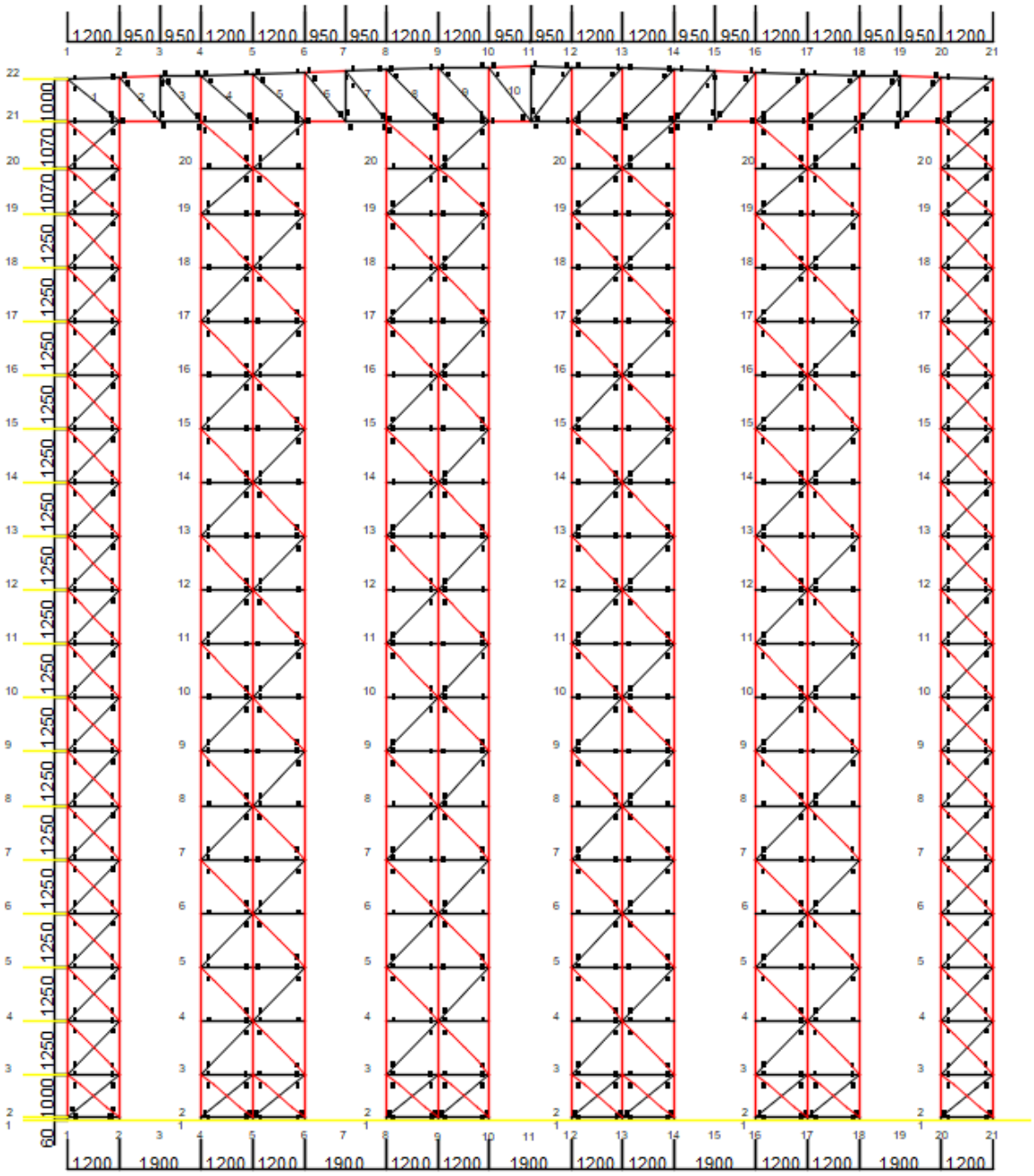

Figure 5.2: Configuration and geometric properties of the ARSW test case

5.2 Fiber Model

In Fiber Model, all structural components are simulated by nonlinear fiber beam elements and thus, it is the most demanding in terms of CPU and RAM usage. Details about this model are given in Table 5.4.

Table 5.4: Fiber Model analysis assignments

	uprights	**diagonal bracings**	**horizontal bracings**	**truss beam bracing**
Geometric Transformation	P-delta	Corotational	Linear	Linear
Element Type	Force-Based	Force-Based	Force-Based	Force-Based
Int. Points	3	3	3	3
Material	Steel02 (5% hardening)	Steel02 (5% hardening)	Steel02 (5% hardening)	Steel02 (5% hardening)
Releases	no	pinned	pinned	pinned
Imperfection	no	no	L/200	no
Group Elements	320	472	190	81
Group Nodes	336	708	380	162
Total Elements	1063			
Total Nodes	1586			

5.3 Truss Model

As discussed in Chapter 4, in Truss Model, computationally expensive diagonal bracings are substituted for simple truss elements that approximate their nonlinear behaviour in tension and compression. Diagonal bracings' ultimate positive and negative strength for each X-column are given in Table 5.5. Finally, details about this model are shown in Table 5.6.

Table 5.5: Axial (positive and negative) strength of the equivalent truss elements

	SINGLE X-COLUMN				**DOUBLE X-COLUMN**		
Box No.	Element tag	N^+ (kN)	N^- (kN)		Element tag	N^+ (kN)	N^- (kN)
2	L40x40x5xS355_156	131.07	-17.91		L40x40x5xS355_156	131.00	17.91
3	L40x40x5xS355_173	131.07	-14.92		RHS30x30x2.5xS355	96.12	21.24

Table 5.5: Axial (positive and negative) strength of the equivalent truss elements (continuation)

	SINGLE X-COLUMN				DOUBLE X-COLUMN		
Box No.	Element tag	N^+ (kN)	N^- (kN)		Element tag	N^+ (kN)	N^- (kN)
4	L40x40x5xS355_173	131.07	-14.92		RHS30x30x2.5xS355	96.12	21.24
5	L40x40x4xS275_173	82.38	-11.52		RHS30x30x2.5xS355	96.12	21.24
6	L40x40x4xS275_173	82.38	-11.52		RHS30x30x2.5xS355	96.12	21.24
7	L40x40x4xS275_173	82.38	-11.52		RHS30x30x2.5xS355	96.12	21.24
8	L40x40x4xS275_173	82.38	-11.52		RHS30x30x2.5xS275	74.53	19.45
9	L40x40x4xS275_173	82.38	-11.52		RHS30x30x2.5xS275	74.53	19.45
10	L40x40x4xS275_173	82.38	-11.52		RHS30x30x2.5xS275	74.53	19.45
11	L35x35x4xS275_173	71.55	-7.87		RHS30x30x2.5xS275	74.53	19.45
12	L35x35x4xS235_173	61.18	-7.58		RHS30x30x2.5xS275	74.53	19.45
13	L35x35x4xS235_173	61.18	-7.58		RHS30x30x2.5xS235	63.73	18.23
14	L35x35x4xS235_173	61.18	-7.58		RHS30x30x2.5xS235	63.73	18.23
15	L30x30x4xS235_173	51.91	-4.87		RHS30x30x2.5xS235	63.73	18.23
16	L30x30x4xS235_173	51.91	-4.87		RHS30x30x2xS235	51.91	15.22
17	L30x30x4xS235_173	51.91	-4.87		RHS30x30x2xS235	51.91	15.22
18	L30x30x4xS235_173	51.91	-4.87		RHS30x30x2xS235	51.91	15.22
19	L30x30x4xS235_160	51.91	-5.55		RHS30x30x2xS235_160	51.91	16.90
20	L30x30x4xS235_160	51.91	-5.55		RHS30x30x2xS235_160	51.91	16.90

Table 5.6: Truss Model analysis assignments

	uprights	**diagonal bracings**	**horizontal bracings**	**truss beam bracing**
Geometric Transformation	P-delta	Linear	Linear	Linear
Element Type	Elastic E-B Beam	Truss	Truss	Truss
Material	-	Pinching4 (Osees)	Elastic	Elastic
Preparation of data	NO	YES	NO	NO

Table 5.6: Truss Model analysis assignments (continuation)

	uprights	diagonal bracings	horizontal bracings	truss beam bracing
Group Elements	320	236	190	81
Group Nodes	336	0	0	26
Total Elements	827			
Total Nodes	362			

5.4 Link Model

As done before, X-columns are substituted for Two Node Link Elements that consider shear-degradation. Uprights are not expected to behave nonlinearly (as they consist of hollowed cross-sections of considerable size), so bending and axial failures are assumed not to develop during the analyses. The linear properties of the X-columns are given in Table 5.7, while heights and distances between them are shown in Figure 5.3. Concerning their nonlinear characteristics, the method implemented in Chapter 4 was followed. Here, we will focus on the equivalent properties of the truss beam. One can think of it as a horizontal Z-column, but with variable h_0 and a. For each Z-box the linear properties $A_{eq,beam}$, $I_{eq,beam}$ and $A_{eff,beam}$ are calculated and then their average is used:

$A_{eq,beam} = 1.38e^{-3}\ m^2$, $I_{eq,beam} = 5.81e^{-4} m^4$ and $A_{eff,beam} = 5.78e^{-4} m^2$

The average moment of inertia must then be multiplied by L_{eq} / L_{real}, where L_{eq} the length of the equivalent beam (3.7m for single and 4.3m for double) and $L_{real} = 1.9m$ the actual clear distance between the X-columns.

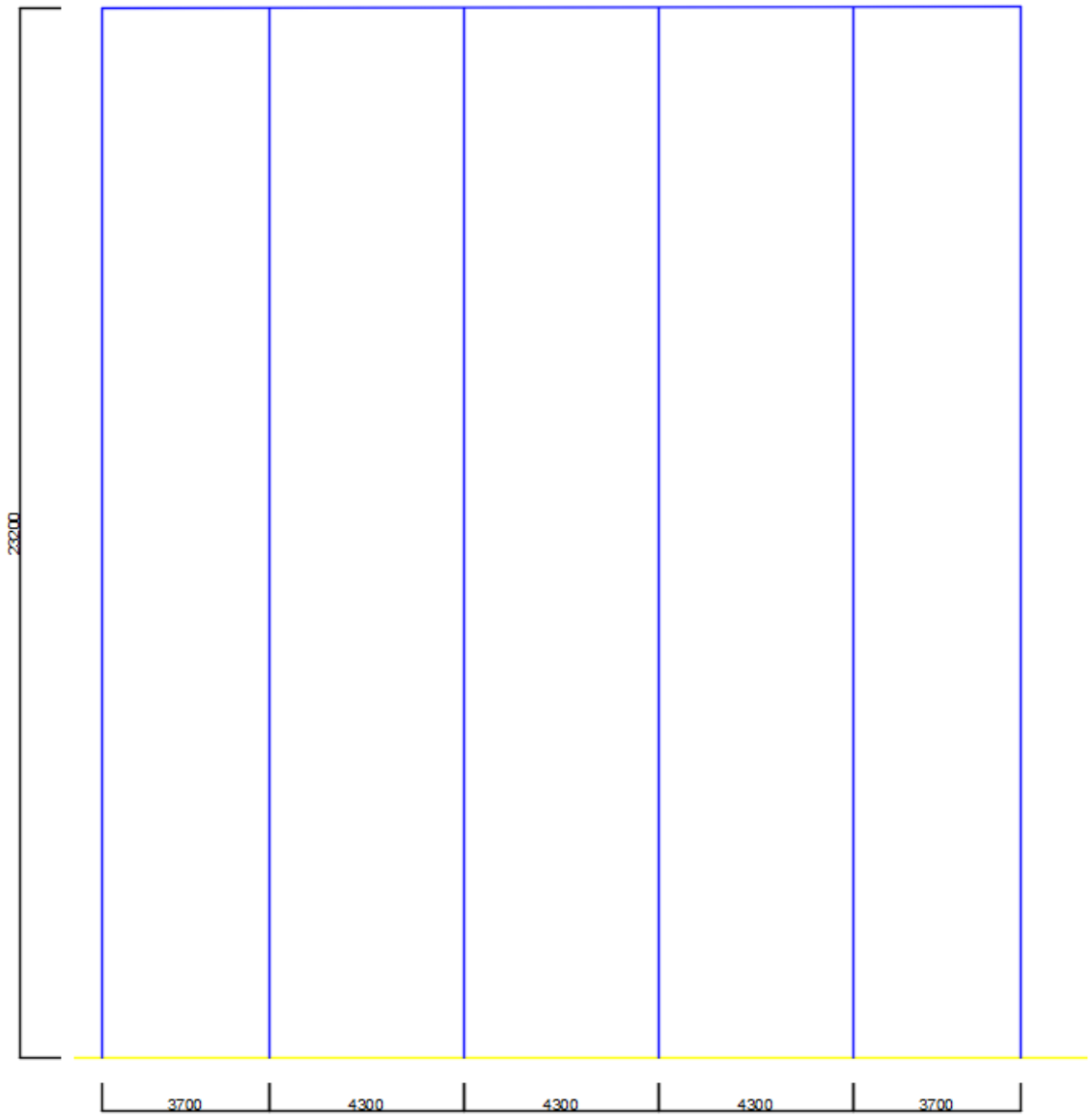

Figure 5.3: Configuration and geometric properties of Link Model

Table 5.7: Linear Properties of X-columns

	SINGLE X-COLUMN				DOUBLE X-COLUMN	
Box No.	A_{eq} (m^2)	I_{eq} (m^4)	A_{eff} (m^2)	A_{eq} (m^2)	I_{eq} (m^4)	A_{eff} (m^2)
2	7.20E-03	2.59E-03	7.25E-04	1.08E-02	1.04E-02	1.45E-03
3	7.20E-03	2.59E-03	6.75E-04	1.08E-02	1.04E-02	4.95E-04
4	7.20E-03	2.59E-03	6.75E-04	1.08E-02	1.04E-02	4.95E-04
5	7.20E-03	2.59E-03	5.47E-04	1.08E-02	1.04E-02	4.95E-04
6	4.51E-03	1.62E-03	5.47E-04	6.77E-03	6.50E-03	4.95E-04
7	4.51E-03	1.62E-03	5.47E-04	6.77E-03	6.50E-03	4.95E-04
8	4.51E-03	1.62E-03	5.47E-04	6.77E-03	6.50E-03	4.95E-04

Table 5.7: Linear Properties of X-columns (continuation)

	SINGLE X-COLUMN				DOUBLE X-COLUMN		
9	4.51E-03	1.62E-03	5.47E-04		6.77E-03	6.50E-03	4.95E-04
10	3.07E-03	1.11E-03	5.47E-04		4.61E-03	4.42E-03	4.95E-04
11	3.07E-03	1.11E-03	4.75E-04		4.61E-03	4.42E-03	4.95E-04
12	3.07E-03	1.11E-03	4.75E-04		4.61E-03	4.42E-03	4.95E-04
13	3.07E-03	1.11E-03	4.75E-04		4.61E-03	4.42E-03	4.95E-04
14	3.07E-03	1.11E-03	4.75E-04		4.61E-03	4.42E-03	4.95E-04
15	3.07E-03	1.11E-03	4.03E-04		4.61E-03	4.42E-03	4.95E-04
16	3.07E-03	1.11E-03	4.03E-04		4.61E-03	4.42E-03	4.03E-04
17	3.07E-03	1.11E-03	4.03E-04		4.61E-03	4.42E-03	4.03E-04
18	3.07E-03	1.11E-03	4.03E-04		4.61E-03	4.42E-03	4.03E-04
19	3.07E-03	1.11E-03	4.32E-04		4.61E-03	4.42E-03	4.32E-04
20	3.07E-03	1.11E-03	4.32E-04		4.61E-03	4.42E-03	4.32E-04

Table 5.8: Link Model analysis assignments

	Equivalent Columns	**Equivalent Beams**
Geometric Transfor-mation	P-delta	Linear
Element Type	Two Node Link Element	Timoshenko
Material	Pinching4 (Osees)	-
Preparation of data	YES	YES
Total Elements	114	5
Total Nodes	120	0
Total Elements	119	
Total Nodes	120	

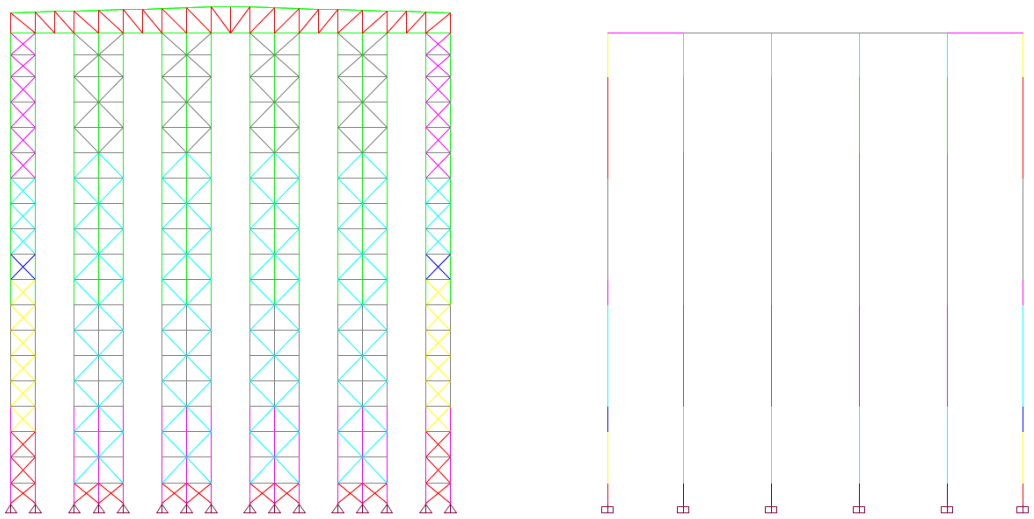

Figure 5.4: FEA Full Model (left) and Link Model (right)

5.5 Modal Analysis

First, Modal Analysis is performed to validate Link Model in the elastic region. The masses are assumed to be lumped, of magnitude 5 kN and distribution as displayed in Figure 5.5. The results for the five first eigenmodes are shown in Figure 5.6 and Figure 5.7. As it is observed, the Link Model predicts well even the higher modes of the system, and so, it is expected to give accurate results in linear dynamic analysis.

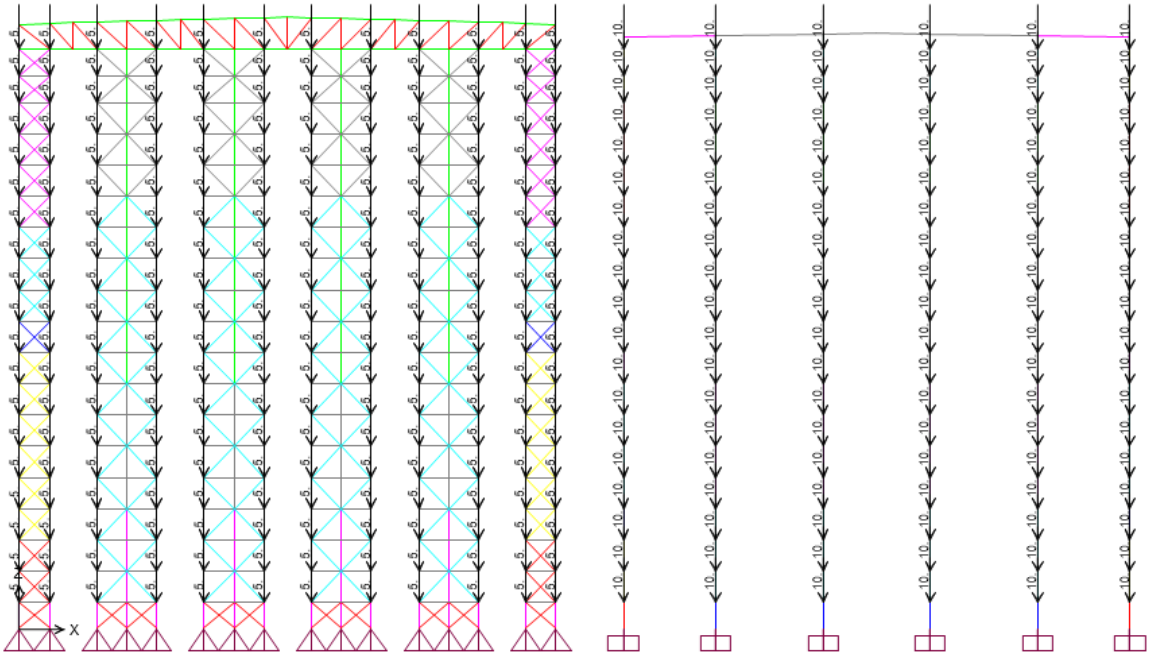

Figure 5.5: Gravity loads (kN) on Full Model (left) and Link Model (right)

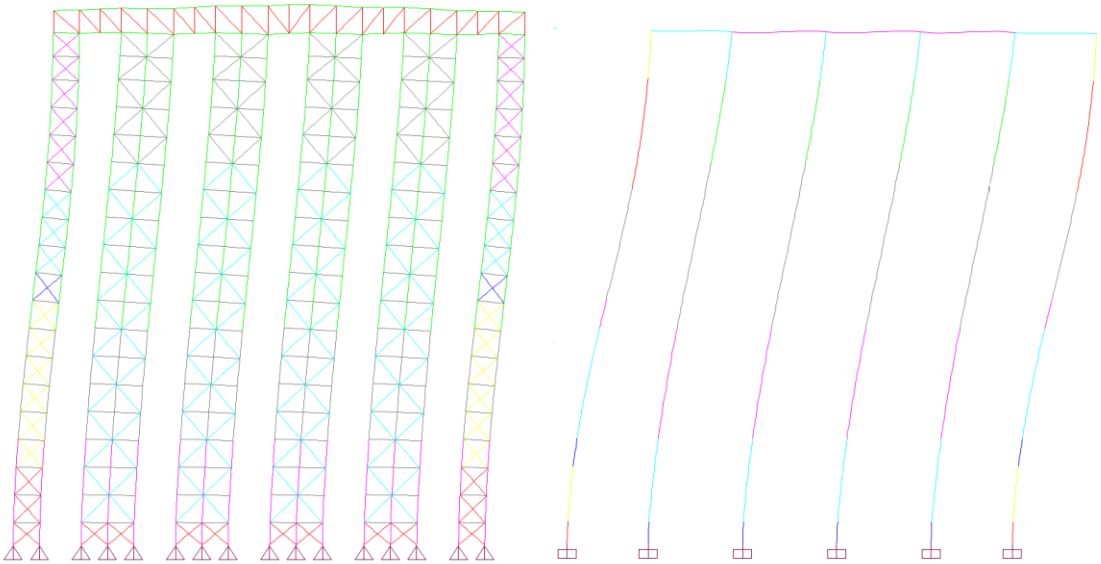

Figure 5.6: First Eigenmode of Full Model ($T_{1,1}$=0.775 sec) and Link Model ($T_{1,2}$=0.784 sec)

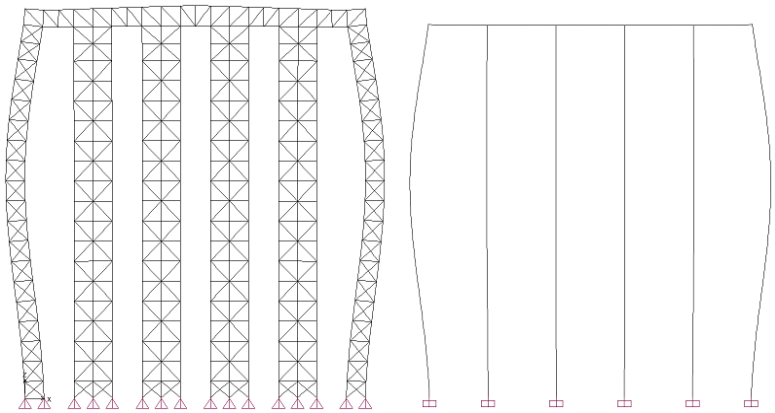

(a) 2nd mode of vibration ($T_{2,1}$=0.386s, $T_{2,2}$=0.37s)

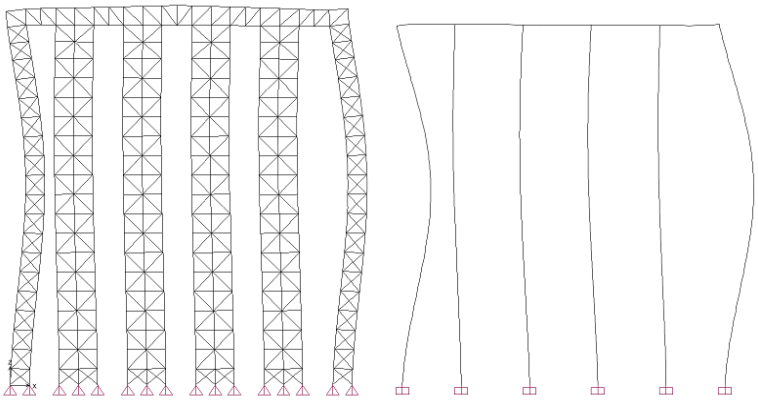

(b) 3rd mode of vibration ($T_{3,1}$=0.358s, $T_{3,2}$=0.342s)

Figure 5.7: 2nd, 3rd, 4th and 5th mode shapes

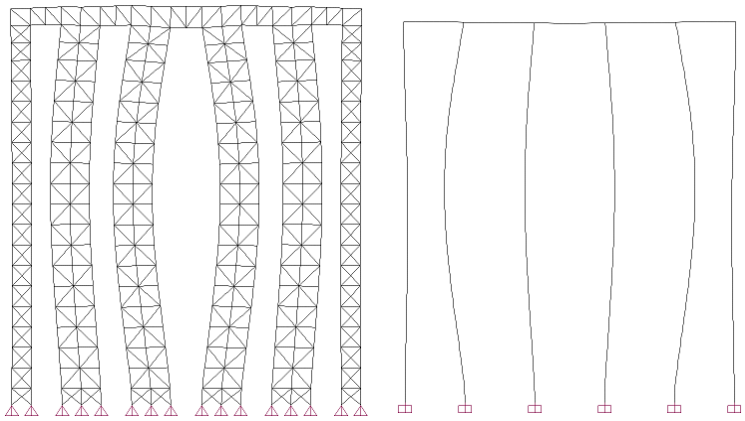

(c) 4th mode of vibration (T4,1=0.271s, T4,2=0.276s)

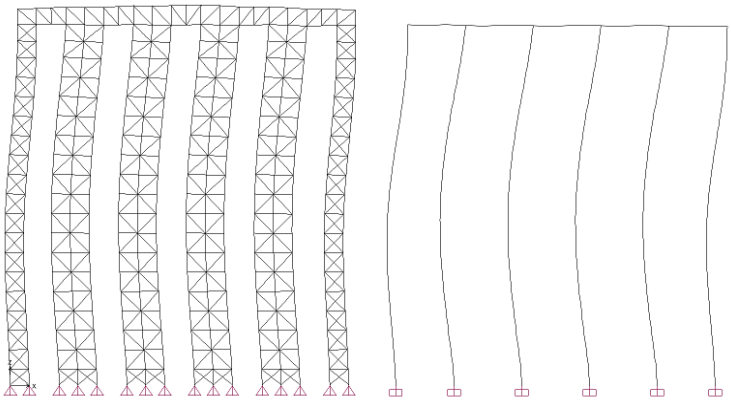

(d) 5th mode of vibration (T5,1=0.209s, T5,2=0.211s)

Figure 5.7: 2nd, 3rd, 4th and 5th mode shapes (continuation)

5.6 Pushover Analysis

Next, Static Pushover Analyses were performed for the three models, assuming triangular distribution for the lateral loads. The analyses were executed until the system reached 10% roof drift or stability and non-convergence problems occurred. The Base-Shear vs Top Node Displacement diagrams are illustrated in Figure 5.8a and Figure 5.8b for 800 kg and 2000 kg pallet load respectively.

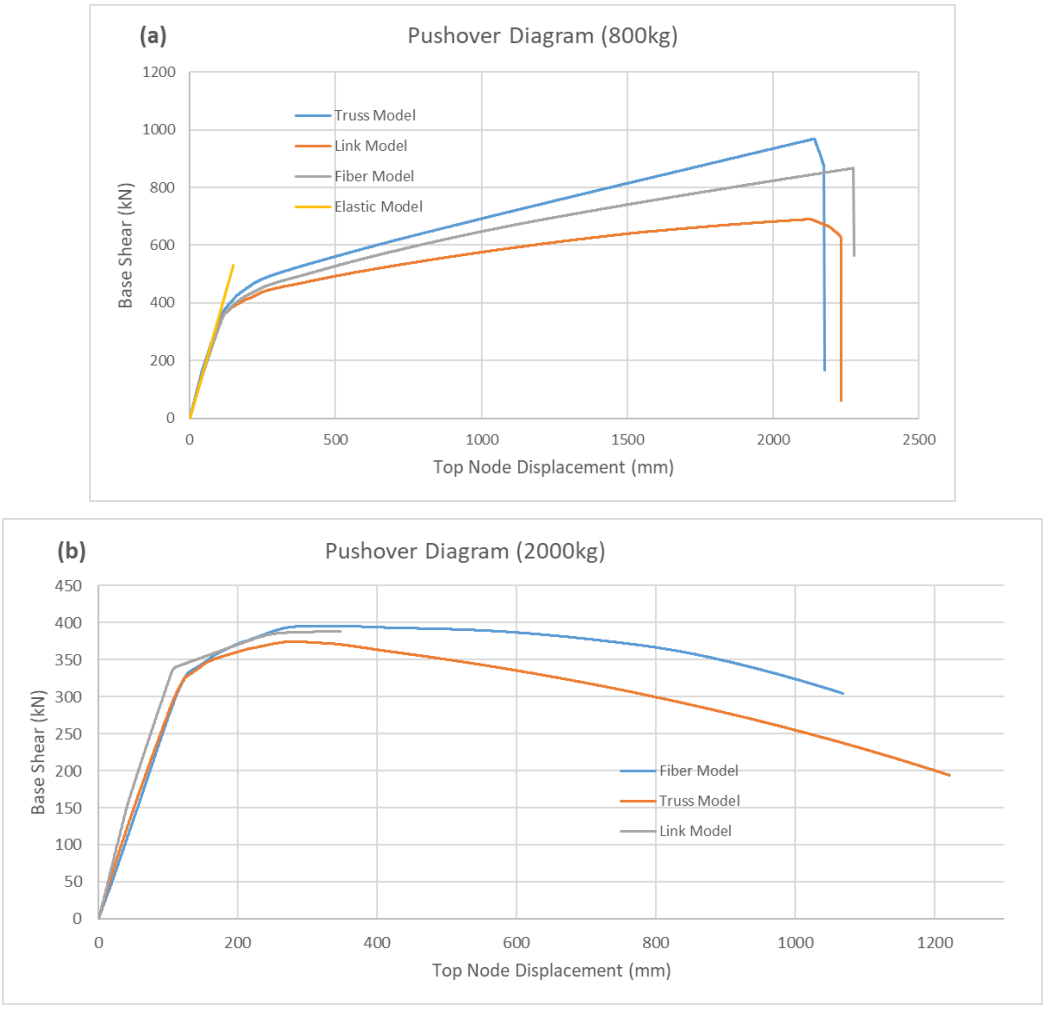

Figure 5.8: Base Shear vs Top Node Displacement of Pushover Analysis for the three models under examination; (a) 800 kg pallet load and (b) 2000 kg pallet load

All models respond linearly and elastic until a roof displacement approximately equal to 150 mm is achieved. After this “limit state” is exceeded, the structure is highly nonlinear, and Pushover’s slope decreases exponentially. This behaviour was attributed to the successive failure of the diagonal bracings in tension. At about 500mm the slope has dropped to 7.2% of the elastic branch for the Link Model, 5.5% for the Truss Model and 7.7% for the Fiber Model. It is mentioned that steel’s strain hardening was chosen equal to 5% which is roughly Pushover’s residual slope.

Pallet load scenarios 800 and 2000 kg have a vast difference in post-capping behaviour. In latter, P-delta phenomena are of major importance and the structure is not able to achieve high ductility and overstrength.

5.7 Dynamic Analysis

Nonlinear dynamic analyses were executed for the Truss and Link Model, and the time-history results are displayed in Figure 5.9a to Figure 5.9f. Structural properties, geometry and distribution of masses were the same as in Pushover Analysis. In addition, both systems were assumed undamped, and thus residual oscillations are expected. It was observed that the Link Model was encouraging accurate, as it was able to predict adequately well the maximum displacement of the system.

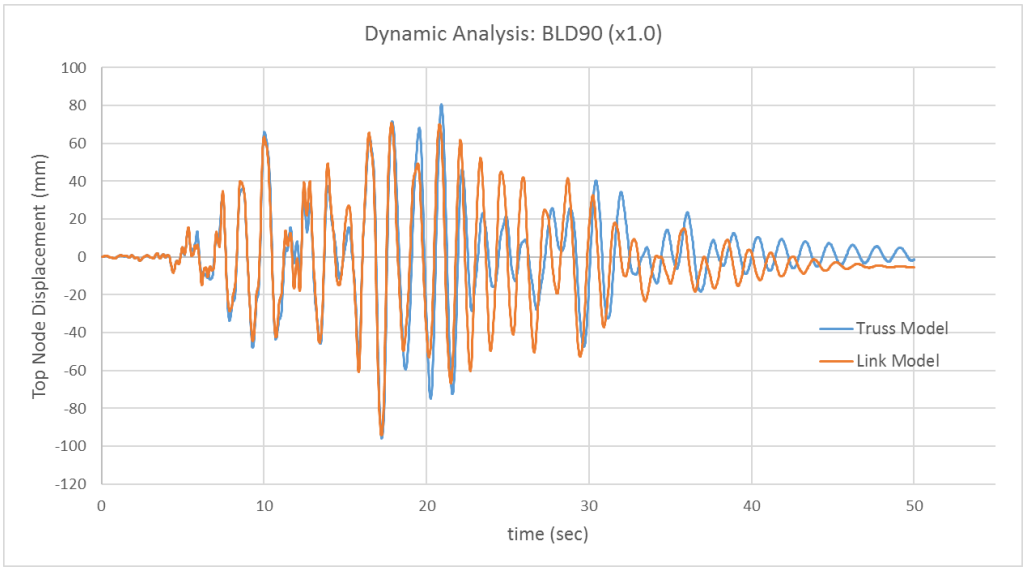

(a) Accelerogram BLD90 (x1.0)

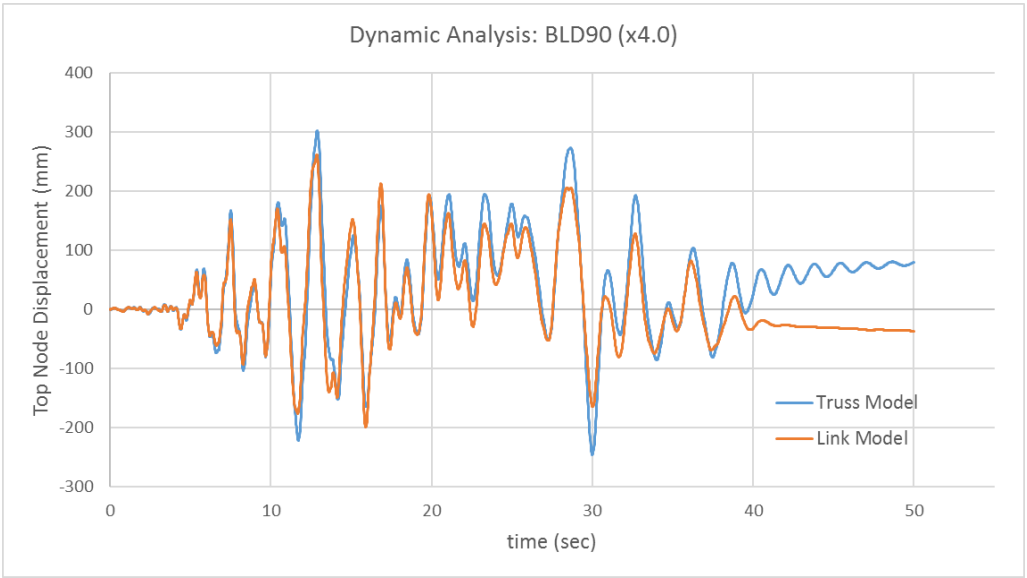

(b) Accelerogram BLD90 (x4.0)

Figure 5.9: Results of time history analyses for the Truss and Link Model

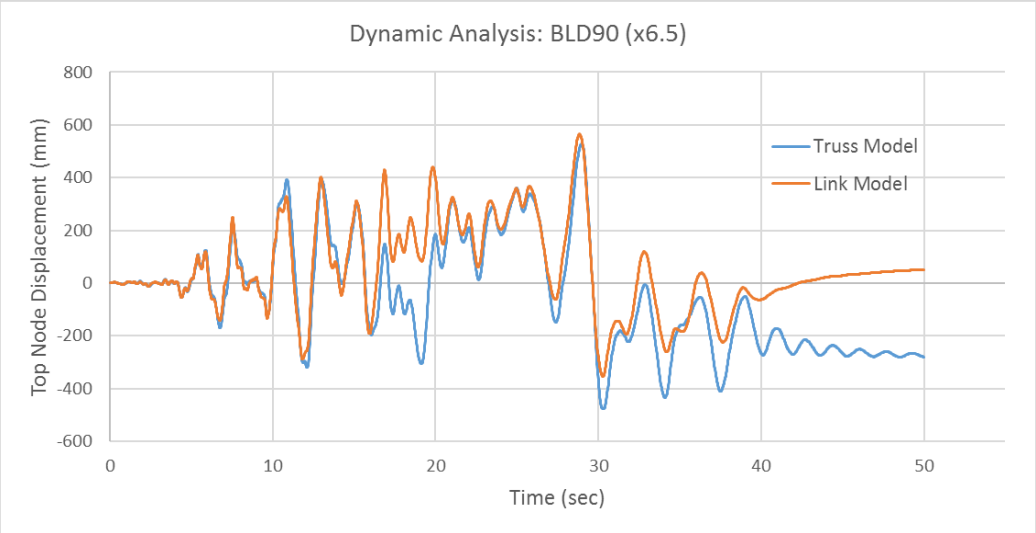

(c) Accelerogram, BLD90 (x6.5)

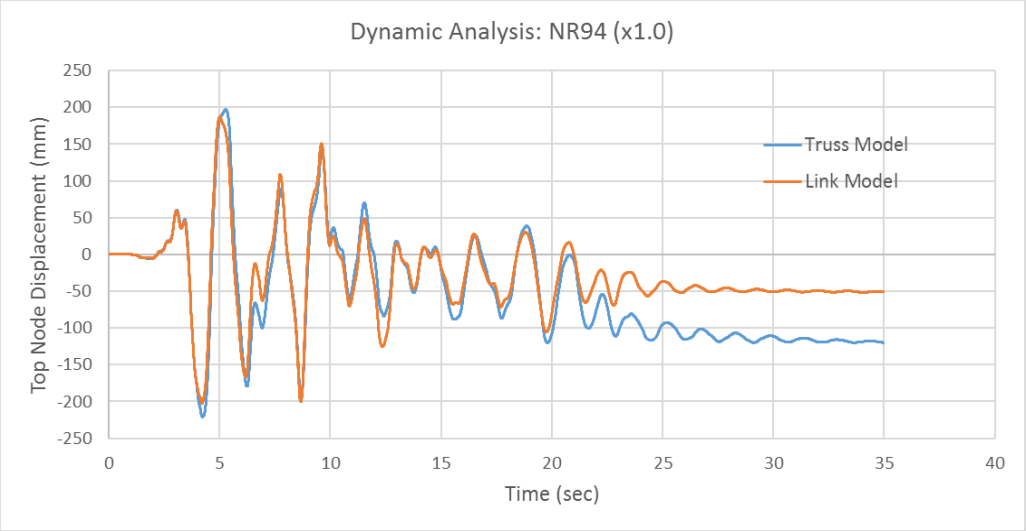

(d) Accelerogram NR94 (x1.0)

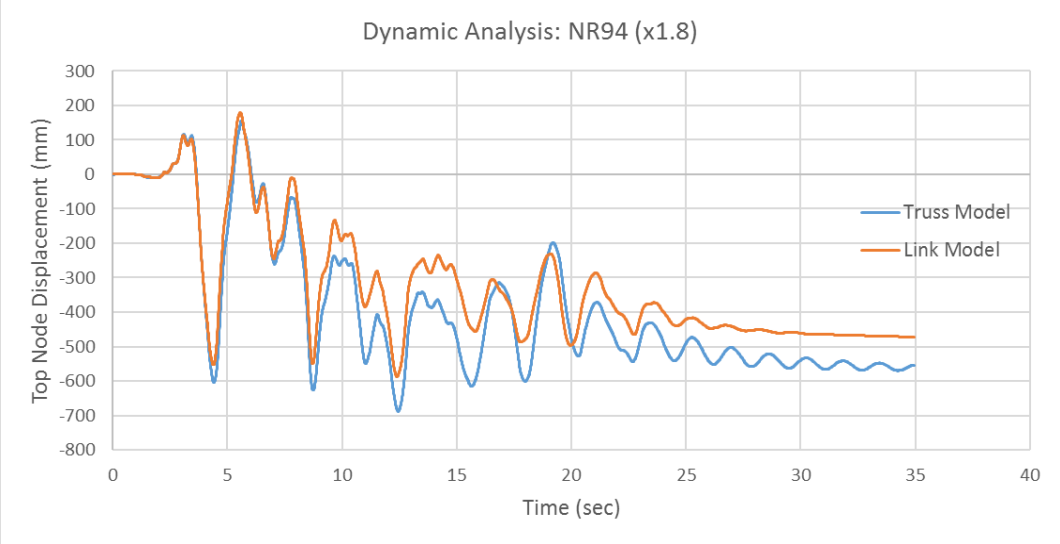

(e) Accelerogram NR94 (x1.8)

Figure 5.9: Results of time history analyses for the Truss and Link Model (continuation)

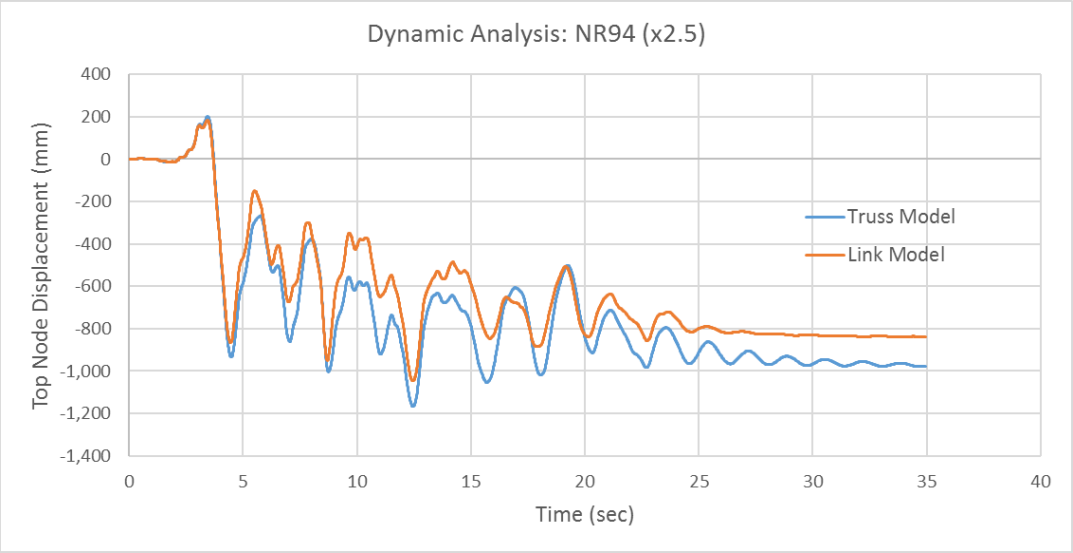

(f) Accelerogram NR94 (x2.5)

Figure 5.9: Results of time history analyses for the Truss and Link Model (continuation)

6 Conclusion and Future Work

The simplified method developed in present thesis was tested on a 2D Automated Rack Supported Warehouse frame for linear, nonlinear static and nonlinear dynamic analyses. In elastic region, the reduced-order model can predict extremely well even the higher eigenmodes of the real structure. A question remains about Linear Buckling Analysis, as upright's local buckling between bracings cannot be considered.

Concerning nonlinear analyses, the introduced model uses Two Node Link Elements to simulate the nonlinear response of upright frames and Timoshenko Beam Elements for the roof. In this specific test case, uprights were considerably stiff, so they did not participate in structure's plastic mechanism. Thus, we concentrated on bracings' compression and tension failure, which corresponds to shear degradation for the equivalent link element. As it was observed, X-column was "transformed" to Z type after buckling of the diagonal bracing occurs and the system loses shear stiffness.

Despite the promising results of the introduced methodology, the following questions/problems are yet to be answered:

- Extension of the method for 3D FEA simulations. A modelling strategy that will be tested is illustrated in Figure 6.1. It includes the summation of beams in down-aisle direction to an equivalent element with plastic hinges assigned to its ends.

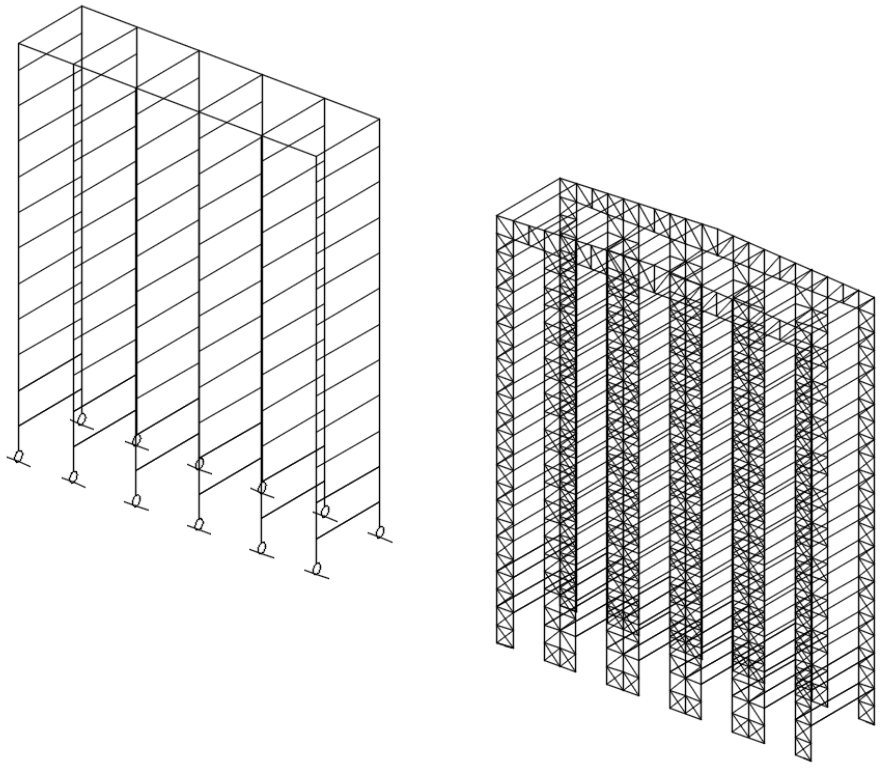

Figure 6.1: Modelling strategies for the simulation of Automated Rack Supported Warehouses

- Combination of shear, axial and bending failure. As it was discussed, an upright buckles when an interaction of axial force and bending moment on the link element occurs.

However, Two Node Link Element is not, at the moment, able to couple its springs. Author's intention is to extend its capabilities by programming a new "coupled" link element. If this attempt is not successful, a possible solution might be the assignment of ZeroLength elements with nonlinear fiber sections that consider moment-force interactions.

- Modify the introduced method so it can be adapted by commercial programs. For example, FEA program SAP2000 does not support Two Node Link Elements but nonlinear shear springs together with moment-force interaction hinges might overcome this problem.

7 References

1. BS EN 15512-2009, "*Terms and definitions*", Section 3
2. EN 16681, "*Low dissipative concept*", Section 8.3.2
3. EU-RFCS Steel RTD Programme RFSR-CT-2004-00045 "*SEISRACKS: Storage Racks in Seismic Areas*" 2004.12.01 - 2007.05.31
4. EU-RFCS Steel RTD Programme RFSR-CT-2011-00031 "*SEISRACKS2: Seismic Behavior of Steel Storage Pallet Racking Systems*" 2011.07.01 - 2014.06.30.
5. K.J. Bathe, "*Finite Element Procedures*", 1st Edition, Prentice Hall, 1996; 2nd Edition, Watertown, MA: Klaus-Jürgen Bathe, 2014.
6. McGraw-Hill, "*Fundamentals of Finite Element Analysis*", 1 edition (June 27, 2003)
7. G. Thomas Mase, George E. Mase "*Continuum Mechanics for Engineers*", CRC-Press, 1999
8. Thomas J. R. Hughes, "*The Finite Element Method: Linear Static and Dynamic Finite Element Analysis*", Dover Publications, 1 edition (August 16, 2000)
9. Henri P. Gavin, "*Structural Element Stiffness, Mass, and Damping Matrices*", online courses, Department of Civil and Environmental Engineering Duke University (Fall 2018)
10. BS EN 15512-2009, "*Simplified method for cross-aisle stability analysis in circumstances where there is uniform distribution of compartment loads over the height of the upright frame*", Annex G
11. Timoshenko, S. P., "*On the correction factor for shear of the differential equation for transverse vibrations of bars of uniform cross-section*", Philosophical Magazine, 1921 p. 744.
12. BS EN 15512-2009, "*Structural analysis*", Section 9
13. EN 16681, "*Structural types and behaviour factor*", Section 8.3
14. http://opensees.berkeley.edu/
15. J. N. Reddy, "*An Introduction to Continuum Mechanics*", Cambridge University Press, 2007
16. Sitaropoulos K. E. (2016). "*Uniaxial spring model of steel braces for the seismic assessment of steel structures*", Diploma Thesis EMK ΔΕ 2016/44, Institute of Steel Structures, National Technical University of Athens, Greece

Annex A. Post-capping behaviour of upright frames

A question arises about the post-capping behaviour of an upright-frame and the corresponding shear degradation. The test cases examined in this thesis assumed that X-column is collapsing after fracture of the diagonal bracing in tension. Here, we will investigate this hypothesis for every type of upright frame and we will try to understand the failure mechanism.

1. D-column

The D-column test case is derived by removing the unnecessary elements (diagonal and horizontal bracings) of the single X-column that was examined in 4.2. Pushover Analysis was performed in FEA program SAP2000 and the corresponding diagram is shown in Figure A.1.

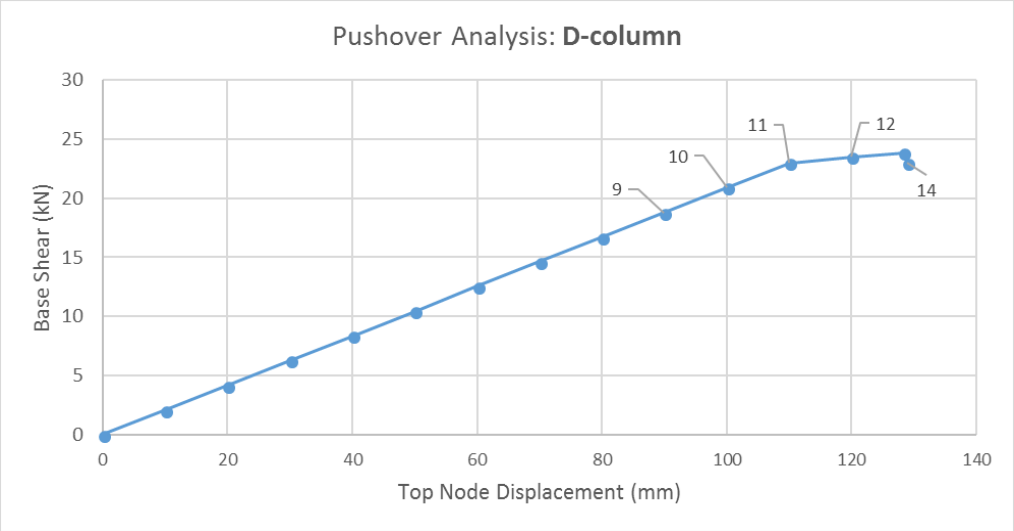

Figure A.1: Pushover Analysis of a single D-column

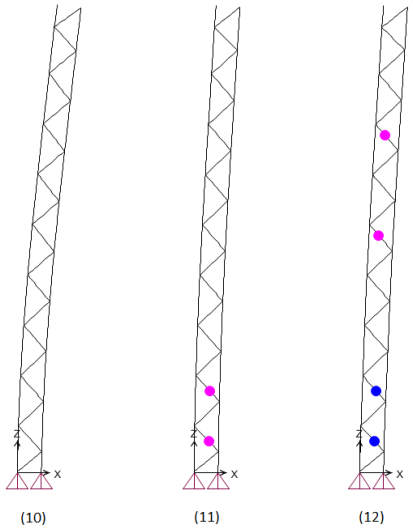

Figure A.2: Failure of bracings under compression in Steps 10, 11 and 12

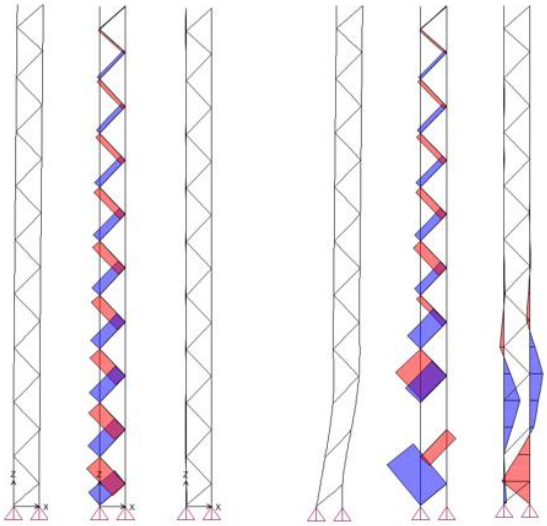

Figure A.3: Deformed shape, Axial Force Diagram and Bending Moment Diagram of **1.** Initial Model (left) and **2.** Damaged Model (right)

Step 10 (see Figure A.1) is the last linear step of the analysis. After that, two bracings fail, and the slope is decreased to 24% in Step 11, 20% in Step 12 and goes negative in Step 13. The configurations of Steps 10, 11 and 12 are given in Figure A.2.

One can claim that in Step 11 the upright-frame is structurally the same as if we have removed completely the bracings that failed. Indeed, the slope of this equivalent D-column is 20%, which is approximately the same as in Step 11. Thus, the load increment from Step 11 to 12 will be carried by the damaged system, whose Axial-Force and Bending-Moment diagrams are shown in Figure A.3. It was observed that, in the damaged system, the bracings near the ones that have failed concentrate axial forces of very large magnitude, while the bending moments on the uprights close to this area explode. It is concluded that:

"The shear resistance of D-column after a bracing fails, is close to zero. In Link Model, one can assume no post-capping shear strength. Ultimate shear displacement is 1 to 1.2 times the yield shear displacement (see Figure A.4)".

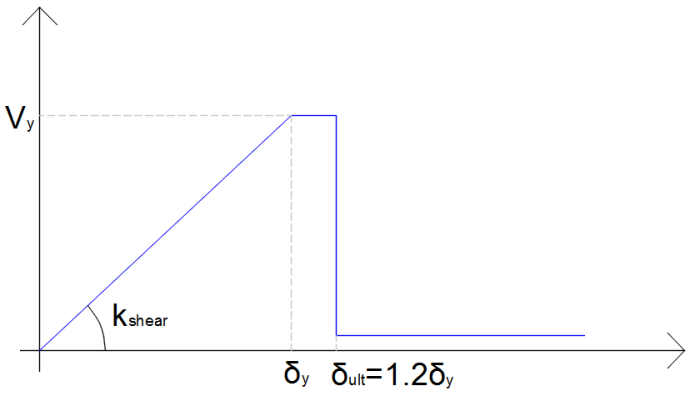

Figure A.4: Shear degradation law for a D-column (Link Model)

2. Z-column

In contrast to D-column, Z-column is an asymmetric upright-frame, so its behaviour depends not only on elements' strengths but on load's direction too (diagonal bracings may experience tension or compression). We distinguish four situations:

a. Diagonal bracing in tension, horizontal bracing in compression and $\boxed{N_{h,rd}^{-} > \frac{N_{d,rd}^{+}}{\cos\phi}}$

The first component that exceeds linear region is the diagonal bracing in tension. Assuming that steel has strain-hardening 5%, the decreased shear area of the Z-column is:

$$A_{eff,y} = \frac{\frac{E\left(5\%A_d\right)}{G}\frac{h_0^2}{d^2}\frac{a}{d}}{1+\frac{h_0^3}{d^3}\frac{\left(5\%A_d\right)}{A_h}} \qquad \text{Eq. (A.1)}$$

Equation A.1 implies that the system continues to resist to shear forces with the Z-column mechanism, but with reduced stiffness. The Pushover Diagram is illustrated in Figure A.5, while the deformed shapes in steps 38, 41, 46 and 49 are given in Figure A.6. Finally, the column collapses when one diagonal bracing reaches its ultimate strain (fracture strain) OR a horizontal bracing buckles.

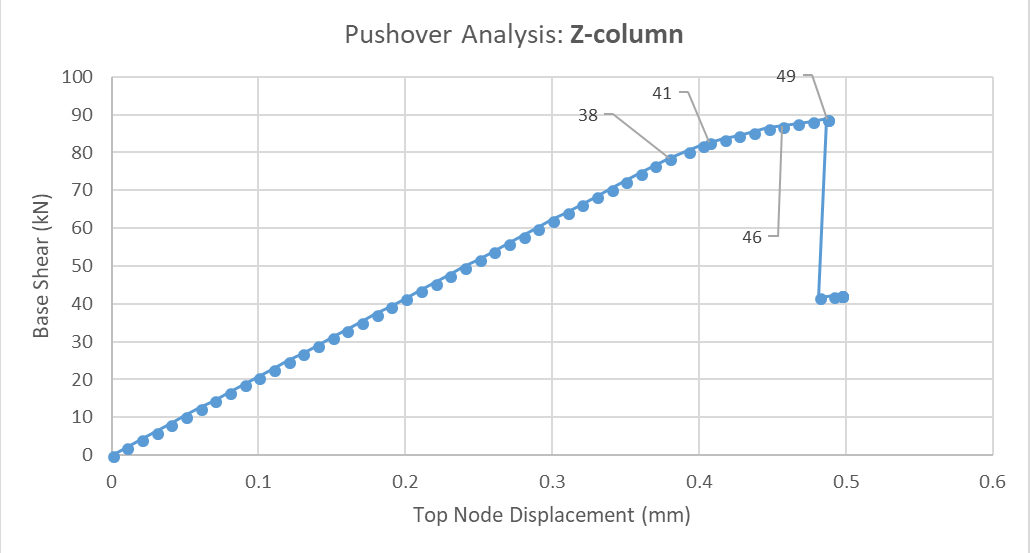

Figure A.5: Pushover Analysis of a single Z-column (tension failure first)

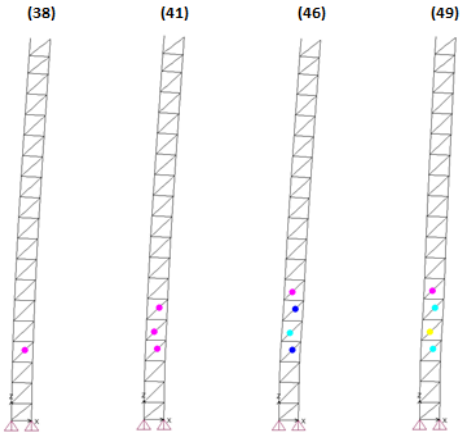

Figure A.6: Deformed configurations in steps 38, 41, 46 and 49 (see Figure A.5)

It is concluded that:

"The shear resistance of Z-column in which the diagonal bracing in tension reached its yield force, the horizontal bracing is in compression and $N_{h,rd}^{-} > N_{d,rd}^{+} / \cos\phi$*, is decreased according to the strain-hardening of the material (Eq. A.1). When a diagonal bracing reaches fracture stain or a horizontal bracing buckles, the upright frame collapses".*

b. <u>Diagonal bracing in tension, horizontal bracing in compression and</u> $\boxed{N_{h,rd}^{-} < \frac{N_{d,rd}^{+}}{\cos\phi}}$

In this situation, the first component that fails is the horizontal bracing in compression.

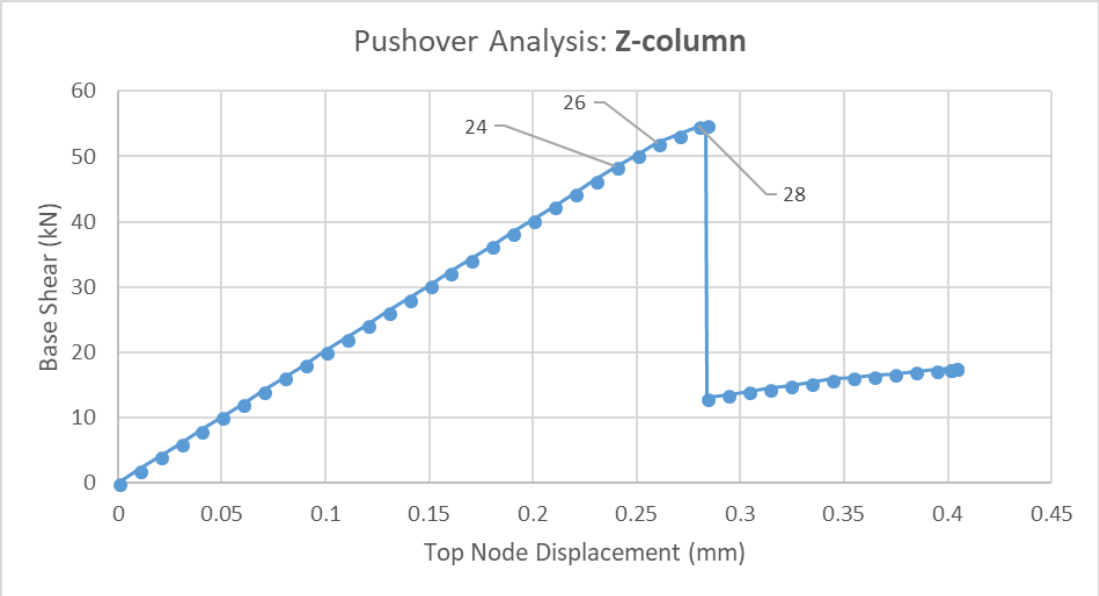

Figure A.7 Pushover Analysis of a single Z-column (buckling first)

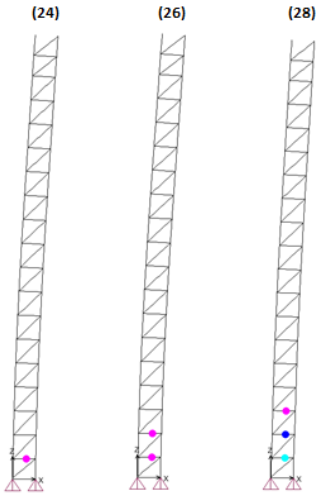

Figure A.8 Deformed configurations in steps 24, 26 and 28 (see Figure A.6)

c. Diagonal bracing in compression, horizontal bracing in tension and $N_{h,rd}^{+} > \frac{N_{d,rd}^{-}}{\cos\phi}$

Here, the diagonal bracing fails in compression due to buckling. The behaviour is similar to the one in case (b), so it is concluded that:

"The shear-resistance of Z-column in which the diagonal bracing in compression failed due to buckling, the horizontal bracing is in tension and $N_{h,rd}^{-} < N_{d,rd}^{+} / \cos\phi$*, is close to zero. In Link Model, one can assume no post-capping shear strength. Ultimate shear displacement is 1 to 1.2 times the yield shear displacement (see Figure A.4)".*

d. Diagonal bracing in compression, horizontal bracing in tension and $N_{h,rd}^{+} < \frac{N_{d,rd}^{-}}{\cos\phi}$

This scenario is very unlikely to happen, but it is mentioned for reasons of completeness. The horizontal bracing reaches yield force before the diagonal buckles and the shear area is decreased to:

$$A_{eff,y} = \frac{\frac{EA_d}{G}\frac{h_0^2}{d^2}\frac{a}{d}}{1+\frac{h_0^3}{d^3}\frac{A_d}{5\%A_h}} \qquad \text{Eq. (A.2)}$$

Then, the diagonal bracing buckles or the horizontal reaches its fracture strain.

It is concluded that:

"The shear-resistance of Z-column in which the diagonal bracing is in compression, the horizontal bracing in tension reached its yield force and $N_{h,rd}^{+} < N_{d,rd}^{-} / \cos\phi$*, is decreased according to the strain-hardening of the material (Eq. A.2). The upright frame collapses when a diagonal bracing buckles or a horizontal bracing reaches its fracture strain.".*

3. X-column

In this type of upright frame, the diagonal bracing in compression is guaranteed to fail first. As was discussed in §4.2, X-column is transformed into a Z-column when a diagonal bracing buckles. It is concluded that:

"A X-column is transformed into a Z-column when the diagonal bracing in compression fails".

4. K-column

Not fully investigated yet. It was observed that before buckling of the diagonal bracing, the upright frame behaves as a D-column. After that, the response is more complex, as shear deformation is developed due to bracings' axial compression-elongation and uprights' bending.

Annex B. How to implement tensile fracture

In contrast to the buckling failure, tension yielding has a smoother behaviour, as steel always has some strain-hardening. A typical configuration of a diagonal bracing in tension is illustrated in Figure B.1. If ε_f is the fracture strain of the material (e.g. 10% strain for steel), then the following equation holds:

$$\delta_f = u_f \cos\phi \Rightarrow$$

$$\varepsilon_f d = u_f \frac{h_0}{d} \Rightarrow$$

$$\boxed{u_f = \frac{d^2}{h_0}\varepsilon_f} \qquad \text{Eq. (B.3)}$$

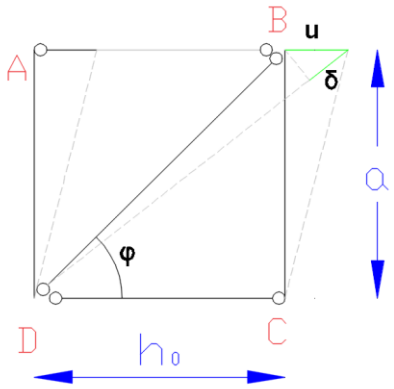

Figure B.1: Deformed configuration of a diagonal bracing